Correlation Effects and Temperature Dependencies in Thin Ferromagnetic Films: Magnetism and Electronic Structure

D I S S E R T A T I O N

zur Erlangung des akademischen Grades
d o c t o r r e r u m n a t u r a l i u m
(Dr. rer. nat.)
im Fach Physik

eingereicht an der
Mathematisch-Naturwissenschaftlichen Fakultät I
der Humboldt-Universität zu Berlin

von

Dipl.-Phys. Roland Schiller

geboren am 13. Mai 1972 in Berlin

Präsident der Humboldt-Universität zu Berlin
Prof. Dr. Jürgen Mlynek

Dekan der Mathematisch-Naturwissenschaftlichen Fakultät I
Prof. Dr. Bernhard Ronacher

Gutachter:

1. PD Dr. Volker Eyert
2. Prof. Dr. Wolfgang Nolting
3. Prof. Dr. Johannes Pollmann

eingereicht am:	17. Juli 2000
Tag der mündlichen Prüfung:	1. November 2000

Abstract

This dissertation is concerned with the theoretical investigation of the electronic and magnetic properties of *4f* systems with film geometry. The presented theory is based on the *s-f* model which features an intra-atomic exchange between a system of localized magnetic moments and the conduction electrons.

The model is investigated for the special case of zero band occupation of the conduction bands which is applicable to the situation in ferromagnetic semiconductors such as the europium chalcogenides EuO and EuS. For the special case of ferromagnetic saturation of the local-moment system the problem is exactly solvable. For finite temperatures, the presented approach is based on a moment-conserving decoupling approximation for suitably defined Green functions and evolves continuously from the exact limiting case. The theory is used to calculate the temperature-dependent quasiparticle spectrum of a ferromagnetic model film. Within these calculations, one finds a marked correlation-induced splitting of the spectra resulting in the existence of a new quasiparticle, the magnetic polaron.

The second part of the thesis is devoted to the calculation of the electronic and magnetic properties of a real ferromagnetic semiconductor film. The original *s-f* model is extended to a multi-band *s-f* model to account for the multiple conduction bands in a real system. Based on the resulting model, the temperature-dependent band structures of bulk EuO and EuO(100) films are calculated. Here, the $T = 0$ band structures of the systems, which have to be taken as input for the model calculations, are calculated using the TB-LMTO-ASA band-structure technique. Due to the special form of the solution of the *s-f* model for the exactly solvable limiting case of $T = 0$ the employed approach for combining the first-principles calculations with the model calculations prevents the problem of double counting of relevant interactions. The calculated temperature-dependent band structures yield a valuable insight into the temperature-dependent interplay between the magnetic and electronic properties in the EuO systems and allow to make verifiable predictions for future experiments. In particular, the existence of a EuO(100) surface state has been predicted and been shown to possibly induce a surface insulator-metal transition.

Zusammenfassung

Diese Dissertation beschäftigt sich mit theoretischen Untersuchung der elektronischen und magnetischen Eigenschaften von *4f*-Systemen mit Filmgeometrie. Die vorgestellte Theorie basiert auf dem *s-f*-Modell, welches durch einen intra-atomaren Austausch zwischen einem System lokaler magnetischer Momente und den Leitungselektronen charakterisiert ist.

Das Modell wird für den Fall des leeren Leitungsbandes untersucht. Der untersuchte Spezialfall ist anwendbar auf die Klasse der ferromagnetischen Halbleiter mit den Europiumchalkogeniden EuO und EuS als Prototypen solcher Substanzen. Für den Grenzfall ferromagnetischer Sättigung des Systems lokaler magnetischer Momente existiert eine exakte Lösung für das Problem. Für endliche Temperaturen wird eine Methode vorgestellt, die auf einer momentenerhaltenden Entkopplungsprozedur für passend definierte Green-Funktionen basiert. Die Theorie für endliche Temperaturen leitet sich dabei übergangslos aus dem exakt lösbaren Grenzfall ab. Mit Hilfe der vorgestellten Theorie wird das temperaturabhängige Quasiteilchenspektrum eines ferromagnetischen Modellfilmes berechnet. Die Rechnungen zeigen ein deutliches korrelationsinduziertes Aufspalten der Spektren, das in der Existenz eines neuen Quasiteilchens, des magnetischen Polarons, resultiert.

Der zweite Teil der Dissertation beschäftigt sich mit der Berechnung der elektronischen und magnetischen Eigenschaften eines realen ferromagnetischen Halbleiterfilms. Um den vielfachen Leitungsbändern eines realen Systems Rechnung tragen zu können, wird das ursprüngliche *s-f*-Modell zu einem Mehrbandmodell erweitert. Das so erweiterte *s-f*-Modell wird dazu benutzt, die temperaturabhängige Bandstruktur von Volumen-EuO und von EuO(100)-Filmen zu berechnen. Die $T = 0$-Bandstrukturen, die als Input für die Modellrechnungen dienen, werden hierbei mittels einer TB-LMTO-ASA-Bandstrukturrechnung berechnet. Die spezielle Struktur der Lösung des *s-f*-Modells für den exakt lösbaren Grenzfall von $T = 0$ verhindert dabei das Auftreten von Doppelzählungen relevanter Wechselwirkungen bei der Kombination von ab-initio-Rechnungen und *s-f*-Modellrechnungen. Die erhaltenen temperaturabhängigen Bandstrukturen geben wertvolle Einblicke in das Wechselspiel zwischen elektronischen und magnetischen Eigenschaften in EuO-Systemen und gestatten es, verifizierbare Vorhersagen für künftige Experimente zu machen. Insbesondere wird die Existenz eines EuO(100)-Oberflächenzustandes vorhergesagt, der das Auftreten eines Oberflächen-Metall-Isolator-Übergangs induzieren kann.

Contents

1 Introduction

A highly interesting field of research in contemporary solid state physics is the interaction between electronic and magnetic properties of materials. The highlights in this respect include phenomena like the colossal magnetoresistance (CMR) effect and the related correlation-induced metal-insulator transition. On the experimental side, the interest is fueled by the prospect for applications on the ever more important fields of storage media and sensor technology. From a theoretical point of view, the investigation of the respective many-particle interactions promises insight into the physics of these materials.

This thesis is focused on the electronic and magnetic properties of rare-earth systems. Due to the importance of the highly localized *4f* shells for the physical properties these materials are often referred to as *4f* system. In magnetic *4f* systems, the electrons of the *4f* shell couple to a finite magnetic moment which is strictly localized at the site of the rare-earth ion. An exchange interaction between the resulting system of localized magnetic moments and the conduction bands gives rise to characteristic mutual dependencies between the magnetic and the electronic properties in magnetic *4f* systems.

The most spectacular of these effects is the red shift of the optical absorption edge with decreasing temperature $T < T_C$, which was first found in 1964 for the ferromagnetic semiconductor EuO [1, 2]. It was later found, that the respective shift of the conduction bands, which for antiferromagnetic materials can also be a blue shift, appears to be a universal property of magnetic semiconductors [3].

The model of choice for the magnetic *4f* systems is the *s-f* model [4] which is due to Zener, Kasuya and Yosida [5, 6, 7] and models the interaction between localized magnetic moments and the conduction electrons as an intra-atomic ferromagnetic exchange. In recent years, the model has been extensively applied to explain the CMR phenomena in the perovskite manganites [8, 9]. Here, the exchange interaction occurs between localized $3d_{t_{2g}}$ spins and partly occupied $3d_{e_g}$ levels. For these systems, the model is referred to as the ferromagnetic Kondo-lattice model (FKLM) or the double-exchange model (DEX) [10, 11, 12].

The second aspect of this thesis is that of reduced dimensionality. Magnetic phenomena at surfaces and in thin films attract attention both theoretically and experimentally due to the question of phase transitions and the variation of magnetic and electronic properties in dimensionally reduced systems [13, 14, 15, 16, 17, 18, 19, 20, 21, 22, 23, 24, 25]. One of the most remarkable examples of the outstanding magnetic

properties at surfaces is the existence of a ferromagnetically ordered surface at temperatures where the bulk material is paramagnetic. This effect was first documented for the Gd(0001) surface by Weller *et al.* [26] and since then has been measured by different groups using a variety of experimental techniques [27, 28, 29, 30], with the enhancement of the Curie temperature at the surface compared to the bulk Curie temperature ranging from 17 K to 60 K. Following the results for Gd, Tb also was found to have a higher surface Curie temperature, relative to the bulk [29, 31]. The occurrence of an enhanced surface Curie temperature is not restricted to the rare earths but has also been found e. g. for the (100) $p(1 \times 1)$ surface of the transition metal vanadium [32].

Contrary to the results on the enhanced Curie temperature of the Gd(0001) surface [26, 27, 28, 29, 30], Donath *et al.* [33], using spin-resolved photoemission did not find any indications for an enhanced Curie temperature of the Gd(0001) surface. They attribute the measured enhancements of the Curie temperature of Gd(0001) surfaces measured by the other groups to a complex film morphology. With respect to the enhanced or not-enhanced surface Curie temperature at Gd(0001) surfaces, the existence of a Gd(0001) surface state, first predicted by band structure calculations [34] and subsequently measured by Li *et al.* [35] appears to be playing a crucial role and its temperature-dependent behavior has been discussed intensely [20, 33, 36, 37, 38, 39, 40, 41, 42]. Here, the discussion is on whether the surface states for the two spin directions collapse Stoner-like for $T \to T_C$ or a finite splitting of the surface states can be found even for $T > T_C$ indicating a spin-mixing type of behavior. Of special interest is the general question, by which mechanism a surface state can lead to an enhanced surface Curie temperature.

In this thesis, the *s-f* model is investigated for film symmetries for the special case of zero band occupation of the conduction band, $n = 0$. In this limit, the model applies to magnetic-semiconductor films. Here, apart from calculations for model films, special focus will be laid on the calculation of the magnetic and electronic properties of real substances. For both the model-film and the real-film calculations, the interplay between correlation effects and geometry of the system will be investigated. Furthermore the conditions for the existence and the temperature-dependent behavior of surface states will be investigated. Clearly, the limit of $n = 0$ is not applicable to local-moment metals such as Gd. However, by presenting the methodical approach for dealing with magnetic-semiconductor films, this work provides the clues to the treatment of the local-moment metals.

The thesis is organized as follows: In the following chapter, the experimental justification for the application of the *s-f* model to magnetic *4f* systems is presented followed by an introduction of the actual model and its special limiting cases. In the last section of chapter 2 the *s-f* model is put into a broader context by discussing its relation to models describing similar physical situations. The main part of the thesis can be divided into two parts. In the first, the *s-f* model is solved for model films containing a single-nondegenerated *s*-like band. In chapter 3 the *s-f* model is introduced and a solution for the case of zero band occupation is presented. Here, due to the zero band occupation, the problem can be divided into an electronic problem and a mag-

netic problem, which can be solved separately. Chapter 4 is devoted to the evaluation of the theory presented earlier for a sc(100) film with the electron hopping given in tight-binding approximation. Here, the calculation of the magnetic properties within the Heisenberg model is followed by the results for the temperature-dependent electronic structure. The second part of the thesis is concerned with the calculations for real magnetic-semiconductor films. Chapter 5 deals with the extensions to the theory which become necessary for a system with multiple degenerated conduction bands. It is followed by the evaluation of the magnetic and electronic properties of EuO(100) films in chapter 6. Starting with the magnetic properties of the EuO(100) films, the results of band structure calculations are presented, followed by the temperature-dependent band structures calculated within the *s-f* model. Here, the calculations are performed both for bulk EuO and for EuO(100) films. The thesis concludes with a summary of the results and an outlook concerning the potentials of the presented approach.

2 The Model

In this chapter we first want to classify the substances we are interested in, namely EuO and EuS. Coming from some general characteristics of *4f* systems, we will focus on the interesting class of magnetic semiconductors [43,44,45], with special emphasis on the europium monochalcogenides [46,44,47]. Based on experimental justifications we will then in Section 2.2 introduce the *s-f* model [43,44,45,48] and continue with known exact results for the model. The last section of this chapter puts the *s-f* model into a broader context by briefly discussing models describing similar physical situations.

2.1 Magnetic *4f* systems

In *4f systems* the electronic properties are largely determined by the existence of a partially filled *4f* shell. Accordingly, *4f* systems have to contain rare earths* (RE). The electron configuration of neutral rare earth atoms is that of xenon plus additional *4f*, *6s*, and for some cases *5d* contributions

$$[\mathrm{RE}] = [\mathrm{Xe}](4f)^n(5d)^m(6s)^2, \qquad (0 \leq n \leq 14;\ m = 0, 1).$$

The typical ionic state of rare earths in a solid is trivalent with exceptions in the middle of the series, where Hund's rule energy can be gained by aligning the maximum number of spins.

One of the main characteristics of *4f* systems is the strong localization of the *4f* electrons, with the *4f* shell lying well inside the xenon core [49]. As a result, the completely filled *5s-5p* core shells shield the fields arising from neighboring atoms very effectively and the *4f* shell is dominated by Hund's rules even in a crystal environment. If the *4f* electrons couple according to Hund's rules to a total angular momentum of $J \neq 0$, the *4f* shell accounts for a permanent magnetic moment which is strongly localized at the position of the rare earth. In *magnetic 4f systems* some sort of exchange interaction between these localized moments leads to a collective magnetic order below a characteristic critical temperature.

Prototypes of magnetic *4f* systems are the rare earths Gd, Tb and Dy and the europium chalcogenides EuX† (X = O, S, Se, Te). The europium chalcogenides belong to the class of magnetic semiconductors, with EuO and EuS being ferromagnetic.

*As *rare earths* we will understand the elements 57 (La) through 71 (Lu).

†With *europium chalcogenides* in this work we refer to the europium monochalcogenides only.

The existence of ferromagnetic semiconductors was severely discussed in the mid fifties by theoretical physicists [47] and stayed an open question until 1960 when Tsubokawa [50] identified $CrBr_3$ as such a material. In 1961 Matthias *et al.* [51] classified EuO as a ferromagnetic semiconductor, which in 1962 was followed by the other europium chalcogenides, where EuS is a ferromagnetic, EuSe a metamagnetic, and EuTe an antiferromagnetic semiconductor [52, 53, 54]. Other classes of magnetic semiconductors include the chalcogenide spinels AB_2X_4[‡], some europium silicates and some ternary europium compounds, such as EuY_2S_4 and $EuGd_2S_4$ [44].

Due to the strong localization of the magnetic moments in magnetic *4f* systems, the electronic and magnetic properties of these materials can be attributed to groups of itinerant and localized electrons, respectively. Some of the most intriguing properties of magnetic *4f* systems arise from the mutual influence between itinerant and localized electrons. The first evidence of such an effect was given by Wachter [1] and Busch *et al.* [2] in 1964 who found a red shift of the absorption edge of the optical *4f*-$5d_{t_{2g}}$ transition [55, 56, 57, 58, 47] in the ferromagnetic semiconductor EuO.

The red shift is caused by a substantial diminution of the gap E_g between the occupied *4f* level and the lower edge of the empty *5d* conduction bands with decreasing temperature below the Curie temperature T_C. Subsequently, this property has been found for all known ferromagnetic semiconductors [3, 44] and must therefore be regarded as a characteristic attribute of these substances.

In the following section we want to introduce a model for magnetic semiconductors, which takes into account both the separate characteristics of the itinerant conduction electrons and the localized moments and the interaction between these two groups of electrons. Here, we will concentrate on the special situation in the ferromagnetic europium chalcogenides EuO and EuS.

2.2 The *s*-*f* model

A Hamiltonian for the class of the magnetic semiconductors has to take into account the two different groups of electrons, itinerant and localized. We take the conduction electrons to be simple *s* electrons

$$\mathcal{H}_s = \sum_{ij\sigma} T_{ij} c^+_{i\sigma} c_{j\sigma}. \tag{2.1}$$

Here, $c^+_{i\sigma}$ and $c_{i\sigma}$ are the creation and annihilation operators of an electron with spin σ at the lattice site $\mathbf{R}_i$ and T_{ij} is the hopping integral between the two lattice sites $\mathbf{R}_i$ and $\mathbf{R}_j$. Since we are interested in the special situation of a semiconductor with an empty conduction band, $n = 0$, in what follows the chemical potential μ as well as any Hubbard type interaction can be disregarded.

[‡]Here A denotes a transition metal or Mg, Zn, Cd, Hg; B is a transition metal or Ga, Al, In; and X stands for S, Se, Te.

The magnetism in the europium chalcogenides is caused by localized magnetic $4f$ moments with a spin of $S = 7/2$. The magnetic properties associated with these localized moments can best be described within the framework of the Heisenberg model

$$\mathcal{H}_f = -\sum_{ij} J_{ij}\, \mathbf{S}_i \cdot \mathbf{S}_j, \tag{2.2}$$

where $\mathbf{S}_i$ denotes the operator of the $4f$ spin localized at the lattice site $\mathbf{R}_i$. The Heisenberg exchange interaction J_{ij} can be restricted within the tight-binding approximation to nearest (Δ) and next nearest neighbors ($\bar{\Delta}$)

$$\mathcal{H}_{f,tb} = -J_1 \sum_{i\Delta} \mathbf{S}_i \cdot \mathbf{S}_{i+\Delta} - J_2 \sum_{i\bar{\Delta}} \mathbf{S}_i \cdot \mathbf{S}_{i+\bar{\Delta}}. \tag{2.3}$$

The mean field evaluation of this expression can be used to derive numerical values for the two exchange constants J_1 and J_2 which, together with the measured critical temperatures are given in Table 2.1.

	Magnetic Order	$T_{C,N}$ (K)	J_1/k_B (K)	J_2/k_B (K)
EuO	FM	69.33	$+0.606$	$+0.119$
EuS	FM	16.57	$+0.228$	-0.102
EuSe	MM[§]	—	$+0.073$	-0.011
EuTe	AFM	9.58	$+0.043$	-0.150

Table 2.1: Magnetic properties of the europium monochalcogenides [47].

The tight-binding approximation of the Heisenberg Hamiltonian up to the next nearest neighbor interactions (2.3) has been found to be an accurate description for the situation in the europium chalcogenides [60]. Furthermore, EuO and EuS are commonly regarded as prototypical Heisenberg ferromagnets [61, 62, 63]. It should be noted that more recent experimental work has been focused on the importance of a biquadratic exchange interaction of the type $-K_{ij}(\mathbf{S}_i \cdot \mathbf{S}_j)^2$ found to be existing in the europium chalcogenides [64, 65]. However, for our purpose of investigating the interplay between electronic and magnetic properties the description of the magnetic properties via the Heisenberg Hamiltonian (2.2) and its tight-binding approximation (2.3) is appropriate.

For an explanation of magnetooptical effects, such as the red shift discussed in Section 2.1, in addition to the Hamiltonian for the kinetic energy of the conduction-band

[§]The magnetic phase diagram of the metamagnet EuSe includes different kinds of complicated antiferromagnetic and ferrimagnetic order and has been discussed e. g. by Griessen *et al.* [59].

electrons (2.1) and the Heisenberg Hamiltonian for the localized *4f* electrons (2.2), we have to introduce an interaction between both groups of electrons. The most accepted way to do this is to consider an intra-atomic exchange interaction J between the spin of the conduction electron $\boldsymbol{\sigma}_i$ and the spin $\mathbf{S}_i$ of the local f moment

$$\mathcal{H}_{sf} = -\frac{J}{\hbar}\sum_i \mathbf{S}_i \cdot \boldsymbol{\sigma}_i . \tag{2.4}$$

For the materials we are interested in the *s-f* exchange interaction is positive $J > 0$, favoring a parallel alignment of the spins $\boldsymbol{\sigma}_i$ and $\mathbf{S}_i$. Using the formalism of second quantization for the electron operators,

$$\frac{1}{\hbar}\sigma_i^{\pm} = c^{+}_{i\uparrow(\downarrow)}c_{i\downarrow(\uparrow)}, \qquad \frac{1}{\hbar}\sigma_i^{z} = \frac{1}{2}\sum_\sigma z_\sigma n_{i\sigma} \quad (z_{\uparrow(\downarrow)} = \pm 1), \tag{2.5}$$

we get for the *s-f* interaction

$$\mathcal{H}_{sf} = -\frac{J}{2}\sum_{i\sigma}(z_\sigma S_i^z n_{i\sigma} + S_i^\sigma c^{+}_{i-\sigma}c_{i\sigma}). \tag{2.6}$$

Together with Eqs. (2.1) and (2.2) we now have the Hamiltonian of the *s-f* model for magnetic semiconductors as

$$\mathcal{H} = \mathcal{H}_s + \mathcal{H}_f + \mathcal{H}_{sf}. \tag{2.7}$$

The original *s-f* model [66, 5, 6, 7, 67, 68] is completely defined by the above Hamiltonian. An additional model extension, however, becomes necessary when the assumption of an empty conduction band does not hold, e. g. when doping the europium chalcogenides with electron donors like the trivalent Gd or La or when describing the metallic rare earths Gd, Tb and Dy. In this case an additional Coulomb term has to be added to the Hamiltonian (2.7) in order to account for the interaction between the charge carriers within the conduction band [44, 48].

In the form (2.7) the model is well suited to describe the situation in an idealized ferromagnetic semiconductor with a single e. g. tight-binding *s* band. For the description of real substances the inclusion of multiple conduction bands in the kinetic Hamiltonian (2.1) and in the *s-f* exchange interaction becomes important. The respective extensions of the *s-f* model will be dealt with in chapter 5.

2.3 Limiting cases and exact results

In this section we want to discuss the *s-f* model in the form (2.7) with respect to special solutions in order to get some insight into the physics of the model. Starting with the weak coupling limit, we will then come to two exactly solvable special cases which prove as a valuable testing ground for more general approximative theories.

The weak coupling limit

The weak coupling limit assumes that the *s-f* Hamiltonian (2.4) represents a small perturbation compared to the kinetic contribution of the conduction electrons (2.1), i. e.

$$J \ll W, \tag{2.8}$$

where W is the free bandwidth of the conduction electrons.

Writing the electron creation and annihilation operators in Bloch representation we get for the *s-f* Hamiltonian

$$\mathcal{H}_{sf} = -\frac{J}{2N}\sum_{i\sigma}\sum_{\mathbf{kq}} \mathrm{e}^{i(\mathbf{k}-\mathbf{q})\mathbf{R}_i}\left(z_\sigma S_i^z c^+_{\mathbf{q}\sigma} c_{\mathbf{k}\sigma} + S_i^\sigma c^+_{\mathbf{q}-\sigma} c_{\mathbf{k}\sigma}\right). \tag{2.9}$$

For the perturbational treatment [44] we divide the original *s-f* Hamiltonian (2.7) into an unperturbed operator $\mathcal{H}_0$ and a perturbation $\mathcal{H}_1 = \mathcal{H} - \mathcal{H}_0$, where

$$\mathcal{H}_0 = \mathcal{H}_s + \mathcal{H}_f - \frac{J}{2N}\sum_{i\sigma}\sum_{\mathbf{k}} z_\sigma S_i^z c^+_{\mathbf{k}\sigma} c_{\mathbf{k}\sigma}, \tag{2.10}$$

$$\mathcal{H}_1 = -\frac{J}{2N}\sum_{i\sigma}\sum_{\mathbf{kq}} \mathrm{e}^{i(\mathbf{k}-\mathbf{q})\mathbf{R}_i}\left((1-\delta_{\mathbf{kq}}) z_\sigma S_i^z c^+_{\mathbf{q}\sigma} c_{\mathbf{k}\sigma} + S_i^\sigma c^+_{\mathbf{q}-\sigma} c_{\mathbf{k}\sigma}\right). \tag{2.11}$$

The unperturbed Hamiltonian (2.10) is completely separable and its eigenstates $|\mathbf{k}\sigma;\alpha\rangle$ can be written as a direct product of the Bloch states $|\varphi_\mathbf{k}\rangle$, the spin states $|\chi_\sigma\rangle$, and $(2S+1)^N$ possible eigenstates of the Heisenberg Hamiltonian $\mathcal{H}_f$,

$$|\mathbf{k}\sigma;\alpha\rangle = |\varphi_\mathbf{k}\rangle|\chi_\sigma\rangle|\alpha\rangle. \tag{2.12}$$

$W_\alpha(T)$ shall be the probability for the f system to be in the state $|\alpha\rangle$ at the temperature T. We can then choose the quantization direction along the z axis,

$$\langle S_i^z\rangle = \sum_\alpha W_\alpha(T)\langle\alpha|S_i^z|\alpha\rangle \equiv \langle S^z\rangle, \quad \langle S_i^x\rangle = \langle S_i^y\rangle = 0, \tag{2.13}$$

and get for the unperturbed energies

$$E_0(\mathbf{k}\sigma;\alpha) \equiv \langle\mathbf{k}\sigma;\alpha|\mathcal{H}_0|\mathbf{k}\sigma;\alpha\rangle = \epsilon(\mathbf{k}) + E_f^{(\alpha)} - \frac{Jz_\sigma}{2N}\sum_i\langle\alpha|S_i^z|\alpha\rangle, \tag{2.14}$$

with the Bloch energies $\epsilon(\mathbf{k})$ and the eigenenergies of the f-spin system $E_f^{(\alpha)}$. Since we are not so much interested in particular configurations of the f-spin systems, we can average the above expressions over all $|\alpha\rangle$

$$E_0(\mathbf{k}\sigma) = \sum_\alpha W_\alpha(T) E_0(\mathbf{k}\sigma;\alpha) = \epsilon(\mathbf{k}) + E_f(T) - \tfrac{1}{2}Jz_\sigma\langle S^z\rangle. \tag{2.15}$$

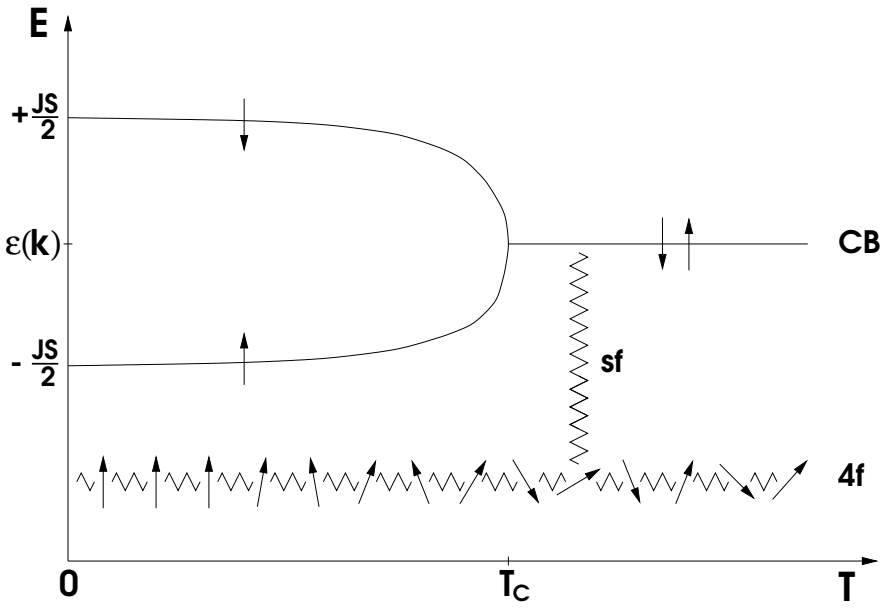

Figure 2.1: Schematics of the mean field picture of the *s*-*f* model.

As a consequence of the special choice of the unperturbed operator $\mathcal{H}_0$, the energy correction in first order perturbation theory becomes zero

$$\Delta E^{(1)}(\mathbf{k}\sigma;\alpha) = \langle \mathbf{k}\sigma;\alpha|\mathcal{H}_1|\mathbf{k}\sigma;\alpha\rangle = 0, \tag{2.16}$$

i. e. for a small *s*-*f* interaction, $J \ll W$, Eq. (2.15) represents a reasonable approximation for the energy of electrons in the conduction band. The energy $E_f(T)$ associated with the *f*-spin system is typically smaller by two orders of magnitude than the other energies in Eq. (2.15) and shall be neglected:

$$E_0(\mathbf{k}\sigma) = \epsilon(\mathbf{k}) - \tfrac{1}{2} J z_\sigma \langle S^z\rangle. \tag{2.17}$$

Due to the neglect of the Heisenberg contribution, the expectation value $\langle S^z\rangle$ in Eq. (2.17) has to be regarded as an externally given parameter, which can be calculated within the Heisenberg model. As a result, for each $\mathbf{k}$ value the free Bloch energy $\epsilon(\mathbf{k})$ splits into a spin-↑ and a spin-↓ level. The splitting is proportional to the magnetization of the *4f*-spin system $\langle S^z\rangle$. With increasing temperature T it will decrease from its maximum value $\Delta E_{\uparrow\downarrow} = JS$ for $T = 0$ to $\Delta E_{\uparrow\downarrow} = 0$ for $T \geq T_C$ (see Fig. 2.1).

According to Eq. (2.17) the lower edge of the spin-↑ band will be lowered with decreasing temperature below the Curie temperature. The weak coupling limit of the *s*-*f* model is therefore able to qualitatively describe the discussed red shift in the europium chalcogenides. The total red shift of the spin-↑ band amounts to $\Delta E_\uparrow = \frac{1}{2} JS$, which with $S = 7/2$ and with the experimentally observed red shifts of 0.27eV and 0.18eV for EuO and EuS [47], respectively, results in an approximation for the *s*-*f* interaction:

$$J_{\mathrm{EuO}} \approx 0.15\mathrm{eV}, \qquad J_{\mathrm{EuS}} \approx 0.1\mathrm{eV}. \tag{2.18}$$

The atomic limit

We want to neglect the dispersion of the conduction band. In order to achieve this we take the lattice constant to be infinite which results in the reduction of the conduction band to a degenerate level T_0. The original Hamiltonian (2.7) becomes:

$$\hat{\mathcal{H}} = T_0 \sum_\sigma n_\sigma - \frac{J}{2} \sum_\sigma (z_\sigma S^z n_\sigma + S^\sigma c^+_{-\sigma} c_\sigma). \tag{2.19}$$

Since $J_{ii} = 0$, the Heisenberg interaction (2.2) is missing in this limiting case.

For the solution of the atomic limit [48, 44, 4] the equations of motions for some suitably chosen Green functions[¶] can be shown to lead to a closed system of equations, which leads to a two-pole expression for the single-electron Green function:

$$G_\sigma = \langle\langle c_\sigma ; c^+_\sigma \rangle\rangle = \hbar \left(\frac{\alpha_{1\sigma}}{E - E_1} + \frac{\alpha_{2\sigma}}{E - E_2} \right), \tag{2.20}$$

where the two spectral weights $\alpha_{1(2)\sigma}$ and the energy positions of the two peaks $E_{1(2)}$ are given by

$$\begin{aligned} E_{1(2)} &= T_0 + \frac{J\hbar}{2}\left(\tfrac{1}{2} \mp (S + \tfrac{1}{2})\right), \\ \alpha_{1(2)\sigma} &= \frac{1}{2S+1}\left(S + \tfrac{1}{2} \pm (\tfrac{1}{2} + \frac{z_\sigma}{\hbar}\langle S^z \rangle)\right). \end{aligned} \tag{2.21}$$

It shall be stressed that Eqs. (2.20) and (2.21) represent an exact result. From Eqs. (2.21) the center of gravity of the spin-σ band can be calculated:

$$E_\sigma = \alpha_{1\sigma} E_1 + \alpha_{2\sigma} E_2 = T_0 - \tfrac{1}{2} J z_\sigma \langle S^z \rangle. \tag{2.22}$$

Hence, for the energy position of the center of gravity in the atomic limit one gets the same result as for the whole spin-σ band in the weak coupling limit in Eq. (2.17). However, the difference between the two cases is that according to Eqs. (2.21) the positions of the levels E_1 and E_2 in the atomic limit are fixed. The movement of the centers of gravity of the spin-σ bands is solely due to the shift of the spectral weights $\alpha_{1(2)\sigma}$. Here, it should be noted that the shift of the center of gravity of the spin-σ band given by Eq. 2.22 is a general result for the *s-f* model [44].

The magnetic polaron

For the *s-f* model (2.7) there exists a special exactly solvable case, which describes the situation of a single electron ($n = 0$) for the case of ferromagnetic saturation of the *4f* moments ($T = 0$) [48, 44, 4]. Due to the perfect alignment of the *f* spins,

[¶] For the concepts of many-body theory see, e. g. [48, 69].

the Heisenberg Hamiltonian in Eq. (2.7) yields a constant energy shift which can be neglected

$$\hat{\mathcal{H}} = \sum_{ij\sigma} T_{ij} c^+_{i\sigma} c_{j\sigma} - \frac{J}{2} \sum_{i\sigma} \left(z_\sigma S^z_i n_{i\sigma} + S^\sigma_i c^+_{i-\sigma} c_{i\sigma} \right). \tag{2.23}$$

The electronic properties of the system are completely determined by the single-electron Green function (cf. Eq. (3.9))

$$G_{ij\sigma}(E) \equiv \langle\langle c_{i\sigma}; c^+_{j\sigma} \rangle\rangle_E, \tag{2.24}$$

which can be calculated using its equation of motion,

$$\sum_k (E\delta_{ik} - T_{ik}) G_{jj\sigma}(E) = \hbar\delta_{ij} - \frac{J}{2}(z_\sigma \Gamma_{iij\sigma}(E) + F_{iij\sigma}(E)). \tag{2.25}$$

The two higher Green functions on the right hand side of the above equation,

$$\Gamma_{ikj\sigma}(E) = \langle\langle S^z_i c_{k\sigma}; c^+_{j\sigma} \rangle\rangle_E, \tag{2.26}$$

$$F_{ikj\sigma}(E) = \langle\langle S^{-\sigma}_i c_{k\sigma}; c^+_{j\sigma} \rangle\rangle_E, \tag{2.27}$$

originate form the two terms of the *s-f* interaction in Eq. (2.23). For the special case we are interested in, the first of these higher Green functions can be reduced to the single-electron Green function,

$$\Gamma_{ikj\sigma}(E) \xrightarrow{n\to 0, T\to 0} \hbar S G_{kj\sigma}(E), \tag{2.28}$$

leaving us with the task of calculating the so called *spin-flip* function $F_{ikj\sigma}(E)$.

Spin-↑ electron: The spin-↑ electron has no possibility to exchange its spin with the perfectly aligned *4f* system leading to

$$F_{ikj\uparrow}(E) \xrightarrow{n\to 0, T\to 0} 0, \tag{2.29}$$

resulting in the immediate solution of the equation of motion (2.25):

$$G_{\mathbf{k}\uparrow}(E) = \frac{\hbar}{E - \epsilon(\mathbf{k}) + \frac{1}{2} J\hbar S}. \tag{2.30}$$

Hence, the spectral density and accordingly the density of states of the spin-↑ electron are merely constantly shifted to lower energies compared to the free Bloch spectral density and the free density of states $\rho_0(E)$, respectively

$$S_{\mathbf{k}\uparrow}(E) = \hbar\delta(E - (\epsilon(\mathbf{k}) - \tfrac{1}{2} J\hbar S)), \tag{2.31}$$

$$\rho_\uparrow(E) = \frac{1}{N} \sum_{\mathbf{K}} S_{\mathbf{k}\uparrow}(E) = \rho_0(E + \tfrac{1}{2} J\hbar S). \tag{2.32}$$

Spin-↓ electron: For the spin-↓ electron we have to determine the spin-flip function $F_{ikj\sigma}(E)$ from its equation of motion. After some manipulations one gets [48]

$$\frac{1}{\sqrt{N}}\sum_{\mathbf{q}} F_{\mathbf{kq}\downarrow}(E) = -\frac{J\hbar^2 SB(E)}{1-\frac{1}{2}J\hbar B(E)}G_{\mathbf{k}\downarrow}(E), \tag{2.33}$$

$$B(E) = \frac{1}{N}\sum_{\mathbf{q}}\left\{E+\tfrac{1}{2}J\hbar S-\epsilon(\mathbf{q})\right\}^{-1}. \tag{2.34}$$

The combination with the Fourier transformed equation of motion (2.25) yields the spin-↓ single electron Green function

$$G_{\mathbf{k}\downarrow}(E) = \frac{\hbar}{E-\epsilon(\mathbf{k})-\Sigma_{\downarrow}(E)}, \tag{2.35}$$

with the spin-↓ self-energy

$$\Sigma_{\downarrow}(E) = \tfrac{1}{2}J\hbar S\left(1+\frac{J\hbar B(E)}{1-\frac{1}{2}J\hbar B(E)}\right). \tag{2.36}$$

For the further discussion we split the complex propagator $B(E)$ into its real and imaginary part. The imaginary part can be reduced, except for a factor, to the spin-↑ density of states, and the real part has to be calculated as a principal value integral,

$$I_B(E) = \mathrm{Im}(B(E)) = -\pi\rho_0(E+\tfrac{1}{2}J\hbar S) = \pi\rho_{\uparrow}(E), \tag{2.37a}$$

$$R_B(E) = \mathrm{Re}(B(E)) = \mathcal{P}\int dx\,\frac{\rho_0(x)}{E+\frac{1}{2}J\hbar S-x}. \tag{2.37b}$$

Combining Eqs. (2.37) and Eq. (2.36), the real and imaginary part of the self-energy are

$$\mathrm{Re}(\Sigma_{\downarrow}(E)) = \tfrac{1}{2}J\hbar S\left(1+J\hbar\frac{R_B(E)(1-\frac{1}{2}J\hbar R_B(E))-\frac{1}{2}J\hbar I_B^2(E)}{(1-\frac{1}{2}J\hbar R_B(E))^2+\frac{1}{4}J^2\hbar^2 I_B^2(E)}\right), \tag{2.38a}$$

$$\mathrm{Im}(\Sigma_{\downarrow}(E)) = \tfrac{1}{2}J\hbar S\frac{I_B(E)}{(1-\frac{1}{2}J\hbar R_B(E))^2+\frac{1}{4}J^2\hbar^2 I_B^2(E)}. \tag{2.38b}$$

The imaginary part of the self-energy, $\mathrm{Im}(\Sigma_{\downarrow}(E))$, determines the lifetime of the quasiparticles which can be attributed to the different peaks in the spectral density $S_{\mathbf{k}\downarrow}(E)$. A finite lifetime ($\mathrm{Im}(\Sigma_{\downarrow}(E)) \neq 0$) corresponds to a non-vanishing spin-↑ density of states in Eq. (2.37a). The respective part of the spectrum represents a scattering region where the spin-↓ electron flips its spin to become a spin-↑ electron. For the sake of spin conservation this process has to be accompanied by a magnon emission reducing the collective spin of the localized *4f* moments.

For all poles of the Green function (2.35) which lie outside the region where $\rho_{\uparrow}(E) \neq 0$ the corresponding quasiparticle has an infinite lifetime. This quasiparticle is called the *magnetic polaron* and can be interpreted as a bound state between

the spin-↓ electron and the ferromagnetically saturated local-moment system, which is realized by a repeated emission and reabsorption of magnons by the spin-↓ electron. As will be shown in Sec. 4.2 a sufficiently strong *s-f* exchange interaction can lead to a complete separation of the scattering part and the polaron part of the spectrum.

2.4 Models of magnetic impurities

We want to put the *s-f* model into a broader context with other models describing similar physical situations. The respective group of models is that of magnetic impurities [49, 70]. We will start by briefly recalling the original *s-d* model first introduced in the 50s. We will then discuss the Anderson and the Kondo model, which both have been introduced to describe the situation in dilute magnetic alloys. Here, the Kondo model is effectively a non-periodic *s-d* model. It can be related to the Anderson model via the Schrieffer-Wolff transformation which will be described at the end of this section.

The *s-d* exchange model

The original *s-f* model was introduced as the so-called *s-d* model for the description of collective magnetism in the transition metals, e. g. Ni, Fe, Co, Cr, Mn etc., and is commonly attributed[‖] to Zener [5], Kasuya [6] and Yosida [7]. The Hamiltonian of the *s-d* (*s-f*) model is written as follows,

$$\mathcal{H}_{sd} = \sum_{\mathbf{k}\sigma} \epsilon(\mathbf{k}) c^+_{\mathbf{k}\sigma} c_{\mathbf{k}\sigma} - N^{-1} \sum_{\mathbf{k}\mathbf{k}'n} J(\mathbf{k}-\mathbf{k}') \mathrm{e}^{i(\mathbf{k}-\mathbf{k}')\mathbf{R}_n} \times \left\{ (c^+_{\mathbf{k}'\uparrow} c_{\mathbf{k}\uparrow} - c^+_{\mathbf{k}'\downarrow} c_{\mathbf{k}\downarrow}) S^z_n + c^+_{\mathbf{k}'\uparrow} c_{\mathbf{k}\downarrow} S^-_n + c^+_{\mathbf{k}'\downarrow} c_{\mathbf{k}\uparrow} S^+_n \right\}, \quad (2.39)$$

where the first term is the kinetic energy of the electrons. The second term describes the interaction between the conduction electrons and the *d* core spins of e. g. Mn ions where the exchange integral

$$J(\mathbf{k}-\mathbf{k}') = N \iint d\mathbf{r}_1 d\mathbf{r}_2 \mathrm{e}^{-i(\mathbf{k}-\mathbf{k}')\mathbf{R}_n} \phi^+_{\mathbf{k}'}(\mathbf{r}_1) \phi^+_d(\mathbf{r}_2 - \mathbf{R}_n) \frac{e^2}{r_{12}} \phi_{\mathbf{k}}(\mathbf{r}_2) \phi_d(\mathbf{r}_1 - \mathbf{R}_n) \quad (2.40)$$

is independent on the lattice vector $\mathbf{R}_n$. $\phi_{\mathbf{k}}(\mathbf{r})$ and $\phi_d(\mathbf{r})$ are the wave functions of the conduction and the *d* electrons, respectively. With the assumption that $J(\mathbf{k}-\mathbf{k}')$ depends only on $|\mathbf{k}-\mathbf{k}'|$ and with the introduction of the conduction-electron spin operators $\boldsymbol{\sigma}_{\mathbf{k}}$ and the spin operator of the *d* electrons $\mathbf{S}_{\mathbf{k}}$ as in Eq. (2.5) the Hamiltonian

[‖] The *s-d* interaction was first discussed on a phenomenological basis by Zener, later derived from the Coulomb interaction by Kasuya, and further discussed by Yosida.

can be written in the form [6]

$$\mathcal{H}_{sd} = \sum_{\mathbf{k}\sigma} \epsilon(\mathbf{k}) c^{+}_{\mathbf{k}\sigma} c_{\mathbf{k}\sigma} - \sum_{\mathbf{q}} J(q) \mathbf{S}_{\mathbf{q}} \cdot \boldsymbol{\sigma}_{-\mathbf{q}}. \tag{2.41}$$

The relation of the above Hamiltonian to the *s*-*f* Hamiltonian (2.7) without the Heisenberg contribution is immediate when assuming a wave-vector independent interaction in Eq. (2.41), $J(q) \equiv J$, according to a solely intra-atomic *s*-*d* coupling.

The Anderson model

Magnetic impurities can originate from the *3d* transition metal elements or from the rare earth series in the periodic table. One manifestation of the effect of magnetic impurities has been known since the 30s. This is the observation of a resistance minimum for some metals as a function of temperature [71]. The effect was first found by de Haas *et al.* in 1934 [72] for very pure specimens of gold. It was only recognized later that this minimum was due to *3d* transition metal impurities such as Fe [70].

In 1961 Anderson proposed a model for describing localized magnetic states in metals [73]. In its original form the *Anderson model*,

$$\mathcal{H}_{AM} = \mathcal{H}_s + \mathcal{H}_d + \mathcal{H}_{corr} + \mathcal{H}_{sd}, \tag{2.42}$$

describes the situation of a single *d*-type impurity level in a free-electron sea. It is therefore often referred to as the single-impurity Anderson model (SIAM) as opposed to the periodic Anderson model which assumes a periodic arrangement of impurities.

The first term of the Hamiltonian (2.42) is the kinetic energy of the free electrons, and the second term describes the unperturbed energy of the *d* states on the impurity atom,

$$\mathcal{H}_s = \sum_{\mathbf{k}\sigma} \epsilon(\mathbf{k}) c^{+}_{\mathbf{k}\sigma} c_{\mathbf{k}\sigma}, \qquad \mathcal{H}_d = \epsilon_d (n_{d\uparrow} + n_{d\downarrow}). \tag{2.43}$$

The third term, $\mathcal{H}_{corr}$, is the repulsive Hubbard interaction among the *d* electrons,

$$\mathcal{H}_{corr} = U n_{d\uparrow} n_{d\downarrow}, \tag{2.44}$$

and the last term,

$$\mathcal{H}_{sd} = \sum_{\mathbf{k}\sigma} V_{\mathbf{k}d} (c^{+}_{\mathbf{k}\sigma} c_{d\sigma} + c^{+}_{d\sigma} c_{\mathbf{k}\sigma}), \tag{2.45}$$

describes the *s*-*d* interaction as an hybridization between the localized *d* level and the free-electron bands. The *s*-*d* energy is therefore purely one-electron like and entirely different [73] from the *s*-*d* exchange interaction in the *s*-*d* model (2.41).

The Kondo model

Based on the *s-d* exchange model by Zener, Kasuya and Yosida (Eq. (2.39)), with a wave-vector independent *s-d* exchange integral Kondo in 1964 [74] calculated the scattering probabilities of the conduction electrons within the second order perturbation theory, taking as the unperturbed Hamiltonian

$$\mathcal{H}_0 = \sum_{\mathbf{k}\sigma} \epsilon(\mathbf{k}) c^+_{\mathbf{k}\sigma} c_{\mathbf{k}\sigma}, \tag{2.46}$$

and as perturbation

$$\mathcal{H}_1 = \frac{J}{N} \sum_{\mathbf{k}\mathbf{k}'n} \mathrm{e}^{i(\mathbf{k}-\mathbf{k}')\mathbf{R}_n} \left\{ (c^+_{\mathbf{k}'\uparrow} c_{\mathbf{k}\uparrow} - c^+_{\mathbf{k}'\downarrow} c_{\mathbf{k}\downarrow}) S^z_n + c^+_{\mathbf{k}'\uparrow} c_{\mathbf{k}\downarrow} S^-_n + c^+_{\mathbf{k}'\downarrow} c_{\mathbf{k}\uparrow} S^+_n \right\}. \tag{2.47}$$

From the calculated scattering probabilities of the conduction electrons it is easily possible to calculate a contribution to the resistivity which is due to the perturbation $\mathcal{H}_1$. When concentrating on those scattering processes which involve a single or double spin flip of the conduction electron, the respective expression for the resistivity as a function of temperature [74] reads,

$$\rho_{\mathrm{spin}}(T) = c\rho_{\mathrm{M}}(1 + (3nJ/E_{\mathrm{F}}) \ln T), \tag{2.48}$$

where c is the concentration of impurity atoms, n is the number of conduction electrons per atom, and E_{F} is the Fermi energy. Here, ρ_{M} denotes a constant, which has to be fit with the experiment. The problem with the expression (2.48) is the singularity at $T = 0$ which indicates that the perturbational treatment cannot be valid at low temperatures. The search for a more comprehensive theory known as the *Kondo problem* attracted intense theoretical interest in the late 60s and early 70s [70] until the earlier work by Anderson (1970) [75] and especially that of Wilson in 1974, 1975 [76, 77] based on a non-perturbative *numerical renormalization group* analysis marked the solution of the problem.

The theory by Kondo [74, 78] was the first to explain the resistance minimum in dilute magnetic alloys. By combining the spin-flip resistivity (2.48) with the lattice resistivity, $\rho_{\mathrm{L}}(T) \sim T^5$, and with the resistivity $c\rho_{\mathrm{A}}$ arising from the various effects due to the scattering potential it is possible to explain the resistance minimum under the condition that the *s-d* exchange interaction is assumed to be negative**, $J < 0$.

In contrast to the *s-d* (*s-f*) type models, where the common nomenclature implies a positive or ferromagnetic *s-d* exchange interaction J, the *Kondo model*†† is characterized by a negative J. This explains the rather recent notation of the *Ferromagnetic Kondo Lattice Model* describing the *s-d* model with $J > 0$.

**In the work by Kondo there is reference to Coles [79] who observed an anomalous rapidly decreasing resistivity for alloys of Rh with Fe towards low temperatures instead of the resistivity minimum. This effect can be accounted for by the theory if assuming that the *s-d* exchange is positive [74].

††The effect of the resistance minimum in dilute magnetic alloys is referred to as the *Kondo effect*.

Schrieffer-Wolff transformation

In 1966 Schrieffer and Wolff [80] introduced a canonical transformation between the Kondo model and the Anderson model (2.42) for the limiting case of small *s*-*d* mixing $V_{\mathbf{k}d}$. The Anderson Hamiltonian (2.42) for a single localized *d* electron reads

$$\mathcal{H} = \mathcal{H}_0 + \mathcal{H}_1, \tag{2.49}$$

where

$$\mathcal{H}_0 = \sum_{\mathbf{k}\sigma} \epsilon(\mathbf{k}) c^+_{\mathbf{k}\sigma} c_{\mathbf{k}\sigma} + \epsilon_d (n_{d\uparrow} + n_{d\downarrow}) + U n_{d\uparrow} n_{d\downarrow}, \tag{2.50}$$

$$\mathcal{H}_1 = \sum_{\mathbf{k}\sigma} (V_{\mathbf{k}d} c^+_{\mathbf{k}\sigma} c_{d\sigma} + V^+_{\mathbf{k}d} c^+_{d\sigma} c_{\mathbf{k}\sigma}). \tag{2.51}$$

The model is characterized by the two dimensionless ratios

$$\begin{aligned} r_\pm &= \Gamma_\pm / |\epsilon_\pm|, \\ \Gamma_\pm &= \pi N(\epsilon_\pm) |V_{\mathbf{k}d}|^2_{\text{aver}}, \end{aligned} \qquad (\epsilon_+ = \epsilon_d + U,\ \epsilon_- = \epsilon_d). \tag{2.52}$$

Here $N(\epsilon_\alpha)$ denotes the density of the conduction electron states at energy ϵ_α. If $\epsilon_+ > 0$ and $\epsilon_- < 0$ then for $V_{\mathbf{k}d} \to 0$ the ground state is given by the Fermi sea and a single electron occupying the *d* orbital, which accounts for a localized moment. The interesting case occurs for small but finite mixing between the localized *d* orbitals and the conduction electron states, i. e. $r_\alpha \ll 1$. We are looking for a canonical transformation,

$$\bar{\mathcal{H}} = \mathrm{e}^S \mathcal{H} \mathrm{e}^{-S} = \mathcal{H} + [S, \mathcal{H}] + \tfrac{1}{2}[S, [S, \mathcal{H}]] + \tfrac{1}{6}[S, [S, [S, \mathcal{H}]]] + \ldots, \tag{2.53}$$

which has no terms which are first order in V. By choosing S to be first order in V, one has

$$[\mathcal{H}_0, S] = \mathcal{H}_1, \tag{2.54}$$

$$\bar{\mathcal{H}} = \mathcal{H}_0 + \tfrac{1}{2}[S, \mathcal{H}_1] + \tfrac{1}{3}[S, [S, \mathcal{H}_1]] + \tfrac{1}{8}[S, [S, [S, \mathcal{H}_1]]] + \ldots \tag{2.55}$$

fulfilling this condition. From Eq. (2.54) the generator S is given by:

$$S = \sum_{\mathbf{k}\sigma\alpha} \frac{V_{\mathbf{k}d}}{\epsilon(\mathbf{k}) - \epsilon_\alpha} n^\alpha_{d-\sigma} c^+_{\mathbf{k}\sigma} c_{d\sigma} + \text{h. c.}, \qquad \left(n^\pm_{d-\sigma} = \tfrac{1}{2} \pm (\tfrac{1}{2} - n_{d-\sigma})\right). \tag{2.56}$$

In the limit of small *s*-*d* interaction $V_{\mathbf{k}d}$, according to $r_\alpha \ll 1$, the transformed Hamiltonian (2.55) is well approximated by its first two terms, $\bar{\mathcal{H}} = \mathcal{H}_0 + \mathcal{H}_2$, with

$$\mathcal{H}_2 = \tfrac{1}{2}[S, \mathcal{H}_1] = \mathcal{H}_{\text{ex}} + \mathcal{H}_{\text{dir}} + \mathcal{H}'_0 + \mathcal{H}_{\text{ch}}. \tag{2.57}$$

The four terms on the right hand side of the above expression are:

(a) an *s*-*d* exchange interaction,

$$\mathcal{H}_{\text{ex}} = -\sum_{\mathbf{k}\mathbf{k}'\sigma} \tfrac{1}{2} J_{\mathbf{k}\mathbf{k}'} \big(c^+_{\mathbf{k}\sigma} c_{\mathbf{k}'-\sigma} c^+_{d-\sigma} c_{d\sigma} + \tfrac{1}{2} c^+_{\mathbf{k}\sigma} c_{\mathbf{k}'\sigma} (n_{d\sigma} - n_{d-\sigma}) \big), \tag{2.58a}$$

where

$$J_{\mathbf{k}\mathbf{k}'} = V_{\mathbf{k}d} V_{\mathbf{k}'d} \sum_{\mathbf{q}=\mathbf{k},\mathbf{k}'} \sum_{\alpha} \frac{z_\alpha}{\epsilon(\mathbf{q}) - \epsilon_\alpha} \qquad (z_\pm = \pm 1); \tag{2.58b}$$

(b) a direct, i. e. spin-independent, *s*-*d* interaction,

$$\mathcal{H}_{\text{dir}} = \sum_{\mathbf{k}\mathbf{k}'\sigma} (W_{\mathbf{k}\mathbf{k}'} + \tfrac{1}{4} J_{\mathbf{k}\mathbf{k}'} n_d) c^+_{\mathbf{k}\sigma} c_{\mathbf{k}'\sigma} \tag{2.59a}$$

where $n_d = n_{d\uparrow} + n_{d\downarrow}$ and

$$W_{\mathbf{k}\mathbf{k}'} = \tfrac{1}{2} V_{\mathbf{k}d} V_{\mathbf{k}'d} \sum_{\mathbf{q}=\mathbf{k},\mathbf{k}'} \frac{1}{\epsilon(\mathbf{q}) - \epsilon_-}; \tag{2.59b}$$

(c) a term which can be absorbed into the original $\mathcal{H}_0$,

$$\mathcal{H}'_0 = -\sum_{\mathbf{k}\sigma} (W_{\mathbf{k}\mathbf{k}} + \tfrac{1}{2} J_{\mathbf{k}\mathbf{k}} n_{d-\sigma}) n_{d\sigma}; \tag{2.60}$$

(d) and a term which changes the occupancy of the *d* orbital by two electrons,

$$\mathcal{H}_{\text{ch}} = \tfrac{1}{4} \sum_{\mathbf{k}\mathbf{k}'\sigma} J_{\mathbf{k}\mathbf{k}'} c^+_{\mathbf{k}-\sigma} c^+_{\mathbf{k}'\sigma} c_{d\sigma} c_{d-\sigma} + \text{h. c.} \tag{2.61}$$

All terms in $\mathcal{H}_2$ conserve the number of *d* electrons, except for $\mathcal{H}_{\text{ch}}$, which changes the number by two. Accordingly, $\mathcal{H}_{\text{ch}}$ does not connect the part of the Hilbert space having one *d* electron, the case of interest, with the remainder of the Hilbert space, i. e. zero or two *d* electron states, and can be neglected. Furthermore, in the one-*d*-electron subspace, $n_d = 1$, $\mathcal{H}_{\text{dir}}$ reduces to a one-body potential which can be eliminated by transforming the $\mathbf{k}$ states accordingly. For the case of small *s*-*d* hybridization, $r_\alpha \ll 1$, the resultant shift in the conduction electron wave functions is negligible.

As a result, $\mathcal{H}_2$ can be reduced to the *s*-*d* exchange interaction (2.58). For $\mathbf{k}, \mathbf{k}' \simeq \mathbf{k}_{\text{F}}$, the *s*-*f* exchange interaction is given by,

$$J_{\mathbf{k}_{\text{F}}\mathbf{k}_{\text{F}}} \equiv J_0 = 2|V_{\mathbf{k}_{\text{F}}d}|^2 \frac{U}{\epsilon_d(\epsilon_d + U)} < 0, \tag{2.62}$$

according to an antiferromagnetic coupling. Concluding, the Anderson model can be replaced by the *s*-*d* exchange model with an effective exchange interaction given by (2.58b) as long as $r_\alpha \ll 1$, i.e. $N(0)|J_0| \ll 1$ [80].

3 The *s-f* model for film geometries

In this work we are interested in the electronic and magnetic properties of systems with film geometry. A *film* consists of n equivalent layers parallel to the surface of the film. Each lattice site is indicated by a greek letter $\alpha, \beta, \gamma, \ldots$, denoting the layer index and a latin letter $i, j, k, \ldots$, numbering the sites within a given layer. Each layer possesses two-dimensional translational geometry. Accordingly, the thermodynamic average of any site dependent operator $A_{i\alpha}$ depends only on the layer index α,

$$\langle A_{i\alpha} \rangle \equiv \langle A_\alpha \rangle. \tag{3.1}$$

For the following expressions and equations the relation to the three-dimensional case is immanent via the index transitions $(i, \alpha) \rightarrow i'$, $(j, \beta) \rightarrow j'$, etc.

3.1 The model Hamiltonian

The complete *s-f* model Hamiltonian consists of three parts,

$$\mathcal{H} = \mathcal{H}_s + \mathcal{H}_f + \mathcal{H}_{sf}, \tag{3.2}$$

the kinetic part $\mathcal{H}_s$ describing the hopping of electrons in the crystal lattice, the Heisenberg part $\mathcal{H}_f$ for the exchange interaction between the localized moments, and a part $\mathcal{H}_{sf}$ containing an intra-atomic exchange interaction between the localized moments and the itinerant electrons (cf. Fig. 2.1). The first part,

$$\mathcal{H}_s = \sum_{ij\alpha\beta} T_{ij}^{\alpha\beta} c_{i\alpha\sigma}^{+} c_{j\beta\sigma}, \tag{3.3}$$

describes the itinerant conduction electrons as *s* electrons. $c_{i\alpha\sigma}^{+}$ and $c_{j\beta\sigma}$ are, respectively, the creation and annihilation operators of an electron with the spin σ at the lattice site $\mathbf{R}_{i\alpha}$. $T_{ij}^{\alpha\beta}$ is the hopping integral between the lattice sites $\mathbf{R}_{i\alpha}$ and $\mathbf{R}_{j\beta}$.

Each lattice site $\mathbf{R}_{i\alpha}$ is occupied by a localized magnetic moment, represented by a spin operator $\mathbf{S}_{i\alpha}$. These localized moments are exchange coupled expressed by the Heisenberg Hamiltonian,

$$\mathcal{H}_f = -\sum_{ij\alpha\beta} J_{ij}^{\alpha\beta} \mathbf{S}_{i\alpha} \mathbf{S}_{j\beta}, \tag{3.4}$$

where $J_{ij}^{\alpha\beta}$ are the exchange integrals between the localized spins at the respective lattice sites.

The distinguishing feature of the *s-f* model is an intra-atomic exchange between the conduction electrons and the localized *f* spins,

$$\mathcal{H}_{sf} = -\frac{J}{\hbar}\sum_{i\alpha}\mathbf{S}_{i\alpha}\sigma_{i\alpha} \tag{3.5}$$

Here, J is the *s-f* exchange interaction and $\sigma_{i\alpha}$ is the Pauli spin operator of the conduction-band electrons. For the materials we are interested in the *s-f* coupling is positive ($J > 0$). In the case where $J < 0$ the model Hamiltonian (3.2) is that of the so-called *Kondo lattice*. Using the second-quantized form of $\sigma_{i\alpha}$ and the abbreviations

$$S_{j\beta}^{\sigma} = S_{j\beta}^{x} + \mathrm{i}z_{\sigma}S_{j\beta}^{y}; \quad z_{\uparrow(\downarrow)} = \pm 1, \tag{3.6}$$

the *s-f* Hamiltonian can be written as

$$\mathcal{H}_{sf} = -\frac{J}{2}\sum_{i\alpha\sigma}\left(z_{\sigma}S_{i\alpha}^{z}n_{i\alpha\sigma} + S_{i\alpha}^{\sigma}c_{i\alpha-\sigma}^{+}c_{i\alpha\sigma}\right). \tag{3.7}$$

The most decisive part of the *s-f* Hamiltonian (3.7) is the second term, which describes spin-exchange processes between the conduction electrons (3.3) and the localized moments (3.4).

3.2 Theoretical approach

In general, the alignment of the localized moments via the Heisenberg interaction (3.4) will be influenced by the *s-f* interaction, which can mediate an indirect interaction (Ruderman-Kittel-Kasuya-Yosida (RKKY)) via the partially occupied conduction band [81]. However, for the description of ferromagnetic semiconductors we are interested in the case of zero band occupation ($n = 0$) according to a single test electron in an otherwise empty conduction band. In this case, the alignment of the localized moments cannot be influenced by the conduction band.

Furthermore, one knows from experiment that typical Heisenberg exchange integrals are smaller by some orders of magnitudes than their *s-f* counterparts. (EuO: $J \approx 0.2\,\mathrm{eV}$, $J_{ij}^{\alpha\beta} \approx 10^{-4}\,\mathrm{eV}$ (cf. Sects. 2.2 and 2.3)). Accordingly, the Hamiltonian (3.2) can be split into an electronic part, $\mathcal{H}_s + \mathcal{H}_{sf}$, and a magnetic part, $\mathcal{H}_f$, which can be solved separately [82, 83].

3.2.1 The electronic subsystem

Starting from the Hamiltonian of the electronic subsystem

$$\mathcal{H}^{*} = \mathcal{H}_s + \mathcal{H}_{sf}, \tag{3.8}$$

all physical relevant information of the system can be derived from the retarded single-electron Green function,

$$G_{ij\sigma}^{\alpha\beta}(E) = \left\langle\!\!\left\langle c_{i\alpha\sigma}; c_{j\beta\sigma}^{+} \right\rangle\!\!\right\rangle_E = -\mathrm{i}\int_0^\infty dt\ \mathrm{e}^{-\frac{\mathrm{i}}{\hbar}Et} \left\langle \left[c_{i\alpha\sigma}(t), c_{j\beta\sigma}^{+}(0) \right]_+ \right\rangle. \tag{3.9}$$

Here and in what follows $[.,.]_+$ ($[.,.]_-$) is the anticommutator (commutator). Conforming with the two-dimensional translational symmetry, we perform a Fourier transformation within the layers of the film,

$$G_{\mathbf{k}\sigma}^{\alpha\beta}(E) = \frac{1}{N}\sum_{ij} \mathrm{e}^{\mathrm{i}\mathbf{k}(\mathbf{R}_i - \mathbf{R}_j)} G_{ij\sigma}^{\alpha\beta}(E), \tag{3.10}$$

where N is the number of sites per layer, $\mathbf{k}$ is an in-plane wavevector from the first 2D-Brillouin zone of the layers and $\mathbf{R}_i$ represents the in-plane part of the position vector, $\mathbf{R}_{i\alpha} = \mathbf{R}_i + \mathbf{r}_\alpha$. From Eq. (3.10) we get the local spectral density by

$$S_{\mathbf{k}\sigma}^{\alpha\beta}(E) = -\frac{1}{\pi}\mathrm{Im}G_{\mathbf{k}\sigma}^{\alpha\beta}(E + \mathrm{i}0^+), \tag{3.11}$$

which is directly related to observable quantities within angle- and spin-resolved direct and inverse photoemission experiments. Finally, the wave-vector summation of $S_{\mathbf{k}\sigma}^{\alpha\beta}(E)$ yields the layer-dependent (local) quasiparticle density of states

$$\rho_\sigma^\alpha(E) = \frac{1}{\hbar N}\sum_{\mathbf{k}} S_{\mathbf{k}\sigma}^{\alpha\alpha}(E). \tag{3.12}$$

For the solution of the many-body problem posed by Eq. (3.8) we write down the equation of motion of the single-electron Green function (3.9)

$$E\, G_{ij\sigma}^{\alpha\beta} = \hbar\delta_{ij}^{\alpha\beta} + \sum_{m\mu} T_{im}^{\alpha\mu} G_{mj\sigma}^{\mu\beta} + \langle\!\langle [c_{i\alpha\sigma}, \mathcal{H}_{sf}]_-; c_{j\beta\sigma}^{+} \rangle\!\rangle_E, \tag{3.13}$$

where $\delta_{ij}^{\alpha\beta} \equiv \delta_{\alpha\beta}\delta_{ij}$. The formal solution of Eq. (3.13) can be found by introducing the self-energy $M_{ij\sigma}^{\alpha\beta}(E)$,

$$\left\langle\!\!\left\langle \left[c_{i\alpha\sigma}, \mathcal{H}_{sf}\right]_-; c_{j\beta\sigma}^{+} \right\rangle\!\!\right\rangle_E = \sum_{m\mu} M_{im\sigma}^{\alpha\mu}(E) G_{mj\sigma}^{\mu\beta}(E), \tag{3.14}$$

which contains all information about the correlation between the conduction band and the system of localized moments. After combining Eqs. (3.13) and (3.14) and performing a two-dimensional Fourier transform we see that the formal solution of Eq. (3.13) is given by

$$\mathbf{G}_{\mathbf{k}\sigma}(E) = \hbar\left(E\,\mathbf{I} - \mathbf{T}_{\mathbf{k}} - \mathbf{M}_{\mathbf{k}\sigma}(E)\right)^{-1}, \tag{3.15}$$

where $\mathbf{I}$ represents the $(n \times n)$ identity matrix and where the elements of the matrices $\mathbf{G}_{\mathbf{k}\sigma}(E)$, $\mathbf{T}_{\mathbf{k}}$, and $\mathbf{M}_{\mathbf{k}\sigma}(E)$ are the layer-dependent functions $G^{\alpha\beta}_{\mathbf{k}\sigma}(E)$, $T^{\alpha\beta}_{\mathbf{k}}$, and $M^{\alpha\beta}_{\mathbf{k}\sigma}(E)$, respectively.

To explicitly get the self-energy in Eq. (3.14) we evaluate the Green function

$$\left\langle\!\left\langle \left[c_{i\alpha\sigma}, \mathcal{H}_{sf}\right]_- ; c^+_{j\beta\sigma} \right\rangle\!\right\rangle_E = -\frac{J}{2}\left(z_\sigma \Gamma^{\alpha\alpha\beta}_{iij\sigma} + F^{\alpha\alpha\beta}_{iij\sigma}\right). \tag{3.16}$$

Here the two higher Green functions,

$$\Gamma^{\alpha\gamma\beta}_{ikj\sigma}(E) = \left\langle\!\left\langle S^z_{i\alpha} c_{k\gamma\sigma}; c^+_{j\beta\sigma} \right\rangle\!\right\rangle_E, \tag{3.17}$$

$$F^{\alpha\gamma\beta}_{ikj\sigma}(E) = \left\langle\!\left\langle S^{-\sigma}_{i\alpha} c_{k\gamma-\sigma}; c^+_{j\beta\sigma} \right\rangle\!\right\rangle_E, \tag{3.18}$$

originate form the two terms of the *s-f* Hamiltonian (3.7) and will be referred to as the *Ising* and the *spin-flip* function, respectively. Considering the equations of motion for these two Green functions we encounter the two higher Green functions $\langle\!\langle [S^z_{i\alpha} c_{k\gamma\sigma}, \mathcal{H}_{sf}]_-; c^+_{j\beta\sigma} \rangle\!\rangle_E$ and $\langle\!\langle [S^{-\sigma}_{i\alpha} c_{k\gamma-\sigma}, \mathcal{H}_{sf}]_-; c^+_{j\beta\sigma} \rangle\!\rangle_E$.

Since we consider an empty conduction band, the thermodynamic average in the Green functions has to be computed with the electron vacuum state $|n=0\rangle$. From the definition of the *s-f* Hamiltonian (3.7) we then see that $\langle n=0|\,\mathcal{H}_{sf} = 0$ and, accordingly,

$$\left\langle\!\left\langle \left[S^z_{i\alpha}, \mathcal{H}_{sf}\right]_- c_{k\gamma\sigma}; c^+_{j\beta\sigma} \right\rangle\!\right\rangle_E \xrightarrow{n\to 0} 0,$$

$$\left\langle\!\left\langle \left[S^{-\sigma}_{i\alpha}, \mathcal{H}_{sf}\right]_- c_{k\gamma-\sigma}; c^+_{j\beta\sigma} \right\rangle\!\right\rangle_E \xrightarrow{n\to 0} 0.$$

Hence, for the equations of motion of the Ising and the spin-flip function we get

$$\sum_{m\mu}\left(E\delta^{\gamma\mu}_{km} - T^{\gamma\mu}_{km}\right)\Gamma^{\alpha\mu\beta}_{imj\sigma}(E) = \hbar\left\langle S^z_\alpha\right\rangle \delta^{\gamma\beta}_{kj} + \left\langle\!\left\langle S^z_{i\alpha}\left[c_{k\gamma\sigma}, \mathcal{H}_{sf}\right]_- ; c^+_{j\beta\sigma} \right\rangle\!\right\rangle_E, \tag{3.19}$$

$$\sum_{m\mu}\left(E\delta^{\gamma\mu}_{km} - T^{\gamma\mu}_{km}\right)F^{\alpha\mu\beta}_{imj\sigma}(E) = \left\langle\!\left\langle S^{-\sigma}_{i\alpha}\left[c_{k\gamma-\sigma}, \mathcal{H}_{sf}\right]_- ; c^+_{j\beta\sigma} \right\rangle\!\right\rangle_E. \tag{3.20}$$

On the right-hand side of these equations appear further higher Green functions which prevent a direct solution and require an approximative treatment. The treatment is different for the non-diagonal terms, $(i,\alpha) \neq (k,\gamma)$ and for the diagonal terms, $(i,\alpha) = (k,\gamma)$. In the first case we use a self-consistent so-called *self-energy approach* which results in a decoupling of the equations of motion. For the diagonal terms, $(i,\alpha) = (k,\gamma)$, this approach is replaced by a moment technique which takes the local correlations better into account.

Non-diagonal terms $(i,\alpha) \neq (k,\gamma)$**:** The definition of the self-energy (3.14) formally corresponds to the substitution

$$\left[c_{i\alpha\sigma}, \mathcal{H}_{sf}\right]_- \longrightarrow \sum_{m\mu} M^{\alpha\mu}_{im\sigma}(E) c_{m\mu\sigma} \tag{3.21}$$

within the brackets of the Green function. The inspection of the spectral decomposition of the two functions in Eq. (3.14) reveals that both, $\langle\langle [c_{i\alpha\sigma}, \mathcal{H}_{sf}]_-; c^+_{j\beta\sigma}\rangle\rangle_E$ and $\langle\langle c_{i\alpha\sigma}; c^+_{j\beta\sigma}\rangle\rangle_E$, have the same pole structure and can differ only by the spectral weights of their poles. The equality of both sides in Eq. (3.14) is installed by the self-energy components $M^{\alpha\beta}_{ij\sigma}(E)$. Inspecting now the spectral representations of the two Green functions $\langle\langle S^{-\sigma}_{i\alpha}[c_{k\gamma\sigma}, \mathcal{H}_{sf}]_-; c^+_{j\beta\sigma}\rangle\rangle_E$ and $\langle\langle S^{-\sigma}_{i\alpha} c_{k\gamma\sigma}; c^+_{j\beta\sigma}\rangle\rangle_E$ we notice that the additional spin operator $S^{-\sigma}_{i\alpha}$ selects for both only those poles of the original Green functions without spin operator which are connected with a spin-flip of the electron. Hence, the poles of these two functions build a subset of the poles of the two Green functions from Eq. (3.14) and are identical to each other. Again, only the weights of the poles can differ. In analogy to Eqs. (3.14) and (3.21) we now propose to use the plausible ansatz

$$\left\langle\!\!\left\langle S^{-\sigma}_{i\alpha}\left[c_{k\gamma-\sigma}, \mathcal{H}_{sf}\right]_-; c^+_{j\beta\sigma}\right\rangle\!\!\right\rangle_E \approx \sum_{m\mu} M^{\gamma\mu}_{km-\sigma}(E) \left\langle\!\!\left\langle S^{-\sigma}_{i\alpha} c_{m\mu-\sigma}; c^+_{j\beta\sigma}\right\rangle\!\!\right\rangle_E . \tag{3.22}$$

A similar reasoning can be used for:

$$\left\langle\!\!\left\langle S^{z}_{i\alpha}\left[c_{k\gamma\sigma}, \mathcal{H}_{sf}\right]_-; c^+_{j\beta\sigma}\right\rangle\!\!\right\rangle_E \approx \sum_{m\mu} M^{\gamma\mu}_{km\sigma}(E) \left\langle\!\!\left\langle S^{z}_{i\alpha} c_{m\mu\sigma}; c^+_{j\beta\sigma}\right\rangle\!\!\right\rangle_E , \tag{3.23}$$

with the difference that here the additional spin operator $S^z_{i\alpha}$ does not change the original pole structure but merely modifies the spectral weights of the poles. On the right-hand sides of Eqs. (3.22) and (3.23) we find the already known spin-flip and Ising function, respectively. Hence, for $(i,\alpha) \neq (k,\gamma)$, the Eqs. (3.13), (3.16), (3.19), (3.20), (3.22), and (3.23) build a closed system.

Diagonal elements $(i,\alpha) = (k,\gamma)$**:** We start with the explicit evaluation of the higher Green functions on the right-hand sides of Eqs. (3.19) and (3.20). For Eq. (3.20) we get, for $(i,\alpha) = (k,\gamma)$,

$$\left\langle\!\!\left\langle S^{-\sigma}_{i\alpha}\left[c_{i\alpha-\sigma}, \mathcal{H}_{sf}\right]_-; c^+_{j\beta\sigma}\right\rangle\!\!\right\rangle_E = \frac{J}{2}\left(z_\sigma \dot{F}^{\alpha\alpha\beta}_{iij\sigma}(E) - \ddot{F}^{\alpha\alpha\beta}_{iij\sigma}(E)\right), \tag{3.24}$$

where we have abbreviated

$$\dot{F}^{\alpha\alpha\beta}_{iij\sigma}(E) = \left\langle\!\!\left\langle S^{-\sigma}_{i\alpha} S^{z}_{i\alpha} c_{i\alpha-\sigma}; c^+_{j\beta\sigma}\right\rangle\!\!\right\rangle_E , \tag{3.25a}$$

$$\ddot{F}^{\alpha\alpha\beta}_{iij\sigma}(E) = \left\langle\!\!\left\langle S^{-\sigma}_{i\alpha} S^{\sigma}_{i\alpha} c_{i\alpha\sigma}; c^+_{j\beta\sigma}\right\rangle\!\!\right\rangle_E . \tag{3.25b}$$

The analogous evaluation of the higher Green function in Eq. (3.19) does not require any further higher Green functions, because it can be expressed in terms of already known Green functions,

$$\left\langle\!\left\langle S^z_{i\alpha}[c_{i\alpha\sigma}, \mathcal{H}_{sf}]_-; c^+_{j\beta\sigma}\right\rangle\!\right\rangle_E + z_\sigma \left\langle\!\left\langle S^{-\sigma}_{i\alpha}[c_{i\alpha-\sigma}, \mathcal{H}_{sf}]_-; c^+_{j\beta\sigma}\right\rangle\!\right\rangle_E = \frac{J\hbar}{2}\left(\Gamma^{\alpha\alpha\beta}_{iij\sigma}(E) + z_\sigma F^{\alpha\alpha\beta}_{iij\sigma}(E) - z_\sigma \hbar S(S+1) G^{\alpha\beta}_{ij\sigma}(E)\right). \quad (3.26)$$

As Eq. (3.24), the above relation is still exact. To get a closed system of equations we are left with the determination of the functions $\dot{F}^{\alpha\alpha\beta}_{iij\sigma}(E)$ and $\ddot{F}^{\alpha\alpha\beta}_{iij\sigma}(E)$. Both fulfill exact relations which will be used to derive satisfying approximations. For spin $S = 1/2$ we find for all temperatures:

$$\dot{F}^{\alpha\alpha\beta}_{iij\sigma}(E)\Big|_{S=\frac{1}{2}} = \tfrac{1}{2} z_\sigma \hbar F^{\alpha\alpha\beta}_{iij\sigma}(E), \quad (3.27a)$$

$$\ddot{F}^{\alpha\alpha\beta}_{iij\sigma}(E)\Big|_{S=\frac{1}{2}} = \tfrac{1}{2}\hbar^2 G^{\alpha\beta}_{ij\sigma}(E) - z_\sigma \hbar \Gamma^{\alpha\alpha\beta}_{iij\sigma}(E). \quad (3.27b)$$

On the other hand, in the case of ferromagnetic saturation, $\langle S^z_\alpha \rangle \equiv S$, it holds for arbitrary spin:

$$\dot{F}^{\alpha\alpha\beta}_{iij\sigma}(E)\Big|_{T=0} = \hbar\left((S - \tfrac{1}{2}) + \tfrac{1}{2} z_\sigma\right) F^{\alpha\alpha\beta}_{iij\sigma}(E), \quad (3.28a)$$

$$\ddot{F}^{\alpha\alpha\beta}_{iij\sigma}(E)\Big|_{T=0} = \hbar^2 S G^{\alpha\beta}_{ij\sigma}(E) - z_\sigma \hbar \Gamma^{\alpha\alpha\beta}_{iij\sigma}(E). \quad (3.28b)$$

The exact limiting cases (3.27) and (3.28) suggest the general structures:

$$\dot{F}^{\alpha\alpha\beta}_{iij\sigma}(E) = \kappa^{(1)}_{\alpha\sigma} G^{\alpha\beta}_{ij\sigma}(E) + \lambda^{(1)}_{\alpha\sigma} F^{\alpha\alpha\beta}_{iij\sigma}(E), \quad (3.29a)$$

$$\ddot{F}^{\alpha\alpha\beta}_{iij\sigma}(E) = \kappa^{(2)}_{\alpha\sigma} G^{\alpha\beta}_{ij\sigma}(E) + \lambda^{(2)}_{\alpha\sigma} \Gamma^{\alpha\alpha\beta}_{iij\sigma}(E). \quad (3.29b)$$

For the five Green functions of the type $\langle\!\langle A; B\rangle\!\rangle_E$ in Eqs. (3.29) we can calculate the spectral moments,

$$M^{(n)}_{AB} = \left\langle \left(\mathrm{i}\hbar \frac{\partial}{\partial t}\right)^n [A(t), B(0)]_+ \right\rangle_{t=0}, \quad (3.30)$$

where $n = 1, 2, \ldots$. Because of the equivalent relation

$$M^{(n)}_{AB} = -\frac{1}{\pi\hbar} \int_{-\infty}^{\infty} dE\, E^n \,\mathrm{Im}\,\langle\!\langle A; B\rangle\!\rangle_E, \quad (3.31)$$

the moments can be used to fix the coefficients $\kappa_{\alpha\sigma}^{(m)}$ and $\lambda_{\alpha\sigma}^{(m)}$ in Eqs. (3.29). After tedious but straightforward calculations [82], we get

$$\begin{aligned}\kappa_{\alpha\sigma}^{(1)} &= 0, \quad \kappa_{\alpha\sigma}^{(2)} = \langle S_\alpha^{-\sigma} S_\alpha^{\sigma} \rangle - \lambda_{\alpha\sigma}^{(2)} \langle S_\alpha^z \rangle, \\ \lambda_{\alpha\sigma}^{(1)} &= \frac{\langle S_\alpha^{-\sigma} S_\alpha^{\sigma} S_\alpha^z \rangle + z_\sigma \langle S_\alpha^{-\sigma} S_\alpha^{\sigma} \rangle}{\langle S_\alpha^{-\sigma} S_\alpha^{\sigma} \rangle}, \\ \lambda_{\alpha\sigma}^{(2)} &= \frac{\langle S_\alpha^{-\sigma} S_\alpha^{\sigma} S_\alpha^z \rangle - \langle S_\alpha^z \rangle \langle S_\alpha^{-\sigma} S_\alpha^{\sigma} \rangle}{\langle (S_\alpha^z)^2 \rangle - \langle S_\alpha^z \rangle^2}.\end{aligned} \tag{3.32}$$

The coefficients are determined by f-spin correlation functions, which will be determined in section 3.2.2.

Solution for the electronic subsystem: The Eqs. (3.13), (3.16), (3.19), (3.20), (3.22)–(3.24), (3.26), (3.29), and (3.32) represent a closed system, which can be solved self-consistently. Before proceeding we assume that the self-energy from Eq. (3.14) is an entirely local entity

$$M_{\mathbf{k}\sigma}^{\alpha\beta}(E) \equiv \delta_{\alpha\beta} M_\sigma^\alpha(E). \tag{3.33}$$

The reason for the $\mathbf{k}$ independence can be traced back to the neglect of magnon energies [84]. The restriction to the diagonal elements of the self-energy with respect to the greek layer indices transfers the locality of the self-energy for the three-dimensional case [84] to the film geometries discussed in this chapter.

We can now use Eqs. (3.22)–(3.24), (3.26), (3.29), and (3.32) to evaluate the Ising and the spin-flip functions in Eqs. (3.19) and (3.20). As the result we get the Fourier transformed Ising and spin-flip functions. According to Eq. (3.16), we can restrict our attention to the diagonal elements $\Gamma_{\mathbf{kq}\sigma}^{\alpha\alpha\beta}(E)$ and $F_{\mathbf{kq}\sigma}^{\alpha\alpha\beta}(E)$. After subsequent $\mathbf{q}$-summation we eventually get, using Eqs. (3.15) and (3.33):

$$\begin{aligned}\hbar \sum_{\mathbf{q}} \Gamma_{\mathbf{kq}\sigma}^{\alpha\alpha\beta} &= \sqrt{N}\hbar \langle S_\alpha^z \rangle G_{\mathbf{k}\sigma}^{\alpha\beta} \\ &\quad - G_{\mathbf{0}\sigma}^{\alpha\alpha} \Big\{ M_\sigma^\alpha \sum_{\mathbf{q}} \Gamma_{\mathbf{kq}\sigma}^{\alpha\alpha\beta} - \frac{J}{2} \Big(z_\sigma (\kappa_{\alpha\sigma}^{(2)} - \hbar^2 S(S+1)) \sqrt{N} G_{\mathbf{k}\sigma}^{\alpha\beta} \\ &\quad + (z_\sigma \hbar - \lambda_{\alpha\sigma}^{(1)}) \sum_{\mathbf{q}} F_{\mathbf{kq}\sigma}^{\alpha\alpha\beta} + (\hbar + z_\sigma \lambda_{\alpha\sigma}^{(2)}) \sum_{\mathbf{q}} \Gamma_{\mathbf{kq}\sigma}^{\alpha\alpha\beta} \Big) \Big\},\end{aligned} \tag{3.34a}$$

$$\begin{aligned}\hbar \sum_{\mathbf{q}} F_{\mathbf{kq}\sigma}^{\alpha\alpha\beta} &= - G_{\mathbf{0}-\sigma}^{\alpha\alpha} \Big\{ M_{-\sigma}^\alpha \sum_{\mathbf{q}} F_{\mathbf{kq}\sigma}^{\alpha\alpha\beta} + \frac{J}{2} \Big(\kappa_{\alpha\sigma}^{(2)} \sqrt{N} G_{\mathbf{k}\sigma}^{\alpha\beta} \\ &\quad - z_\sigma \lambda_{\alpha\sigma}^{(1)} \sum_{\mathbf{q}} F_{\mathbf{kq}\sigma}^{\alpha\alpha\beta} + \lambda_{\alpha\sigma}^{(2)} \sum_{\mathbf{q}} \Gamma_{\mathbf{kq}\sigma}^{\alpha\alpha\beta} \Big) \Big\},\end{aligned} \tag{3.34b}$$

where we have introduced

$$G_{\mathbf{0}\sigma}^{\alpha\alpha}(E) = \frac{1}{N} \sum_{\mathbf{k}} G_{\mathbf{k}\sigma}^{\alpha\alpha}(E). \tag{3.35}$$

The set of equations (3.34) can be solved to express the sums $\sum_{\mathbf{q}} \Gamma^{\alpha\alpha\beta}_{\mathbf{kq}\sigma}(E)$ and $\sum_{\mathbf{q}} F^{\alpha\alpha\beta}_{\mathbf{kq}\sigma}(E)$ in terms of the single-electron Green function $G^{\alpha\beta}_{\mathbf{k}\sigma}(E)$. However, by inspecting Eqs. (3.34) we see that these expressions will still contain the layer- and spin-dependent self-energy $M^{\alpha}_{\sigma}(E)$.

To solve this problem we combine Eqs. (3.14) and (3.16) and get, after Fourier transformation:

$$M^{\alpha}_{\sigma} G^{\alpha\beta}_{\mathbf{k}\sigma} = -\frac{J}{2\sqrt{N}}\Big(z_{\sigma} \sum_{\mathbf{q}} \Gamma^{\alpha\alpha\beta}_{\mathbf{kq}\sigma} + \sum_{\mathbf{q}} F^{\alpha\alpha\beta}_{\mathbf{kq}\sigma}\Big). \tag{3.36}$$

Combining this equation with the results obtained for $\sum_{\mathbf{q}} \Gamma^{\alpha\alpha\beta}_{\mathbf{kq}\sigma}(E)$ and $\sum_{\mathbf{q}} F^{\alpha\alpha\beta}_{\mathbf{kq}\sigma}(E)$ from Eqs. (3.34) we eventually get an implicit set of equations for the layer- and spin-dependent electronic self-energy,

$$M^{\alpha}_{\sigma}(E) = -\frac{J}{2} m^{\alpha}_{\sigma}(E), \quad m^{\alpha}_{\sigma}(E) = \frac{Z^{\alpha}_{\sigma}(E)}{N^{\alpha}_{\sigma}(E)}, \tag{3.37}$$

where the numerator and the denominator are given by

$$Z^{\alpha}_{\sigma} = z_{\sigma}\hbar^2 \langle S^z_{\alpha}\rangle + \frac{J}{2} f^1_Z + \frac{J^2}{4} f^2_Z, \tag{3.38a}$$

$$N^{\alpha}_{\sigma} = \hbar^2 - \frac{J}{2} f^1_N + \frac{J^2}{4} f^2_N, \tag{3.38b}$$

with

$$\begin{aligned}
f^1_Z &= \big(\kappa^{(2)}_{\alpha\sigma} - \hbar^2 S(S+1)\big) G^{\alpha\alpha}_{\mathbf{0}\sigma} - \big((\lambda^{(1)}_{\alpha\sigma} + \lambda^{(2)}_{\alpha\sigma} + z_{\sigma} m^{\alpha}_{-\sigma})\hbar\langle S^z_{\alpha}\rangle + \hbar\kappa^{(2)}_{\alpha\sigma}\big) G^{\alpha\alpha}_{\mathbf{0}-\sigma}, \\
f^2_Z &= \big(z_{\sigma}\hbar^2 S(S+1)(\lambda^{(1)}_{\alpha\sigma} + \lambda^{(2)}_{\alpha\sigma} + z_{\sigma} m^{\alpha}_{-\sigma}) + \kappa^{(2)}_{\alpha\sigma}(m^{\alpha}_{\sigma} - m^{\alpha}_{-\sigma})\big) G^{\alpha\alpha}_{\mathbf{0}\sigma} G^{\alpha\alpha}_{\mathbf{0}-\sigma}, \\
f^1_N &= (\hbar + z_{\sigma}\lambda^{(2)}_{\alpha\sigma} + m^{\alpha}_{\sigma}) G^{\alpha\alpha}_{\mathbf{0}\sigma} + (z_{\sigma}\lambda^{(1)}_{\alpha\sigma} + m^{\alpha}_{-\sigma}) G^{\alpha\alpha}_{\mathbf{0}-\sigma}, \\
f^2_N &= \big((m^{\alpha}_{\sigma} + \hbar)(m^{\alpha}_{-\sigma} + z_{\sigma}\lambda^{(1)}_{\alpha\sigma}) + z_{\sigma}\lambda^{(2)}_{\alpha\sigma}(m^{\alpha}_{-\sigma} + \hbar)\big) G^{\alpha\alpha}_{\mathbf{0}\sigma} G^{\alpha\alpha}_{\mathbf{0}-\sigma}.
\end{aligned} \tag{3.38c}$$

The implicit set of equations (3.37) and (3.38) now enables us to self-consistently evaluate the self-energy of the system provided that the *f*-spin correlation functions from Eqs. (3.32) are known. These will be evaluated in the next section.

3.2.2 The local-moment system

Considering the Heisenberg model,

$$\mathcal{H}_f = -\sum_{ij} J_{ij}\, \mathbf{S}_i \cdot \mathbf{S}_j = -\sum_{ij} J_{ij} \left(S^+_i S^-_j + S^z_i S^z_j\right), \tag{3.39}$$

in a system with film geometry one comes to the conclusion that due to the Mermin-Wagner theorem [85, 86] the problem cannot have a solution showing collective magnetic order at finite temperatures $T > 0$.

To steer clear of this obstacle there are two possibilities. First, one can apply a decoupling scheme to the Hamiltonian (3.39) which breaks the Mermin-Wagner theorem. The most common example in the case of the Heisenberg model would be a mean-field decoupling. For us, the main drawback of the mean-field decoupling is its incapability of describing physical properties at the 2D-3D transition.

When choosing a better decoupling approximation to fulfill the Mermin-Wagner theorem, the original Heisenberg Hamiltonian (3.39) has to be extended to break the directional symmetry. The most common extensions are the introduction of an anisotropic exchange interaction,

$$-D \sum_{ij} S_i^z S_j^z - D_\mathrm{s} \sum_{i,j \in \mathrm{surf}} S_i^z S_j^z, \tag{3.40}$$

and/or the single-ion anisotropy,

$$-D_0 \sum_i \left(S_i^z\right)^2 - D_{0,\mathrm{s}} \sum_{i \in \mathrm{surf}} \left(S_i^z\right)^2. \tag{3.41}$$

In Eqs. (3.40) and (3.41) the first sums run over all lattice sites of the film whereas in the second optional terms the summations include positions within the surface layers of the film only, according to a possible variation of the anisotropy in the vicinity of the surface.

Extending the original Heisenberg Hamiltonian (3.39) by Eq. (3.40) or Eq. (3.41) one can now calculate the magnetic properties of films at finite temperatures within a nontrivial decoupling scheme.

For the following calculations [87] we have chosen a single-ion anisotropy which is uniform within the whole film leaving us with the total Hamiltonian

$$\mathcal{H} = \mathcal{H}_f + \mathcal{H}_A = -\sum_{ij\alpha\beta} J_{ij}^{\alpha\beta} \left(S_{i\alpha}^+ S_{j\beta}^- + S_{i\alpha}^z S_{j\beta}^z \right) - D_0 \sum_{i\alpha} \left(S_{i\alpha}^z\right)^2. \tag{3.42}$$

As in Sec. 3.2.1 the greek indices are for the layers of the film and the latin indices denote the sites within a given layer (cf. Fig. 2.1, Eq. (3.1)).

To derive the layer-dependent magnetizations $\langle S_\alpha^z \rangle$ for arbitrary values of the spin S of the localized moments we introduce the so-called retarded Callen Green function [88]:

$$G_{ij\,(a)}^{\alpha\beta}(E) \equiv \langle\langle S_{i\alpha}^+ ; B_{j\beta}^{(a)} \rangle\rangle_E = \langle\langle S_{i\alpha}^+ ; \mathrm{e}^{a S_{j\beta}^z} S_{j\beta}^- \rangle\rangle_E. \tag{3.43}$$

For the equation of motion of the Callen Green function,

$$E\; G_{ij\,(a)}^{\alpha\beta}(E) = \hbar \langle [S_{i\alpha}^+, B_{j\beta}^{(a)}]_- \rangle + \langle\langle [S_{i\alpha}^+, \mathcal{H}]_- ; B_{j\beta}^{(a)} \rangle\rangle_E \tag{3.44}$$

one needs the inhomogeneity,

$$\langle [S^+_{i\alpha}, B^{(a)}_{j\beta}]_- \rangle = \eta^{(a)}_\alpha \delta_{\alpha\beta}\delta_{ij}, \tag{3.45}$$

and the commutators

$$[S^+_{i\alpha}, \mathcal{H}_f]_- = -2\hbar \sum_{k\gamma} J^{\alpha\gamma}_{ik} \left(S^z_{i\alpha} S^+_{k\gamma} - S^z_{k\gamma} S^+_{i\alpha} \right), \tag{3.46}$$

$$[S^+_{i\alpha}, \mathcal{H}_A]_- = D_0 \hbar \left(S^+_{i\alpha} S^z_{i\alpha} + S^z_{i\alpha} S^+_{i\alpha} \right). \tag{3.47}$$

For the higher Green function on the right hand side of the equation of motion (3.44) resulting from the commutator relationship (3.46) one can apply the Random Phase Approximation (RPA) which has proved to yield reasonable results throughout the entire temperature range:

$$\begin{aligned} \langle\langle S^z_{i\alpha} S^+_{k\gamma};\, B^{(a)}_{j\beta} \rangle\rangle_E &\longrightarrow \langle S^z_\alpha \rangle \langle\langle S^+_{k\gamma};\, B^{(a)}_{j\beta} \rangle\rangle_E, \\ \langle\langle S^z_{k\gamma} S^+_{i\alpha};\, B^{(a)}_{j\beta} \rangle\rangle_E &\longrightarrow \langle S^z_\gamma \rangle \langle\langle S^+_{i\alpha};\, B^{(a)}_{j\beta} \rangle\rangle_E. \end{aligned} \tag{3.48}$$

For the higher Green functions resulting from the commutator (3.47) this is not possible due to the strong on-site correlation of the corresponding operators. However, one can look for an acceptable decoupling of the form

$$\langle\langle S^+_{i\alpha} S^z_{i\alpha} + S^z_{i\alpha} S^+_{i\alpha};\, B^{(a)}_{j\beta} \rangle\rangle_E = \Phi_{i\alpha} \langle\langle S^+_{i\alpha};\, B^{(a)}_{j\beta} \rangle\rangle_E. \tag{3.49}$$

As was shown by Lines [89] an appropriate coefficient $\Phi_{i\alpha} = \Phi_\alpha$ can be found for any given function $B^{(a)}_{j\beta} = f(S^-_{j\beta})$, which is all we need to know at the moment. We will come back to the explicit calculation of the Φ_α later.

Using the relations (3.45)–(3.49) and applying a two-dimensional Fourier transform introducing the in-plane wavevector $\mathbf{k}$ the equation of motion (3.44) becomes

$$\begin{aligned} (E - \hbar D_0 \Phi_\alpha)\, G^{\alpha\beta}_{\mathbf{k}(a)} &= \hbar \eta^{(a)}_\alpha \delta_{\alpha\beta} \\ &\quad + 2\hbar \sum_\gamma \left(J^{\alpha\gamma}_{\mathbf{0}} \langle S^z_\gamma \rangle G^{\alpha\beta}_{\mathbf{k}(a)} - J^{\alpha\gamma}_{\mathbf{k}} \langle S^z_\alpha \rangle G^{\gamma\beta}_{\mathbf{k}(a)} \right). \end{aligned} \tag{3.50}$$

Writing Eq. (3.50) in matrix form one immediately gets the solution by simple matrix inversion:

$$G^{\alpha\beta}_{\mathbf{k}(a)}(E) = \hbar \begin{pmatrix} \eta^{(a)}_1 & & 0 \\ & \ddots & \\ 0 & & \eta^{(a)}_n \end{pmatrix} \cdot (E\mathbf{I} - \mathbf{M})^{-1}, \tag{3.51}$$

where $\mathbf{I}$ represents the $(n \times n)$ identity matrix and

$$\frac{(\mathbf{M})^{\alpha\beta}}{\hbar} = \left(D_0 \Phi_\alpha + 2 \sum_\gamma J^{\alpha\gamma}_0 \langle S^z_\gamma \rangle \right) \delta_{\alpha\beta} - 2 J^{\alpha\beta}_{\mathbf{k}} \langle S^z_\alpha \rangle. \tag{3.52}$$

The local, i. e. layer-dependent, spectral density, $S^{\alpha}_{\mathbf{k}(a)} = -\frac{1}{\pi}\mathrm{Im}G^{\alpha\alpha}_{\mathbf{k}(a)}$, can then be written as a sum of δ-functions and with (3.51) one gets:

$$S^{\alpha}_{\mathbf{k}(a)} = \hbar\eta^{(a)}_{\alpha}\sum_{\gamma}\chi_{\alpha\alpha\gamma}(\mathbf{k})\delta\left(E - E_{\gamma}(\mathbf{k})\right), \tag{3.53}$$

where $E_{\gamma}(\mathbf{k})$ are the poles of the Green function (3.51) and $\chi_{\alpha\alpha\gamma}(\mathbf{k})$ are the weights of these poles in the diagonal elements of the Green function, $G^{\alpha\alpha}_{\mathbf{k}(a)}$. Both, the poles and the weights can be calculated numerically.

Extending the procedure by Callen [88] from 3D to film structures* one finds an analytical expression for the layer dependent magnetizations [90, 91],

$$\langle S^{z}_{\alpha}\rangle = \hbar\frac{(1+\varphi_{\alpha})^{2S+1}(S-\varphi_{\alpha}) + \varphi_{\alpha}^{2S+1}(S+1+\varphi_{\alpha})}{(1+\varphi_{\alpha})^{2S+1} - \varphi_{\alpha}^{2S+1}}, \tag{3.54}$$

where

$$\varphi_{\alpha} = \frac{1}{N_{\mathrm{s}}}\sum_{\mathbf{k}}\sum_{\gamma}\frac{\chi_{\alpha\alpha\gamma}(\mathbf{k})}{\mathrm{e}^{\beta E_{\gamma}(\mathbf{k})} - 1}. \tag{3.55}$$

Here, N_{s} is the number of atoms in a layer and $\beta = (k_{\mathrm{B}}T)^{-1}$. The poles and weights in Eq. (3.55) have to be calculated for the special Green function $G^{\alpha\alpha}_{\mathbf{k}(a)}$ with $a = 0$†. In this case the Callen Green function (3.43) simply becomes:

$$G^{\alpha\beta}_{ij\,(0)} = G^{\alpha\beta}_{ij} = \langle\langle S^{+}_{i\alpha};\, B^{(0)}_{j\beta}\rangle\rangle = \langle\langle S^{+}_{i\alpha};\, S^{-}_{j\beta}\rangle\rangle, \tag{3.56}$$

and, according to (3.45),

$$\eta^{(0)}_{\alpha} = \eta_{\alpha} = 2\hbar\langle S^{z}_{\alpha}\rangle. \tag{3.57}$$

Having solved the problem formally we are left with explicitly calculating the coefficients Φ_{α} of Eq. (3.49). Applying the spectral theorem to Eq. (3.49) for the special case of $a = 0$ one gets, using elementary commutator relations:

$$\langle S^{-}_{j\beta}S^{+}_{i\alpha}(2S^{z}_{i\alpha} + \hbar)\rangle = \Phi_{i\alpha}\langle S^{-}_{j\beta}S^{+}_{i\alpha}\rangle. \tag{3.58}$$

We now define the Green function

$$D^{\beta\alpha}_{ji} = \langle\langle S^{-}_{j\beta};\, C_{i\alpha}\rangle\rangle_{E}, \tag{3.59}$$

where $C_{i\alpha}$ is a function of the lattice site. Writing down the equation of motion of $D^{\beta\alpha}_{ji}$ for the limit $D_0 \to 0$,

$$E\; D^{\beta\alpha}_{ji}(E) = \hbar\langle\langle[S^{-}_{j\beta}, C_{i\alpha}]_{-}\rangle\rangle + \langle\langle[S^{-}_{j\beta}, \mathcal{H}_{f}]_{-};\, C_{i\alpha}\rangle\rangle_{E}, \tag{3.60}$$

*The only condition for the extension is that the spectral density has the multi-pole structure (3.53)

†The parameter a had been introduced to derive Eq. (3.54) for arbitrary spin S.

and decoupling all the higher Green functions using the RPA one arrives after transformation into the two-dimensional **k** space at:

$$D_{\mathbf{k}}^{\beta\alpha} = \hbar \begin{pmatrix} \langle [S_1^-, C_1]_- \rangle & & 0 \\ & \ddots & \\ 0 & & \langle [S_n^-, C_n]_- \rangle \end{pmatrix} \cdot (E\mathbf{I} - \mathbf{A})^{-1}, \tag{3.61}$$

where **A** is a matrix which is independent on the choice of $C_{i\alpha}$. Now putting $C_{i\alpha}$ in Eq. (3.59) in turn equal to $S_{i\alpha}^+$ and to $S_{i\alpha}^+(2S_{i\alpha}^z + \hbar)$ and applying the spectral theorem to Eq. (3.61) one eventually gets the relation:

$$\frac{\langle S_{j\beta}^- S_{i\alpha}^+ \rangle}{\langle [S_{i\alpha}^-, S_{i\alpha}^+]_- \rangle} = \frac{\langle S_{j\beta}^- S_{i\alpha}^+ (2S_{i\alpha}^z + \hbar) \rangle}{\langle [S_{i\alpha}^-, S_{i\alpha}^+ (2S_{i\alpha}^z + \hbar)]_- \rangle}. \tag{3.62}$$

The coefficients $\Phi_{i\alpha}$ are then with Eq. (3.58) given by

$$\Phi_{i\alpha} = \frac{\langle [S_{i\alpha}^-, S_{i\alpha}^+ (2S_{i\alpha}^z + \hbar)]_- \rangle}{\langle [S_{i\alpha}^-, S_{i\alpha}^+]_- \rangle} = \frac{2\langle (S_{i\alpha}^z)^2 \rangle - \hbar^2 S(S+1)}{\langle S_{i\alpha}^z \rangle}, \tag{3.63}$$

where, along with commutator relations, the identity

$$S_{i\alpha}^{\pm} S_{i\alpha}^{\mp} = \hbar^2 S(S+1) \pm \hbar S_{i\alpha}^z - (S_{i\alpha}^z)^2 \tag{3.64}$$

has been used. To avoid the unknown expectation values $\langle (S_{i\alpha}^z)^2 \rangle$ we apply the spectral theorem to the spectral density (3.53) with $a = 0$ and get using Eqs. (3.55) and (3.57):

$$\langle S_\alpha^- S_\alpha^+ \rangle = 2\hbar \langle S_\alpha^z \rangle \frac{1}{N_\mathrm{s}} \sum_{\mathbf{k}} \sum_{\gamma} \frac{\chi_{\alpha\alpha\gamma}(\mathbf{k})}{\mathrm{e}^{\beta E_\gamma(\mathbf{k})} - 1} = 2\hbar \langle S_\alpha^z \rangle \varphi_\alpha. \tag{3.65}$$

Hence, with (3.64) and (3.65), we get

$$\langle (S_\alpha^z)^2 \rangle = \hbar^2 S(S+1) - \hbar \langle S_\alpha^z \rangle (1 + 2\varphi_\alpha), \tag{3.66}$$

and the coefficients Φ_α can be written in the convenient form

$$\Phi_\alpha = \frac{2\hbar^2 S(S+1) - 3\hbar \langle S_\alpha^z \rangle (1 + 2\varphi_\alpha)}{\langle S_\alpha^z \rangle}. \tag{3.67}$$

Together with (3.67), Eqs. (3.51), (3.52), (3.54), and (3.55) represent a closed system of equations, which can be solved numerically. As a result, the layer-dependent magnetizations (3.54) and the φ_α according to Eq. (3.55) will be known. Together with Eqs. (3.64)–(3.66) and with the relation

$$\langle (S_\alpha^z)^3 \rangle = \hbar^3 S(S+1)\varphi_\alpha + \hbar^2 \langle S_\alpha^z \rangle \big(S(S+1) + \varphi_\alpha \big) - \hbar \langle (S_\alpha^z)^2 \rangle (1 + 2\varphi_\alpha) \tag{3.68}$$

the temperature dependent coefficients (3.32) can then be calculated. Mediated by Eqs. (3.32), (3.37), and (3.38), the *f*-spin correlation functions contain the whole temperature dependence of the electronic subsystem (3.8).

4 Model calculations for films

The theory presented in the previous chapter shall now be evaluated numerically. The structure of this chapter follows from the separated treatment of the electronic subsystem and the local-moment system in sections 3.2.1 and 3.2.2, respectively. The temperature dependence of the electronic system is determined by the *f*-spin correlation functions in Eq. (3.32). Hence, the numerical calculations for the local-moment system have to precede the numerical evaluation of the electronic structure.

All the calculations for the model system have been performed for a simple cubic (sc) film with its surface parallel to the sc(100) crystal plane. In principle, there is no restriction as to which crystal structure can be calculated with the presented method. The sc(100) film geometry has been chosen merely for clarity.

4.1 Magnetic properties

To describe the situation in europium chalcogenides, the numerical calculations for the local-moment system have been performed for a spin of $S = 7/2$. It should be noted, however, that the formulas presented in section 3.2.2 are valid for arbitrary spin S.

A useful simplification of the original Heisenberg Hamiltonian (3.39) is the tight-binding approximation for the *f*-*f* exchange integrals to nearest neighbor coupling. For a sc(100) film four of the total six nearest neighbors of any atom at the site $\mathbf{R}_{i\alpha}$ are in the same layer α and the other two are one each in one of the adjacent layers $\alpha \pm 1$,

$$J_{ij}^{\alpha\beta} = \delta_{i,j+\Delta}^{\alpha\beta} J^{\alpha\alpha} + \delta_{ij}^{\alpha,\beta\pm1} J^{\alpha\beta}. \tag{4.1}$$

Here, Δ denotes the relative positions of nearest neighbors, both within the same layer, for sc(100) films: $\Delta = (0,1),\ (0,\bar{1}),\ (1,0),\ (\bar{1},0)$. Furthermore, the *f*-*f* exchange interaction has been assumed to be uniform within the whole film,

$$J^{\alpha\alpha} = J^{\alpha\beta} \equiv J_{ff}. \tag{4.2}$$

For the following calculations, the explicit value of the Heisenberg exchange interaction J_{ff} has been chosen to be $J_{ff} = 0.01\,\mathrm{eV}$. The single-ion anisotropy in Eq. (3.42) plays the role of keeping the magnetization of the film finite at finite temperatures and should therefore be small compared to the Heisenberg exchange interaction, $D_0 \ll J_{ff}$. Accordingly, the single-ion anisotropy was set to $D_0/J_{ff} = 0.01$.

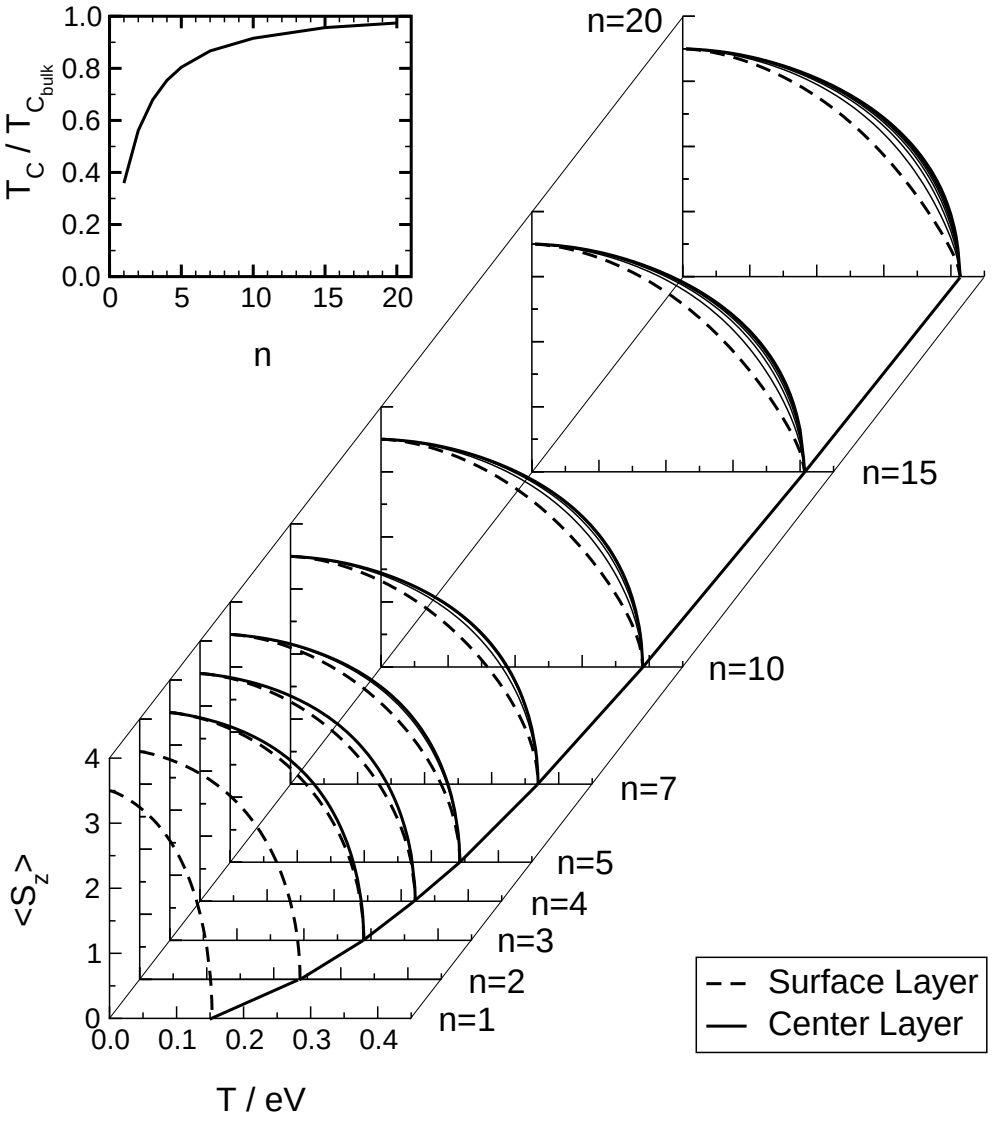

Figure 4.1: Layer-dependent magnetizations, $\langle S_\alpha^z \rangle$, of sc(100) films as a function of temperature for various thicknesses n of the films. For all temperatures and for all film thicknesses, the $\langle S_\alpha^z \rangle$ increase monotonously from the surface layer towards the center of the films. **Inset:** Curie temperature as a function of film thickness.

Fig. 4.1 shows the temperature and layer-dependent magnetizations of sc(100) films of various thicknesses from $n = 1$ up to $n = 20$. For all temperatures and for all film thicknesses the $\langle S_\alpha^z \rangle$ increase from the lowest magnetizations at the surface of the films (bold dashed lines) monotonously towards the highest magnetizations in the center of the films (bold solid lines). This can qualitatively be explained by the lower coordination number of the surface atoms, $Z_{\mathrm{s,sc(100)}} = 5$, compared to the bulk coordination number, $Z_{\mathrm{b,sc}} = 6$, of the sc lattice. The inset of Fig. 4.1 shows the dependence of the Curie temperature on the film thickness n compared to the 3D Curie tempera-

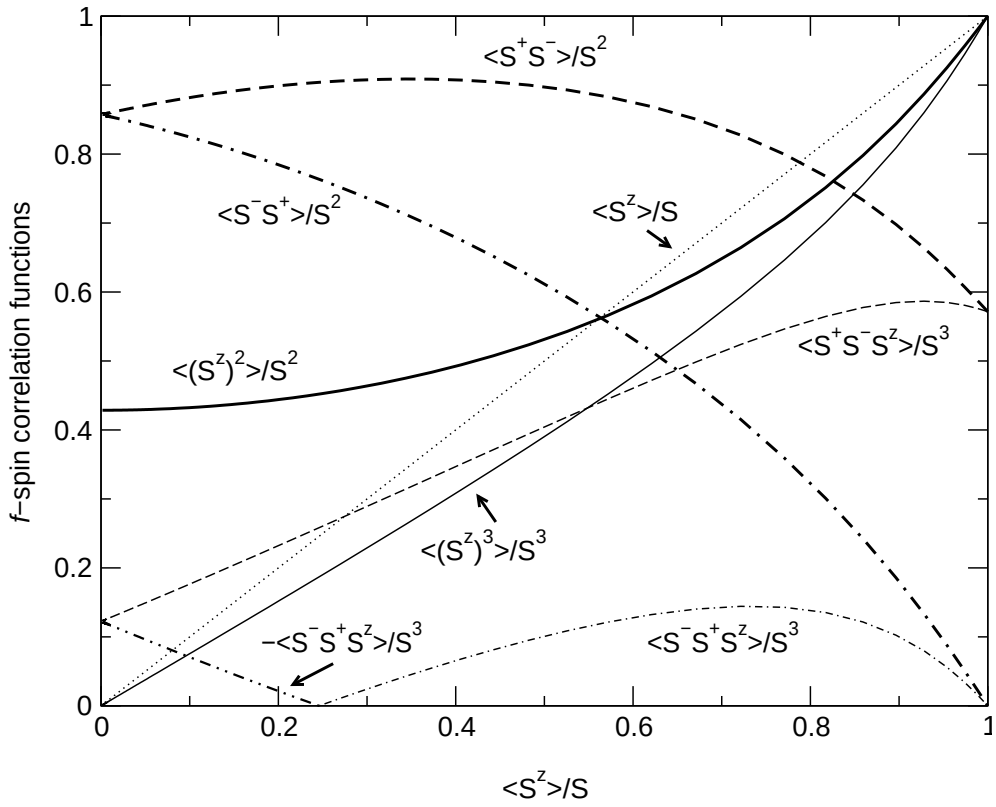

Figure 4.2: Reduced f-spin correlation functions as a function of the reduced magnetization $\langle S^z\rangle/S$ calculated for a local-moment system with $S = 7/2$. The thin dotted line ($y = x$) is a guide for the eye.

ture calculated with the same exchange interaction J_{ff} and with the same single-ion anisotropy D_0. As can be seen both from Fig. 4.1 and its inset the case of a 10-layer film is already a good approximation for thicker films ($n = 20$), concerning both the surface and the center layer magnetization.

For the calculation of the temperature and layer dependent self-energy of the electronic system according to Eqs. (3.37) and (3.38) the coefficients (3.32) have to be calculated from the f-spin correlation functions $\langle(S_\alpha^z)^2\rangle$, $\langle S_\alpha^\pm S_\alpha^\mp\rangle$, $\langle(S_\alpha^z)^3\rangle$, and $\langle S_\alpha^\pm S_\alpha^\mp\rangle$. Using Eqs. (3.54), (3.64)–(3.66), and (3.68), these correlation functions can all be expressed in terms of the φ_α (see Eq. (3.55)). Fig. 4.2 shows the relevant f-spin correlation functions for a system with $S = 7/2$ as a function of the reduced magnetization $\langle S^z\rangle/S$. Figs. 4.1 and 4.2 thereby combine all the information needed to calculate the temperature dependence of the electronic structure.

The equations for the determination of the Callen Green function, Eqs. (3.51) and (3.52) contain the anisotropy energy $E_\mathrm{A} = -D_0\Phi_\alpha$ with the temperature-dependent anisotropy coefficients Φ_α. In the limit of small single-ion anisotropy, $D_0 \ll J_{ff}$, the Φ_α are given by Eq. (3.67). Fig. 4.3 shows the anisotropy coefficient Φ as a function of the reduced magnetization $\langle S^z\rangle/S$. As can be seen from Fig. 4.3, for decreasing

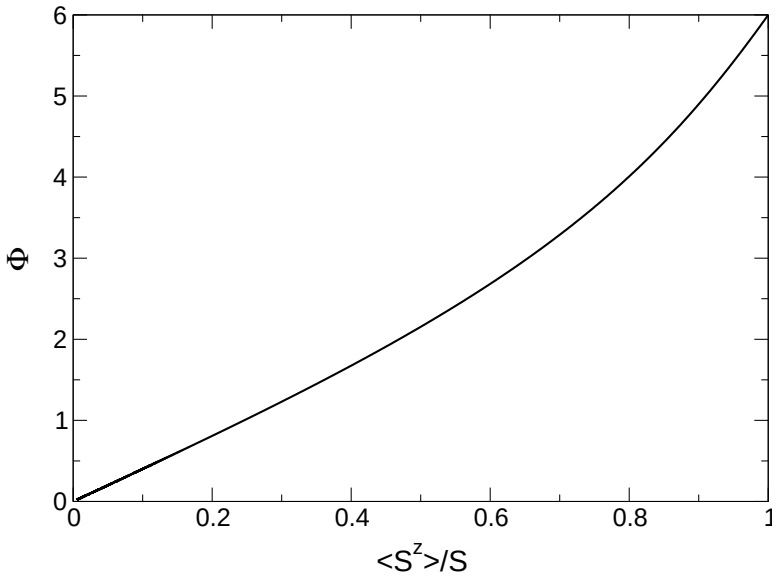

Figure 4.3: Anisotropy coefficient Φ (cf. Eq. (3.67)) as a function of the reduced magnetization $\langle S^z\rangle/S$ calculated for a local-moment system with $S = 7/2$.

magnetization the anisotropy energy increases monotonously from its minimum value of $E_\mathrm{A} = -6D_0$ at $\langle S^z\rangle = S$ to $E_\mathrm{A} = 0$ at $\langle S^z\rangle = 0$.

4.2 Electronic structure

As for the Heisenberg Hamiltonian in Sec. 4.1, for the kinetic Hamiltonian of the itinerant electrons (3.3) we have chosen the tight-binding approximation with a uniform hopping throughout the film,

$$T_{ij}^{\alpha\beta} = \delta_{i,j+\Delta}^{\alpha\beta} T^{\alpha\alpha} + \delta_{ij}^{\alpha,\beta\pm1} T^{\alpha\beta}, \qquad T^{\alpha\alpha} = T^{\alpha\beta} \equiv T, \tag{4.3}$$

with a value of $T = 0.1\,\mathrm{eV}$. The case of non-uniform hopping will be discussed in Sec. 4.2.1.

We discuss our results in terms of the spectral density $S_{\mathbf{k}\sigma}^{\alpha\alpha}(E)$, defined in Eq. (3.11), and the local quasiparticle density of states, Eq. (3.12). We start our discussion of the temperature-dependent electronic structure with the limiting case of the magnetic polaron, $T = 0$ and $n = 0$, which gives us an insight into the underlying physics of the problem. The special case of ferromagnetic saturation, $T = 0$, and empty conduction band, $n = 0$, is exactly solvable, both for the bulk material [92, 93, 84] (cf. Sec. 5) and for film geometries [94]. The limiting case, therefore, provides a good testing ground for the theory for finite temperatures presented in Sec. 3.2.1.

It turns out that for $T = 0$ the $\uparrow$-spectrum is rather simple, since a $\uparrow$-electron has no chance to exchange its spin with the ferromagnetically saturated localized f-spin

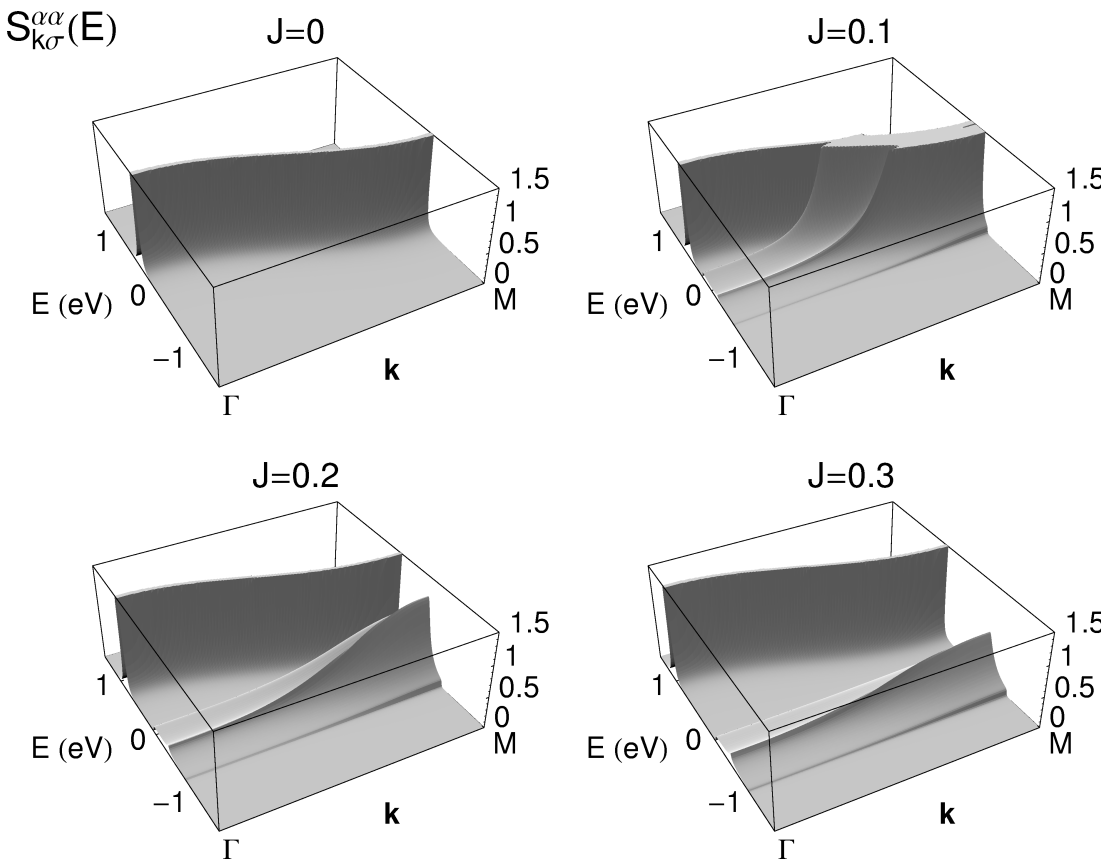

Figure 4.4: Spin-↓ spectral density $S^{\alpha\alpha}_{\mathbf{k}\sigma} = S_{\mathbf{k}\downarrow}$ of a sc(100) monolayer for ferromagnetic saturation of the local-moment system ($T = 0$, $\langle S^z \rangle = S$) as a function of energy and wave vector from $\bar{\Gamma} = (0, 0)$ to $\bar{\mathrm{M}} = (\pi, \pi)$ and different values of *s-f* interaction J (in eV).

system. The quasiparticle band structure is therefore identical to the free Bloch dispersion, only rigidly shifted by a constant energy amount of $-\frac{1}{2}JS$, due to the first Ising-like term in the *s-f* Hamiltonian (3.7).

Fig. 4.4 shows the spin-↓ spectral density of a sc(100) monolayer for the special case of ferromagnetic saturation, $T = 0$, for different *s-f* interactions J. For $J = 0$ the spectral density represents a δ-function located at the point of the free two-dimensional Bloch dispersion. For small *s-f* exchange coupling, $J > 0$, a slight deformation of the original Bloch dispersion sets in and the quasiparticle peaks get a finite width indicating a finite lifetime. For intermediate and strong couplings the spectral density splits into two parts corresponding to two different spin exchange processes between the excited spin-↓ electron and the localized *f*-spin system. The higher energetic part of the spectrum represents a polarization of the immediate spin neighborhood of the electron due to a repeated emission and reabsorption of magnons. The result is a polaron-like quasiparticle called the *magnetic polaron*. The low-energetic part of the spectrum is a scattering band which corresponds to the simple emission of a magnon by

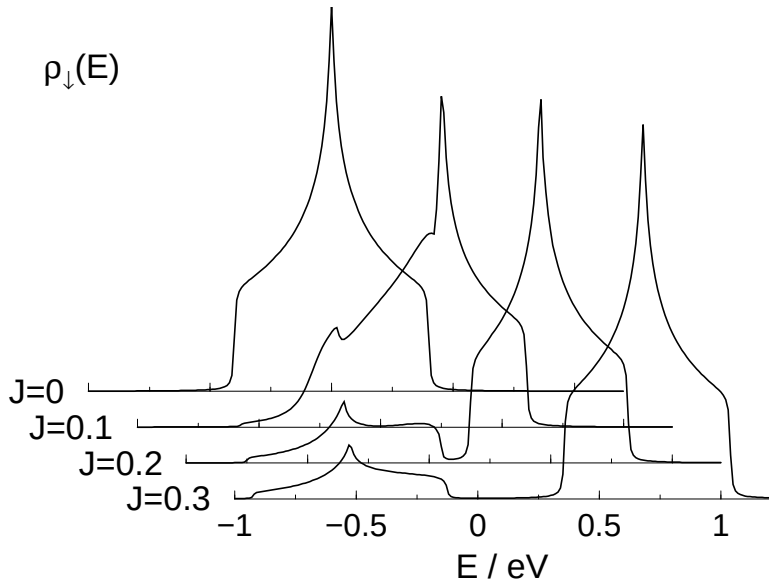

Figure 4.5: Density of states $\rho_\downarrow(E)$ of a sc(100) monolayer for $T = 0$ and for different *s-f* interactions J (in eV).

the spin-$\downarrow$ electron, which is necessarily connected with a spin-flip of the electron [94].

From the spectral density of Fig. 4.4 we get, using Eq. (3.12), the local quasiparticle density of states $\rho_\downarrow(E)$ of a monolayer, displayed in Fig. 4.5. Here we see that the splitting of the spectral density discussed above transfers itself to the quasiparticle density of states as a gap for $J \gtrapprox 0.2$. As for the spectral density, the density of states of the spin-$\uparrow$ electron is only rigidly shifted and therefore not displayed.

However, this does not hold any longer for finite temperatures, $T > 0$. Fig. 4.6 exhibits the density of states of a sc(100) monolayer for different *s-f* interactions and different temperatures. The dotted lines represent the case of vanishing *s-f* exchange, $J = 0$, where spin-$\downarrow$ and spin-$\uparrow$ spectra are equal. Since the electrons are not coupled to the local-moment system, we also have no temperature dependency. For finite *s-f* interaction we see from Fig. 4.5 that in the spin-$\downarrow$ density of states spectral weight is transferred from the high-energetic polaron peak to the low-energetic scattering peak. To explain this effect we have to consider the elementary processes which build the spectrum. The low-energetic scattering peak of the spin-$\downarrow$ electron consists of two elementary processes.

Because of finite deviation of the *f*-spin system from saturation for $T > 0$, the $\downarrow$-electron has a finite probability of entering the local frame as spin-$\uparrow$ electron. This probability is zero for $\langle S_z \rangle = S$ $(T = 0)$ and increases with increasing temperature. On the other hand, the spin-$\downarrow$ electron can first emit a magnon and by that process reverse its spin, becoming a spin-$\uparrow$ electron in the external frame of coordinates. The spectral weight produced by the first elementary process reduces the spectral weight of the high-energetic polaron peak therefore shifting spectral weight from the high-energetic

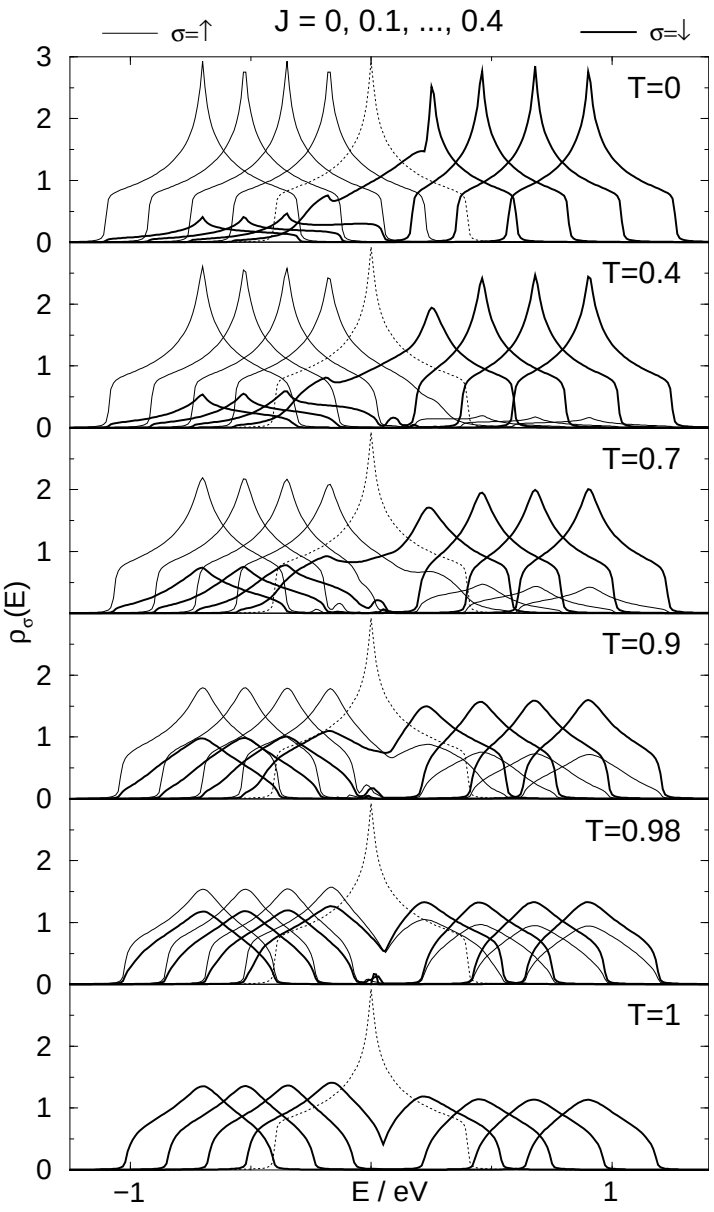

Figure 4.6: Density of states $\rho_\downarrow(E)$ of a sc(100) monolayer for different *s-f* interactions J (in eV) and for different temperatures (in units of T_C). The dotted lines represent the case of $J = 0$, where there is no distinction between spin-↓ and spin-↑ electron, $\rho_\downarrow(E) = \rho_\uparrow(E)$.

polaron peaks towards the low-energetic scattering peak.

For the spin-↑ electron we see from Fig. 4.6 that for increasing temperatures $T > 0$ an additional peak rises at the high-energetic side of the spectra. We can explain this effect by the spin-↑ electron absorbing a magnon and subsequently, as spin-↓ electron forming a polaron. Here the magnon absorption by a spin-↑ electron is equivalent to the magnon emission by a spin-↓ electron. In the case of ferromagnetic saturation the

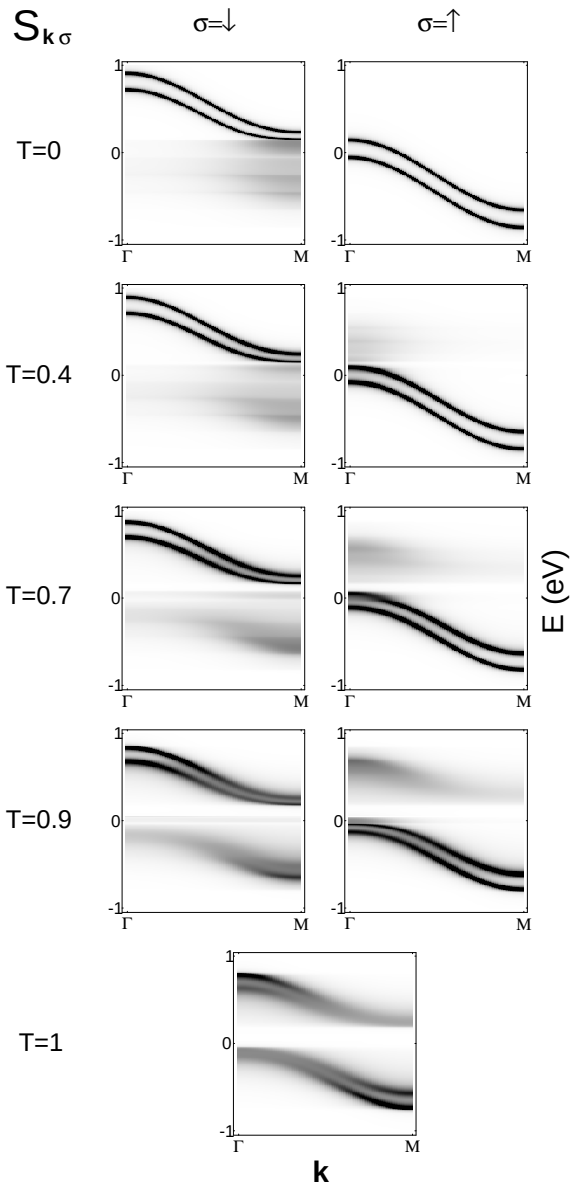

Figure 4.7: Spectral density, $S_{\mathbf{k}\sigma}(E) = S^{11}_{\mathbf{k}\sigma}(E) = S^{22}_{\mathbf{k}\sigma}(E)$, of a sc(100) double layer as a function of energy and wave vector from $\bar{\Gamma} = (0,0)$ to $\bar{\mathrm{M}} = (\pi,\pi)$ for $J = 0.2\,\mathrm{eV}$ and different temperatures (in units of T_C).

system does not contain any magnons, which is the reason why there is no scattering peak in the spin-↑ spectrum at $T = 0$. As a result of the shifting of spectral weights towards lower energies for the spin-↓ electron and towards higher energies for the spin-↑ electron the densities of states for the two spin directions approach each other with increasing temperature.

In the limiting case of $T \to T_\mathrm{C}$ the system has eventually lost its ability to distinct between the two possible spin directions of the test electron because of the loss of

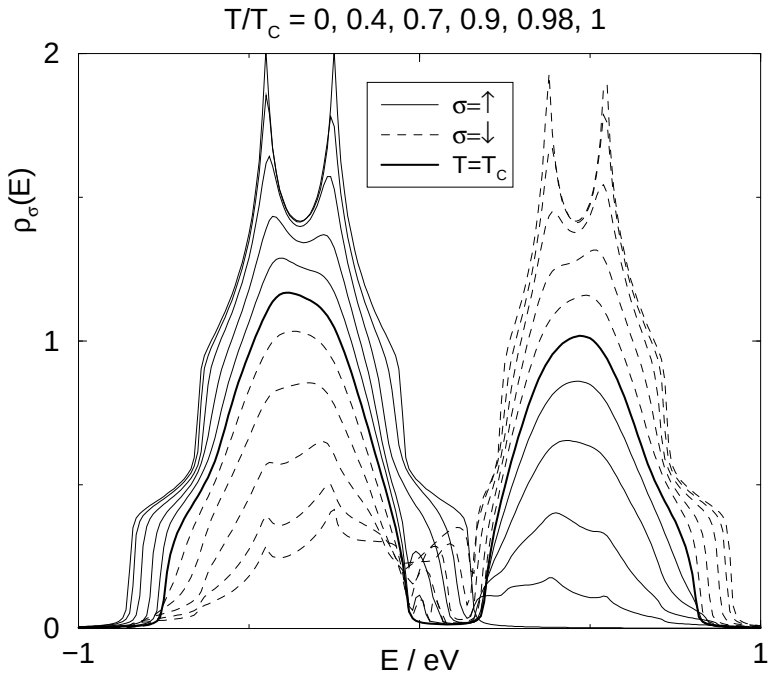

Figure 4.8: Density of states, $\rho_\downarrow(E) = \rho^1_\downarrow(E) = \rho^2_\downarrow(E)$, of a sc(100) double layer for $J = 0.2\,\mathrm{eV}$ and different temperatures (in units of T_C). The curves for $T = 0$ are furthest away from the paramagnetic solution, $T = T_\mathrm{C}$ (**bold** line).

magnetization of the underlying local-moment system, $\langle S^z \rangle \to 0$. Hence as for the case of vanishing *s-f* interaction for $T = T_\mathrm{C}$ the density of states of the spin-$\downarrow$ electron equals that of the spin-$\uparrow$ electron. Another feature which can be seen from Fig. 4.6 is that the positions of the four quasiparticle subbands, two for each spin direction, do not change with temperature.

To further discuss the temperature effects we present with Figs. 4.7 and 4.8 the spectral density and the local density of states, respectively, of a sc(100) double layer ($n = 2$) for $J = 0.2$ and different temperatures. Again we see that the spectra for the two spin directions approach each other for $T \to T_\mathrm{C}$. Another detail which can be observed in Fig. 4.6 is that the increase of temperature results in the narrowing of the subbands. For the case of intermediate coupling, $J = 0.2$, according to Figs. 4.7 and 4.8 this band narrowing results in the opening of a gap between the scattering and the polaron band with increasing temperature.

This temperature-enhanced band splitting has already been found for the three-dimensional case [84]. It can be explained for the spin-$\uparrow$ electron by the fact that for propagating in its own low-energetic subband it needs to find an appropriate lattice site. In the case of ferromagnetic saturation there is no restriction for the propagation of the spin-$\uparrow$ electrons since spin-flip processes are impossible. With increasing temperature there is an increasing deviation of the local moments resulting in the possible magnon absorption by the spin-$\uparrow$ electron and a subsequent change to the higher energetic

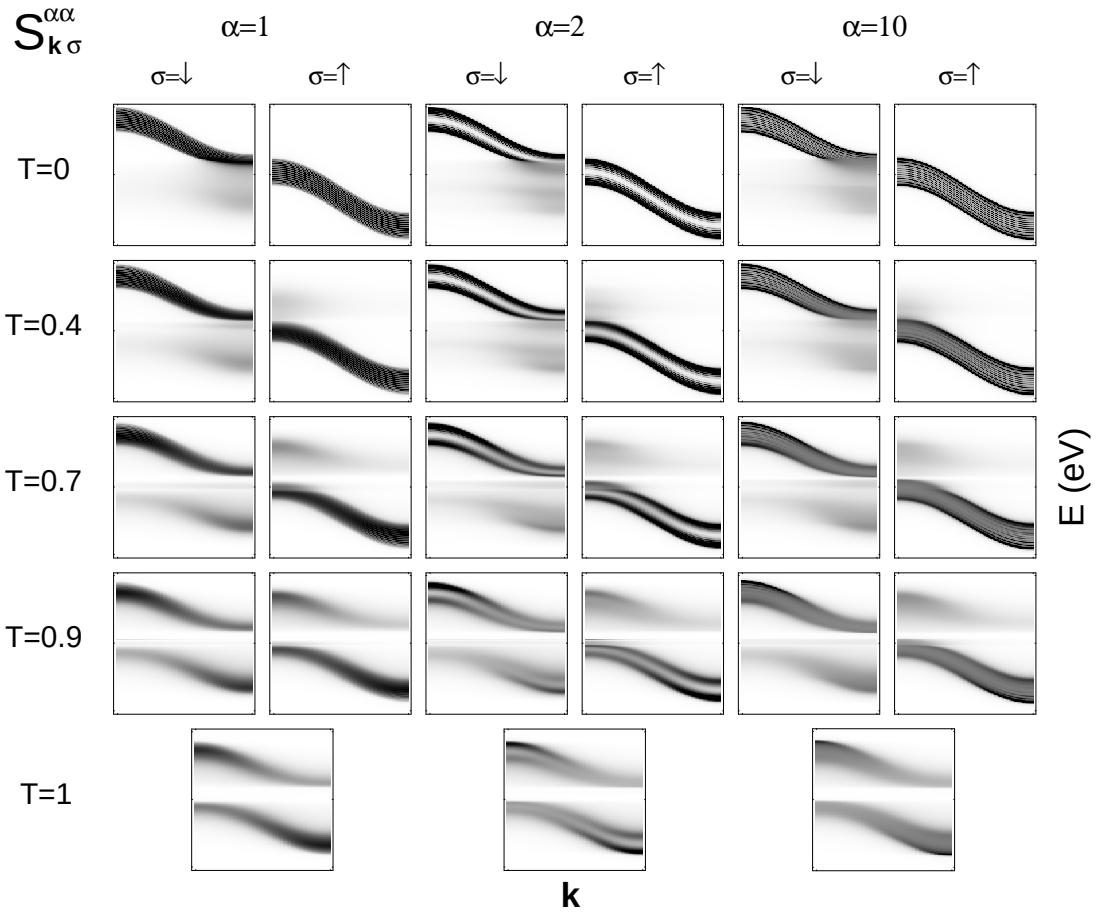

Figure 4.9: Spectral density, $S^{\alpha\alpha}_{\mathbf{k}\sigma}$, as a function of wavevector $\mathbf{k}$ from $\Gamma = (0,0)$ to $\mathrm{M} = (\pi,\pi)$ (horizontal axes) and energy E from $-1\,\mathrm{eV}$ to $1\,\mathrm{eV}$ (vertical axes) of the first ($\alpha = 1, 20$), second ($\alpha = 2, 19$), and center ($\alpha = 10, 11$) layer of a 20-layer sc(100) film for $J = 0.2\,\mathrm{eV}$ and different temperatures (in units of T_C).

polaron subband. Hence, the spin-↑ electron, to propagate in its own subband needs to move further distances with increasing temperature resulting in a reduced effective hopping and in a decreased bandwidth.

In addition to the discussed temperature effects, Figs. 4.7 and 4.8 exhibit a typical two-peak structure which is caused by the coupling of the two layers. This two-peak structure is replaced in the case of an n-layer film by an n-peak structure. Generally, the spectra of the discussed local-moment films are characterized by an interplay between correlation (J), temperature effects, and geometry of the film. Figs. 4.9 and 4.10 display results for the layer-dependent spectral density and the local density of states of a 20-layer sc(100) film. In addition to the dependence on the s-f exchange interaction and the temperature dependence we notice that the spectral density and the density of states show a typical layer dependence due to the broken translational symmetry at the surfaces of the film [94]. For the center layers ($\alpha = 10, 11$) of the 20-layer-film

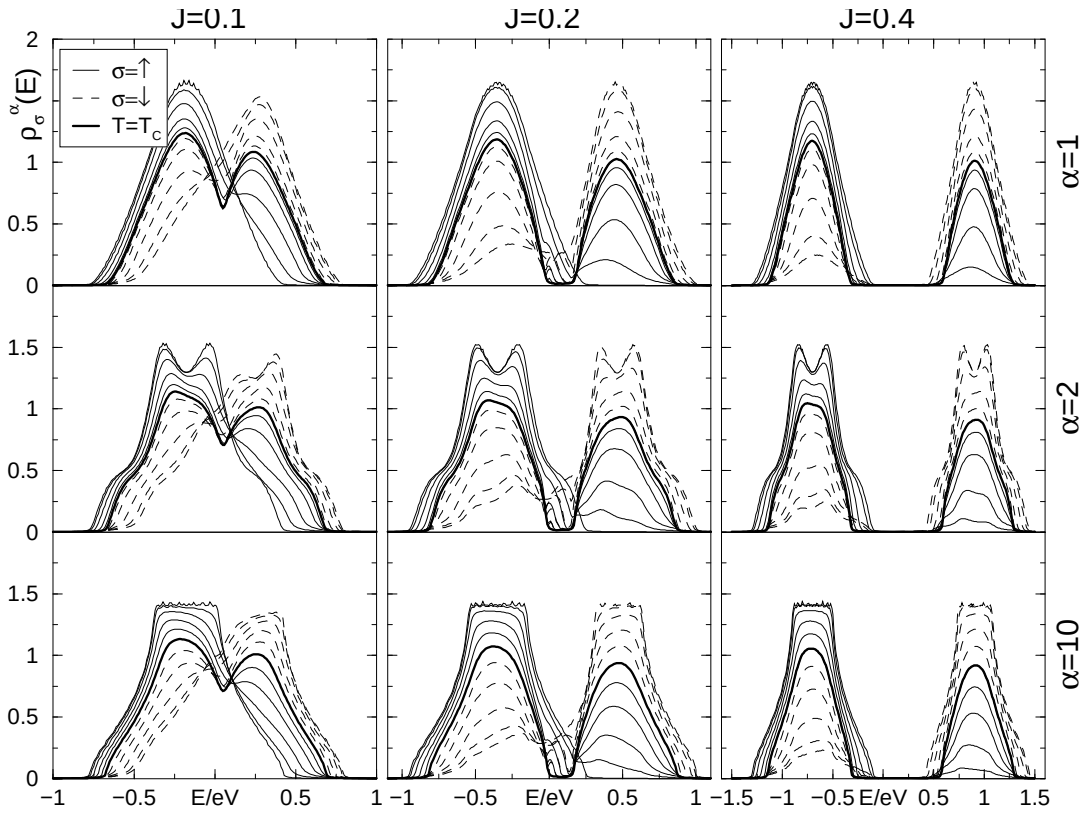

Figure 4.10: Local density of states, $\rho_\sigma^\alpha(E)$, of the first ($\alpha = 1, 20$), second ($\alpha = 2, 19$), and center ($\alpha = 10, 11$) layer of a 20-layer sc(100) film for different *s-f* interactions J and different temperatures $T/T_C = 0, 0.4, 0.7, 0.9, 0.98, 1$. The curves for $T = 0$ are furthest away from the paramagnetic solution, $T = T_C$ (**bold** lines).

we see from Fig. 4.10 that the local density of states of the spin-↑ electron at $T = 0$ has already become pretty similar to the well-known tight-binding density of states of the three-dimensional sc lattice whereas the density of states of the surface layers ($\alpha = 1, 20$) exhibits a semi-elliptic profile, which is typically observed for the local density of states at surfaces.

Whereas up to now we have assumed a hopping which is uniform within the whole film, according to Eq. (4.3), in the following section we will investigate the effects of modified hopping in the vicinity of the surfaces of the film.

4.2.1 Temperature-dependent surface states

Within the framework of the theory presented in Chapter 3 it is possible to describe surface states at the surface of a ferromagnetic semiconductor film like EuO. The aim is to give a contribution to the discussion on the temperature dependent behavior of a Gd(0001) surface state [34, 35, 36, 33, 37, 95, 96, 38, 39, 40, 41, 42]. Here, a thorough account on the surface magnetism and the surface electronic structure of the lanthanides

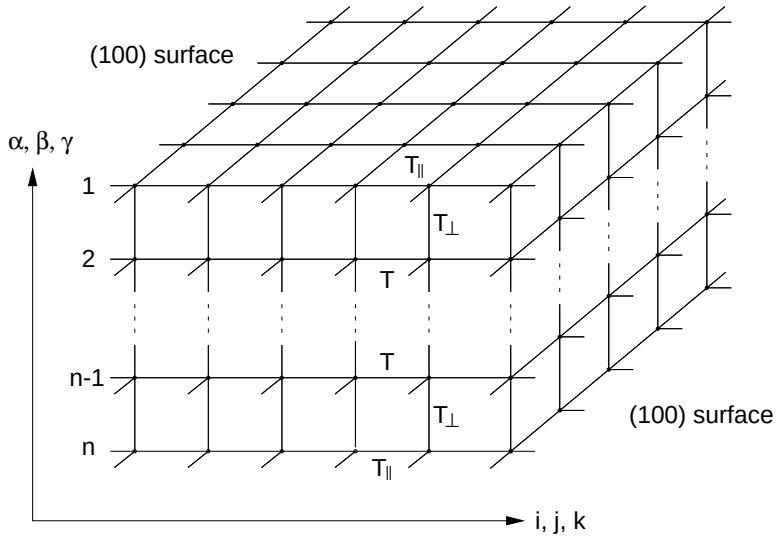

Figure 4.11: Model of an n-layer film with simple cubic structure. The nearest neighbor hopping is assumed to be $T_\parallel$ with in the surface layer, $T_\perp$ between the surface layer and the adjacent layer, and T within and between all other layers.

has been recently given by Dowben *et al.* [19].

The limitations of comparing the results on surface states obtained for a ferromagnetic semiconductor film to the experimental findings for the Gd(0001) surface state stem from the restriction of the theory from Chapter 3 to an empty conduction band, $n = 0$. However, it will be shown that the different observed scenarios for the temperature dependent behavior of the Gd(0001) surfaces states can be reproduced.

We still employ the tight-binding approximation for the hopping matrix elements, according to the first part of Eq. (4.3). However, the hopping in the vicinity of the surface will be allowed to vary,

$$T^{\alpha\beta} = \begin{pmatrix} T_\parallel & T_\perp & 0 & 0 & \cdots & 0 \\ T_\perp & T & T & & \ddots & \vdots \\ 0 & T & & \ddots & & 0 \\ 0 & & \ddots & & T & 0 \\ \vdots & \ddots & & T & T & T_\perp \\ 0 & \cdots & 0 & 0 & T_\perp & T_\parallel \end{pmatrix}, \tag{4.4a}$$

according to Fig. 4.11, and with

$$T_\parallel = \epsilon_\parallel T, \qquad T_\perp = \epsilon_\perp T. \tag{4.4b}$$

Here, $\epsilon_\parallel$ describes the variation of the hopping within the surface layer as compared to the uniform hopping in the center of the film and $\epsilon_\perp$ stands for the modification of the hopping between the surface layer and the layer nearest to the surface layer.

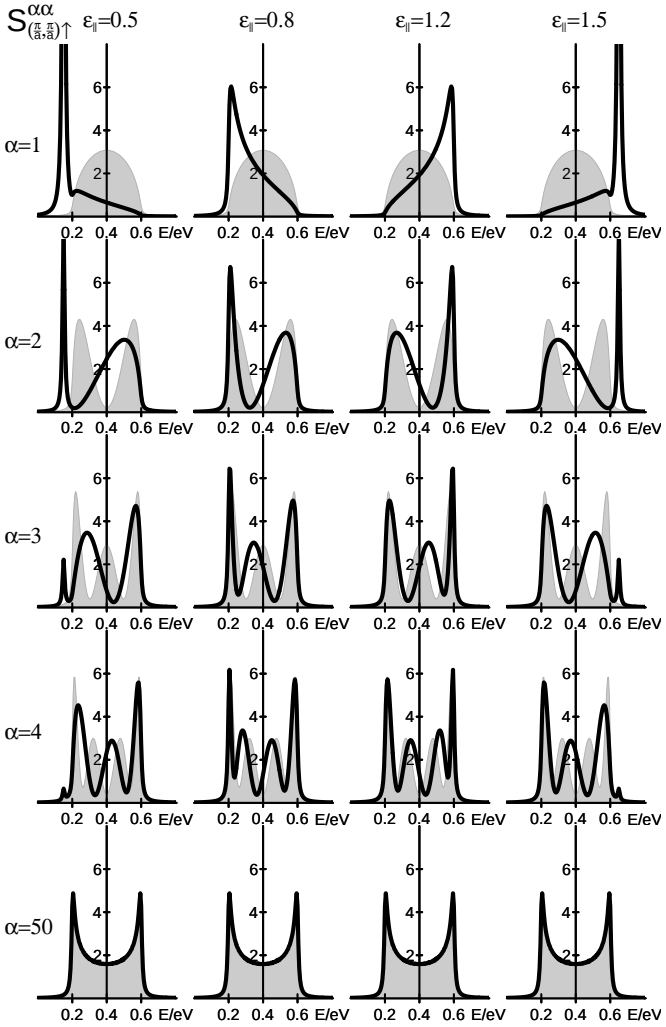

Figure 4.12: Local spin-↑ spectral densities, $S^{\alpha\alpha}_{\mathbf{k}\uparrow}$ of a 100-layer sc(100) film at the $\bar{\mathrm{M}}$-point for ($T = 0$; $J = 0$; $\alpha = 1,\ 2,\ 3,\ 4,\ 50$) as a function of energy. The hopping within the first layer is modified by the factor $\epsilon_{\|}$ whereas the hopping between the first and the second layer remains unchanged, $\epsilon_{\perp} \equiv 1$. The grey background shows the local spectral densities for the case of uniform hopping ($\epsilon_{\|} = \epsilon_{\perp} \equiv 1$).

In reality the variation of the hopping integrals in the vicinity of the surface may be caused e. g. by a relaxation of the interlayer distance. According to the scaling law $T \sim r^{-5}$ for the d-electrons [97] a relatively small top-layer relaxation $\Delta r/r$ may result in a strong change of the hopping integral T. Thus e. g. a relaxation of the Gd(0001) surface layer of 3-6 % (cf. [98] and references therein) would yield a modification of the hopping integrals of of up to 30 %.

For the exactly solvable case of a single electron in an otherwise empty conduction band and a ferromagnetically saturated f-spin system, $T = 0$, it can be shown that modifying the hopping in the vicinity of the surface according to Eqs. (4.4) leads to

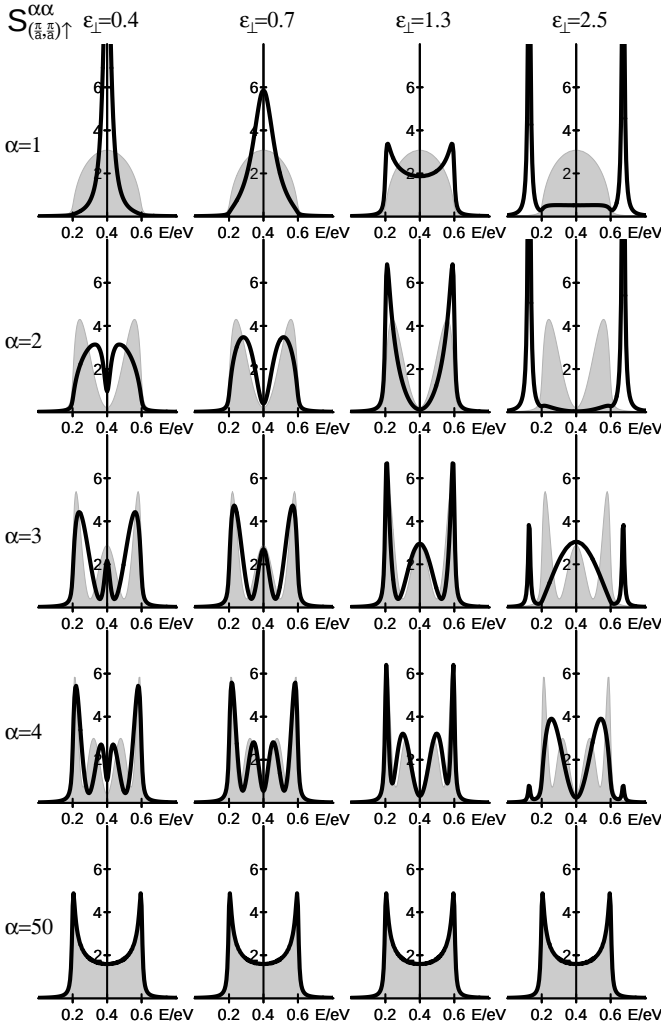

Figure 4.13: Same as Fig. 4.12 but for modified hopping between the first and the second layer according to $\epsilon_\perp$ and with unchanged hopping within the first layer, $\epsilon_\parallel \equiv 1$.

the appearance of surface states in the local spectral density $S^{\alpha\alpha}_{\mathbf{k}\sigma}$ [82, 99, 100, 101]. Modifying the hopping within the surface layer by more than 25 %, i. e. $\epsilon_\parallel \lessapprox 3/4$ or $\epsilon_\parallel \gtrapprox 5/4$, while keeping all the other hopping integrals unchanged results in a single surface state at the lower or the upper edge of the bulk band (cf. Fig. 4.12). This surface state first emerges at the $\bar{\Gamma}$- and at the $\bar{\mathrm{M}}$-point from the bulk band and from there spreads for larger modifications of $\epsilon_\parallel$ to the rest of the Brillouin zone.

On the other hand, when the hopping within the first layer remains constant, $\epsilon_\parallel \equiv 1$, but the hopping between the first and the second layer is significantly increased, $\epsilon_\perp \gtrapprox \sqrt{2}$, then two surface states split off one on each side of the bulk band (cf. Fig. 4.13). In this case the emergence of the surface states from the bulk band is **k**-independent [100]. Both types of surface states for the special case of $T = 0$ can be observed at the single bulk band and on the high-energetic polaron band for the case of

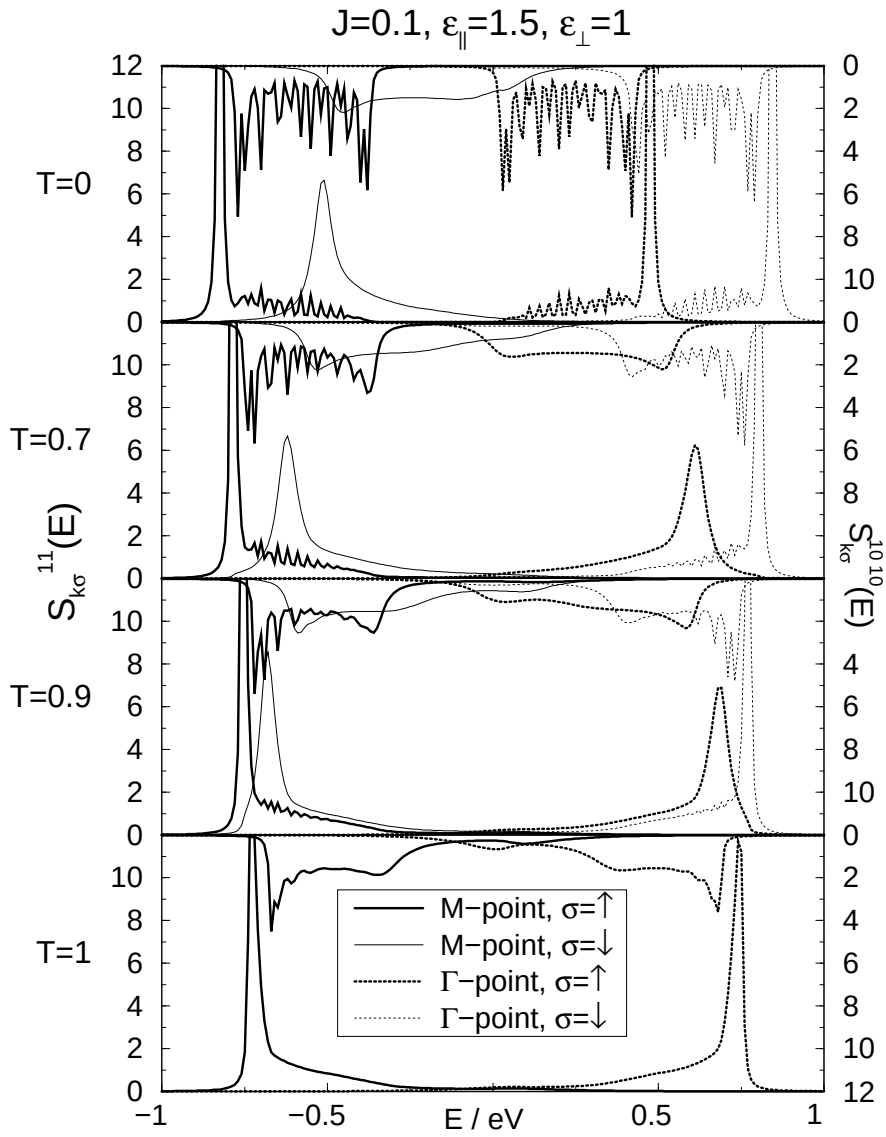

Figure 4.14: Local density of states, $S^{11}_{\mathbf{k}\sigma}(E)$ of the first layer of a 20-layer sc(100) film at the $\bar{\Gamma}$-point and the $\bar{\mathrm{M}}$-point for both spin directions and different temperatures, $T = 0,\ 0.7,\ 0.9,\ 1$ (in units of T_C) and modified hopping within the first layer, $\epsilon_\parallel = 1.5$, while $\epsilon_\perp \equiv 1$. Upside down but in the same scale, the respective local spectral densities of the center layer, $S^{10\,10}_{\mathbf{k}\sigma}(E)$, are displayed.

the spin-↑ electron and the spin-↓ electron, respectively. It should be noted that these findings can be proven analytically for the case of the spin-↑ electron [82, 101].

Figs. 4.14 to 4.16 show the temperature dependence of surface states for the different possible variations of the hopping in the vicinity of the surface. All the calculations for Figs. 4.14 to 4.16 have been performed for a 20-layer sc(100) film. The parameters for the uniform hopping according to Eqs. (4.4) and for the *s*-*f* exchange interaction are $T = -0.1$ and $J = 0.1$, respectively.

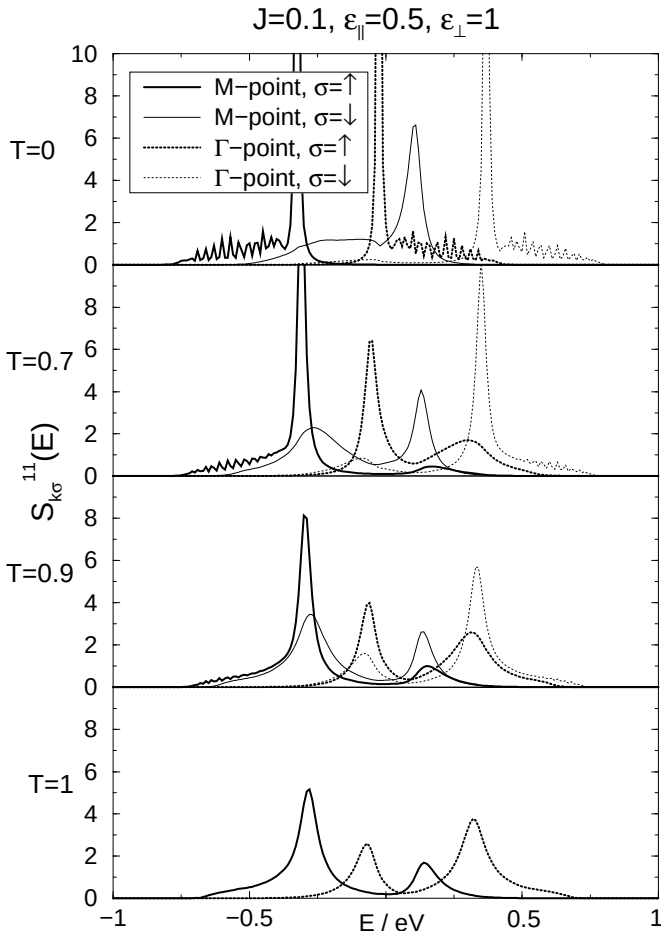

Figure 4.15: Local density of states, $S^{11}_{\mathbf{k}\sigma}(E)$ of the first layer of a 20-layer sc(100) film at the $\bar{\Gamma}$-point and the $\bar{\mathrm{M}}$-point for both spin directions and different temperatures, $T = 0,\ 0.7,\ 0.9,\ 1$ (in units of T_C) and modified hopping within the first layer, $\epsilon_\parallel = 0.5$, while $\epsilon_\perp \equiv 1$.

For the calculations we have employed a modification of the hopping in the surface layer and between the surface layer and the adjacent layer of 50 % ($\epsilon_\parallel = 0.5,\ 1.5$) and 100 % ($\epsilon_\perp = 2$), respectively (cf. Eq. (4.4b)). Such a drastic modification of the hopping integrals in the vicinity of the surface is rather unlikely to occur in reality. However, as has been shown in [99] the actual peak position of a surface states depends only weakly on the variation of $\epsilon_\parallel$ and $\epsilon_\perp$, respectively. The selected strong variation of the hopping parameters $T_\parallel$ and $T_\perp$ give rise to pronounced surface states which enable us to more clearly see the qualitative behavior of the surface states as a function of temperature.

In Fig. 4.14 we have the case that the hopping within the surface layer is enhanced by 50 %, leading to the existence of a surface state on the outer edge of the bulk dispersion. This surface state can most clearly be seen at the $\bar{\Gamma}$-point and the $\bar{\mathrm{M}}$-point in the two-dimensional Brillouin zone. In Fig. 4.14, the spectral density of the first

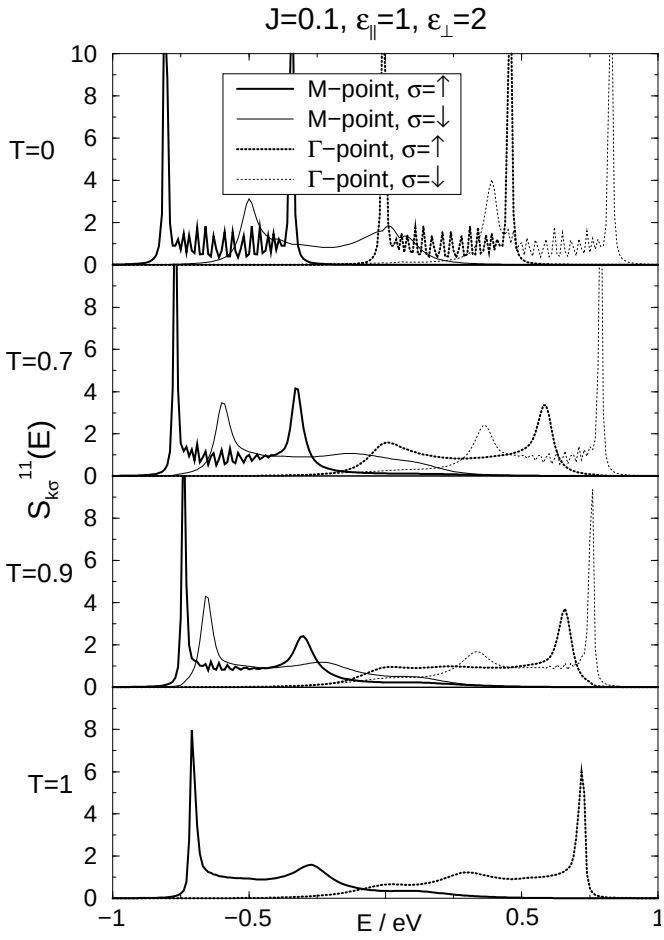

Figure 4.16: Same as Fig. 4.15 for modified hopping between the first and the second layer, $\epsilon_\perp = 2$, while $\epsilon_\parallel \equiv 1$.

layer, $S^{11}_{\mathbf{k}\sigma}(E)$, for both of these points is displayed as a function of energy. If the temperature is increased, we see that the position of the spin-↑ and of the spin-↓ surface states approach each other in a Stoner-like fashion until both peaks are equivalent for $T = T_\mathrm{C}$. The oscillations in the spectral densities, which can be seen in Fig. 4.14 around $-0.6\,\mathrm{eV}$, $0.3\,\mathrm{eV}$, and $0.7\,\mathrm{eV}$ are due to the finite thickness of our model film, as are the respective oscillations in Figs. 4.15 and 4.16.

Also in Fig. 4.14, but upside down, the spectral density of one of the center layers of the 20-layer film, $S^{10\,10}_{\mathbf{k}\sigma}(E)$, can be seen again for the $\bar{\Gamma}$-point and the $\bar{\mathrm{M}}$-point and both spin directions indicating that the positions of the surface states visible in $S^{11}_{\mathbf{k}\sigma}(E)$ lie outside of the bulk spectrum of the crystal for all temperatures. The same is valid for the spectra displayed in Figs. 4.15 and 4.16. In these figures, however, the local spectral densities of the central layers have been omitted for clarity.

In Fig. 4.15, the temperature dependence of surface states is documented for the case where the hopping within the first layer is reduced by 50 %, $\epsilon_\parallel = 0.5$ ($\epsilon_\perp \equiv 1$).

In this case we observe a spin-mixing behavior where the positions of the spin-↑ and of the spin-↓ surface states stay the same when the temperature is risen but spectral weight is being transferred between the different peaks. This results in equal populations of the spin-↓ and the spin-↑ peaks at $T = T_C$.

To round up the picture we see in Fig. 4.16 the case where the hopping between the first and the second layer is modified, $\epsilon_\perp = 2$, while the hopping within the first layer remains equal to the uniform hopping within the film, $\epsilon_\parallel \equiv 1$. Here we have for $T = 0$ two surface states, one on each side of the bulk spectrum. When the temperature is switched on the surface states on the outer side of the bulk dispersion behave Stoner-like, while the surface states on the inner side of the bulk dispersion exhibit a spin-mixing behavior.

Apparently, our model is able to reproduce a Stoner-like collapse of the spin-↓ and the spin-↑ peak positions for T_C as well as a spin-mixing behavior. In the spin-mixing case there are two peaks which both have a majority- and a minority-spin contribution. When the temperature is increased, the spectral weight of these contributions is altered until for $T = T_C$ for each peak the spin-↓ and the spin-↑ contributions have the same spectral weights.

In being able to reproduce both Stoner-like and spin-mixing behavior, depending on the variation of the hopping and the position in the Brillouin zone, our model calculations are in harmony with more recent (inverse) photoemission studies on Gd(0001) films which abandoned the grasp of earlier works that the temperature dependent behavior of the Gd(0001) surface state has to be either Stoner-like or of spin-mixing type [38, 39]. Especially, it has been shown here that for certain parameters it is possible to observe both kinds of behavior at the same time (see Fig. 4.16). This feature of our model calculation seems to be in strong agreement with a scenario proposed by Donath and Gubanka [38].

5 Theory for real systems

In Chapter 3 the theory of a model ferromagnetic semiconductor film based on the *s-f* model Hamiltonian according to Eqs. (3.2)–(3.5) has been presented. We now want to investigate the modifications which are necessary to extend the theoretical description to a *real* ferromagnetic semiconductor film. For the sake of being concrete we will focus on EuO. The presented theory applies, however, all the same to its "sister compound" EuS.

To start with the things which do not change, the Heisenberg Hamiltonian for the local-moment system in the form (3.4) or in the extended form (3.42) including the single-ion anisotropy is surely still an appropriate description for a local-moment system. For EuO the local moments are due to the exactly half-filled *4f*-shells of the Europium atoms. Since EuO has the NaCl crystal structure, these local moments form an fcc lattice.

The kinetic Hamiltonian $\mathcal{H}_s$ in the form (3.3) describes the conduction electrons as *s* electrons. For a real substance the kinetic Hamiltonian has therefore to be modified to allow for a realistic band structure to be incorporated into our model calculation. This band structure will in general include multiple conduction bands, adding the band indices m and m' to the kinetic Hamiltonian,

$$\mathcal{H}_s = \sum_{ij\alpha\beta} \sum_{mm'} T_{ij\alpha\beta}^{mm'} c_{i\alpha m\sigma}^{+} c_{j\beta m'\sigma} . \tag{5.1}$$

In the above equation, $c_{i\alpha m\sigma}^{+}$ and $c_{i\alpha m\sigma}$ are, respectively, the creation and annihilation operator of an electron with spin σ from the m-th subband of the atom at the lattice site $\mathbf{R}_{i\alpha}$. The $T_{ij\alpha\beta}^{mm'}$ describe the hopping between the m-th subband at the lattice site $\mathbf{R}_{i\alpha}$ and the m'-th subband at $\mathbf{R}_{j\beta}$. These hopping integrals have to be determined within a first-principles band-structure calculation, which will be done in Sec. 6.2.

The multiple conduction-band character of the kinetic Hamiltonian (5.1) implies that the *s-f* interaction also has to be modified from the single-conduction-band form (3.5). In the following section we want to derive the form of the *s-f* interaction for the case of a localized moment interacting with multiple conduction bands.

5.1 The multi-band *s-f* model

The fundamental interaction between electrons is the Coulomb interaction. We start from the general form of the Coulomb interaction for electrons at a single isolated lattice site,

$$\mathcal{H}_I = \tfrac{1}{2} \sum_{L_1 \ldots L_4} \sum_{\sigma\sigma'} U_{L_1 \ldots L4} c^+_{L_1\sigma} c^+_{L_2\sigma'} c_{L_3\sigma'} c_{L_4\sigma}, \tag{5.2}$$

since we want to keep the local character of the *s-f* interaction to be derived. The L_1, ..., L_4 denote the different bands of the atom and the $U_{L_1 \ldots L_4}$ are the Coulomb matrix elements.

We restrict the electron scattering processes caused by the Coulomb interaction to two involved subbands and get

$$\begin{aligned} \mathcal{H}_I = \tfrac{1}{2} \sum_{LL'\sigma\sigma'} \big[& U_{LL'} c^+_{L\sigma} c^+_{L'\sigma'} c_{L'\sigma'} c_{L\sigma} + J_{LL'} c^+_{L\sigma} c^+_{L'\sigma'} c_{L\sigma'} c_{L'\sigma} \\ & + J^*_{LL'} c^+_{L\sigma} c^+_{L\sigma'} c_{L'\sigma'} c_{L'\sigma} \big]. \end{aligned} \tag{5.3}$$

The band indices L and L' can be attributed either to a localized band or to a conduction band, with

$$L,\ L' = \begin{cases} m\colon & \text{conduction bands} \\ f\colon & \text{localized bands} \end{cases} \tag{5.4}$$

We can then split the Coulomb interactions into three different parts, depending on whether both L and L' are conduction bands, $\mathcal{H}_I^{CC}$, both belong to localized bands, $\mathcal{H}_I^{LL}$, or there is an interaction between localized and conduction bands involved, $\mathcal{H}_I^{CL}$,

$$\mathcal{H}_I = \mathcal{H}_I^{CC} + \mathcal{H}_I^{LL} + \mathcal{H}_I^{CL}. \tag{5.5}$$

The first of the three parts will yield no contribution, since for the case of a semiconductor the conduction bands are unoccupied, $n = 0$. The second term, $\mathcal{H}_I^{LL}$, is already contained in the description of the localized moments via the Heisenberg model. The third term is the only one which contains an interaction between the localized bands and the conduction bands. Using the nomenclature (5.4), it can be written in the form

$$\begin{aligned} \mathcal{H}_I^{CL} = \sum_{mf\sigma\sigma'} \Big[& U_{mf} c^+_{m\sigma} c^+_{f\sigma'} c_{f\sigma'} c_{m\sigma} + J_{mf} c^+_{m\sigma} c^+_{f\sigma'} c_{m\sigma'} c_{f\sigma} \\ & + \tfrac{1}{2} \big(J^*_{mf} c^+_{m\sigma} c^+_{m\sigma'} c_{f\sigma'} c_{f\sigma} + J^*_{fm} c^+_{f\sigma} c^+_{f\sigma'} c_{m\sigma'} c_{m\sigma} \big) \Big]. \end{aligned} \tag{5.6}$$

The last two terms of the above equation vanish for the special case of EuO,

$$J^*_{mf} c^+_{m\sigma} c^+_{m\sigma'} c_{f\sigma'} c_{f\sigma} = 0 \qquad \text{(Eu, Gd)}, \tag{5.7a}$$

$$J^*_{fm} c^+_{f\sigma} c^+_{f\sigma'} c_{m\sigma'} c_{m\sigma} = 0 \qquad (n = 0). \tag{5.7b}$$

Of these two, the first term yields no contribution since for Eu (as for Gd) the *4f* shell has its maximum spin of $S = 7/2$. As a result of the Pauli principle, all electrons

have to occupy different subbands and none of the 7 subbands of the *4f* shell will be doubly occupied. The second term disappears due to the fact that the conduction band is unoccupied, $n = n_m = 0$.

Using Eqs. (5.7) together with the relations for the electron spin operators,

$$\begin{aligned} \sigma^+ &= c_\uparrow^+ c_\downarrow = \sigma^x + i\sigma^y, \\ \sigma^- &= c_\downarrow^+ c_\uparrow = \sigma^x - i\sigma^y, \end{aligned} \qquad \sigma^z = \tfrac{1}{2}(n_\uparrow - n_\downarrow), \tag{5.8}$$

Eq. (5.6) can be written in the form

$$\mathcal{H}_I^{CL} = \sum_{mf} \Big[U_{mf} n_m n_f - J_{mf} \big(\sigma_m^+ \sigma_f^- + \sigma_m^- \sigma_f^+ + n_{m\uparrow} n_{f\uparrow} + n_{m\downarrow} n_{f\downarrow} \big) \Big], \tag{5.9}$$

where $n = n_\uparrow + n_\downarrow$. Using once more Eqs. (5.8) one arrives at

$$\mathcal{H}_I^{CL} = -2 \sum_{mf} J_{mf} \boldsymbol{\sigma}_m \cdot \boldsymbol{\sigma}_f + \sum_{mf} \big(U_{mf} - \tfrac{1}{2} J_{mf} \big) n_m n_f. \tag{5.10}$$

Here, the last term disappears due to $n = n_m = 0$. By defining the spin operator $\mathbf{S}$ of the local moment which can be attributed to the localized bands as

$$\mathbf{S} = \hbar \sum_f \boldsymbol{\sigma}_f, \tag{5.11}$$

and by assuming the inter-band exchange J_{mf} between the conduction bands and the localized bands to be independent on the band indices m and f,

$$J_{mf} \equiv \frac{J}{2}, \tag{5.12}$$

the inter-band interaction between the localized bands and the conduction bands (5.10) can be written in the final form

$$\mathcal{H}_I^{CL} = -\frac{J}{\hbar} \sum_m \boldsymbol{\sigma}_m \cdot \mathbf{S}. \tag{5.13}$$

Eq. (5.13) represents the inter-band exchange interaction between the localized bands and the conduction bands at a single, e. g. Eu, site. To get the respective Hamiltonian of the whole crystal, we have to sum Eq. (5.13) over all the lattice sites $\mathbf{R}_{i\alpha}$ of the Eu atoms and end up with the Hamiltonian for the multi-band *s-f* interaction

$$\mathcal{H}_{sf} = -\frac{J}{\hbar} \sum_{i\alpha m} \boldsymbol{\sigma}_{i\alpha m} \cdot \mathbf{S}_{i\alpha}. \tag{5.14}$$

Comparing the above Hamiltonian with the Hamiltonian of the single-band *s-f* model (3.5) we see that Hamiltonian of the multi-band *s-f* interaction (5.14) features an additional sum over the different conduction bands.

5.2 Modifications of the original theory

Gathering the information obtained so far in this chapter, the Hamiltonian of the multi-band s-f model for film geometries consists of three parts,

$$\begin{aligned}\mathcal{H} =& \mathcal{H}_s + \mathcal{H}_{sf} + \mathcal{H}_f^* \\ =& \sum_{ij\alpha\beta}\sum_{mm'} T_{ij\alpha\beta}^{mm'} c_{i\alpha m\sigma}^{+} c_{j\beta m'\sigma} - \frac{J}{\hbar}\sum_{i\alpha m} \boldsymbol{\sigma}_{i\alpha m}\cdot \mathbf{S}_{i\alpha} + \mathcal{H}_f^*, \end{aligned} \tag{5.15}$$

where the Hamiltonian of the localized moments consists of a Heisenberg part and an anisotropy contribution, $\mathcal{H}_f^* = \mathcal{H}_f + \mathcal{H}_A$, as defined in Eq. (3.42).

As a result, there are no changes necessary to the theory of the local-moment system as presented in Sec. (3.2.2). In contrast, the theory for the electronic subsystem from Sec. (3.2.1) has to be modified to account for the multiple conduction-band character of both the kinetic and the s-f part of the multi-band s-f Hamiltonian (5.15).

To find the solution for the electronic subsystem for the case of the multi-band s-f model we formally introduce the operator $\mathbf{S}_{i\alpha m}$ in the multi-band s-f interaction,

$$\mathcal{H}_{sf} = -\frac{J}{\hbar}\sum_{i\alpha m} \boldsymbol{\sigma}_{i\alpha m}\cdot \mathbf{S}_{i\alpha m}, \qquad \mathbf{S}_{i\alpha m} \equiv \mathbf{S}_{i\alpha}. \tag{5.16}$$

By introducing the multi-indices $\mathcal{A}$, $\mathcal{B}$, ..., defined by $(\alpha, m) \to \mathcal{A}$, $(\beta, m') \to \mathcal{B}$, ..., the solution for the electronic subsystem of the single-band s-f model presented in Sec. 3.2.1 can be transferred to the case of the multi-band s-f model, with the correspondences $\alpha \mathrel{\widehat{=}} \mathcal{A}$, $\beta \mathrel{\widehat{=}} \mathcal{B}$, etc.

The reason for this straightforward transference is that the commutator relations which govern the solution presented in Sec. 3.2.1 are invariant under the index transition, e. g.

$$\begin{aligned}[c_{i\alpha\sigma}, \mathcal{H}_{sf}^{\mathrm{sb}}]_- &= -\frac{J}{2}\left(z_\sigma S_{i\alpha}^z c_{i\alpha\sigma} + S_{i\alpha}^{-\sigma} c_{i\alpha-\sigma}\right), \\ [c_{i\mathcal{A}\sigma}^{+}, \mathcal{H}_{sf}^{\mathrm{mb}}]_- &= -\frac{J}{2}\left(z_\sigma S_{i\alpha}^z c_{i\alpha m\sigma} + S_{i\alpha}^{-\sigma} c_{i\alpha m-\sigma}\right) = -\frac{J}{2}\left(z_\sigma S_{i\mathcal{A}}^z c_{i\mathcal{A}\sigma} + S_{i\mathcal{A}}^{-\sigma} c_{i\mathcal{A}-\sigma}\right).\end{aligned}$$

Slight modifications compared to the case of the single-band s-f model occur in the calculation of the spectral moments (3.30) needed for the coefficients in Eqs. (3.32) (cf. [82]). However, the form of the coefficients will stay the same.

As a result, we get the solution of the electronic subsystem in an analogous form to Eqs. (3.37) and (3.38). Different to the case of the single-band s-f model the respective implicit set of matrix equations for the determination of the self-energy for the case of the multi-band s-f model with L conduction bands in an n-layer film consists of $(n \times n)$ matrices with $(L \times L)$ blocks as the matrix elements.

5.3 Brief introduction to density-functional theory

The hopping matrix elements $T_{ij\alpha\beta}^{mm'}$ from the kinetic Hamiltonian (5.1) have to be calculated within a first-principles band-structure calculation. In this section we want to introduce the basic concepts of density-functional theory and give an overview over some of the most common band-structure techniques. An overview over the field of density-functional theory can be found e. g. in [102, 103, 104, 105, 106, 107], whereas selected band-structure techniques are reviewed in [107, 108, 109, 110, 111, 112].

The fundamentals of density-functional theory (DFT) are due to Hohenberg and Kohn [113] and Kohn and Sham [114] and can be described as a reduction of the complicated many-body problem of interacting electrons to a set of effective single-particle problems. We consider a system of N interacting electrons moving in some fixed external potential v_{ext}, described by the Hamiltonian

$$\mathcal{H} = \mathcal{T} + \mathcal{U} + \mathcal{V} = \sum_i \Big(-\frac{\hbar^2}{2m}\nabla_i^2 \Big) + \frac{1}{2}\frac{e^2}{4\pi\epsilon_0}\sum_{ij}^{i\neq j}\frac{1}{|\mathbf{r}_i - \mathbf{r}_j|} + \sum_i v_{\text{ext}}(\mathbf{r}_i). \quad (5.17)$$

Here, $\mathcal{T}$ is the kinetic energy, $\mathcal{U}$ is the electron-electron Coulomb repulsion, and $\mathcal{V}$ is the interaction with the external potential, which includes the electrostatic interactions with the fixed nuclei.

Firstly, Hohenberg and Kohn [113] showed that the external potential is a unique functional of the electron density $n(\mathbf{r})$. Furthermore, the ground state ϕ and the energy functionals

$$E[n] = \langle\phi|\mathcal{H}|\phi\rangle = F[n] + \int v_{\text{ext}}(\mathbf{r})n(\mathbf{r})\mathrm{d}\mathbf{r}, \quad (5.18)$$

$$F[n] = \langle\phi|\mathcal{T} + \mathcal{U}|\phi\rangle, \quad (5.19)$$

are unique functionals of $n(\mathbf{r})$, with $E[n]$ assuming its minimal value E for the correct ground state density.

By defining yet another functional, the Hartree contribution can be separated from the functional $F[n]$,

$$F[n] = \frac{e^2}{8\pi\epsilon_0}\iint\frac{n(\mathbf{r})n(\mathbf{r}')}{|\mathbf{r}-\mathbf{r}'|}\mathrm{d}\mathbf{r}\mathrm{d}\mathbf{r}' + G[n]. \quad (5.20)$$

Thus, the newly defined functional $G[n]$ represents the kinetic energy plus the difference between the true interaction energy and that given by the Hartree interaction.

The theorem by Hohenberg and Kohn [113] applies equally to the case of non-interacting electrons, given by the Hamiltonian

$$\mathcal{H}_s = \mathcal{T} + \mathcal{V} = \sum_i \Big(-\frac{\hbar^2}{2m}\nabla_i^2 \Big) + \sum_i v_{\text{s}}(\mathbf{r}_i), \quad (5.21)$$

where $v_s(\mathbf{r}_i)$ is the external potential of the free system. The ground state ϕ_s of this single-particle problem is obtained by populating the lowest lying one-electron orbitals defined by the Schrödinger equation

$$\Big[-\frac{\hbar^2}{2m}\nabla^2 + v_s(\mathrm{r})\Big]\psi_j(\mathbf{k},\mathbf{r}) = E_j(\mathbf{k})\psi_j(\mathbf{k},\mathbf{r}), \tag{5.22}$$

with the density given by

$$n(\mathbf{r}) = \sum_{j\mathbf{k}}^{\text{occ.}} |\psi_j(\mathbf{k},\mathbf{r})|^2. \tag{5.23}$$

Kohn and Sham [114] considered the system of non-interacting electrons (5.21) together with the real system of interacting electrons and proceeded to determine the external potential $v_s(\mathbf{r})$ such that Eq. (5.23) constitutes also the ground state density of the real system. Within their approach, the functional $G[n]$ is written in the form

$$G[n] = T_s[n] + E_{xc}[n], \tag{5.24}$$

where $T_s[n]$ is the kinetic energy functional of the non-interacting electrons,

$$T_s[n] = \langle\phi_s|\mathcal{T}|\phi_s\rangle = \sum_{j\mathbf{k}}^{\text{occ.}} \int \psi_j^*(\mathbf{k},\mathbf{r})(-\frac{\hbar^2}{2m}\nabla^2)\psi_j(\mathbf{k},\mathbf{r})\mathrm{d}\mathbf{r}, \tag{5.25}$$

and $E_{xc}[n]$ is the so-called exchange-correlation energy functional. The latter describes the difference between the true kinetic energy and that of the non-interacting system plus the difference between the true interaction energy and that included by the Hartree contribution. Within the local-density approximation (LDA), the homogeneous electron gas serves to model the exchange-correlation energy in the form

$$E_{xc}[n] = \int \epsilon_{xc}(n(\mathbf{r}))n(\mathbf{r})\mathrm{d}\mathbf{r}. \tag{5.26}$$

The above equation may be viewed as dividing the inhomogeneous interacting electron gas into small boxes, each containing a homogeneous electron gas with a density $n(\mathbf{r})$. This approximation is correct in the limit of slowly varying densities.

Collecting together all the above assumptions and definitions, we can write the energy functional $E[n]$ in the form

$$E[n] = \langle\phi_s|\mathcal{T}|\phi_s\rangle + \int\left\{\frac{e^2}{8\pi\epsilon_0}\int\frac{n(\mathbf{r}')}{|\mathbf{r}-\mathbf{r}'|}\mathrm{d}\mathbf{r}' + v_{ext}(\mathbf{r}) + \epsilon_{xc}(n(\mathbf{r}))\right\}n(\mathbf{r})\mathrm{d}\mathbf{r}. \tag{5.27}$$

Minimization with respect to the density $n(\mathbf{r})$ leeds to the effective single-particle Schrödinger equation

$$\Big[-\frac{\hbar^2}{2m}\nabla^2 + \frac{e^2}{4\pi\epsilon_0}\int\frac{n(\mathbf{r}')}{|\mathbf{r}-\mathbf{r}'|}\mathrm{d}\mathbf{r}' + v_{ext}(\mathbf{r}) + v_{xc}(n(\mathbf{r}))\Big]\psi_j(\mathbf{k},\mathbf{r}) = E_j(\mathbf{k})\psi_j(\mathbf{k},\mathbf{r}) \tag{5.28}$$

Comparing the above equation with Eq. (5.22) we see that the electrons move in the effective potential

$$v_s(\mathbf{r}) = v_H(\mathbf{r}) + v_{ext}(\mathbf{r}) + v_{xc}(n(\mathbf{r})), \tag{5.29}$$

with the Hartree potential,

$$v_H(\mathbf{r}) = \frac{e^2}{4\pi\epsilon_0} \int \frac{n(\mathbf{r}')}{|\mathbf{r} - \mathbf{r}'|} d\mathbf{r}', \tag{5.30}$$

and with the exchange-correlation potential $v_{xc}(n(\mathbf{r}))$ defined by

$$v_{xc}(\mathbf{r}) = \frac{d[n\epsilon_{xc}(n)]}{dn} \equiv \mu_{xc}[n(\mathbf{r})]. \tag{5.31}$$

Here, $\mu_{xc}[n(\mathbf{r})]$ is the exchange correlation part of the chemical potential in a homogeneous electron gas of density $n(\mathbf{r})$. Useful estimates of ϵ_{xc} and μ_{xc} have been given e. g. by Hedin and Lundqvist [115].

Within a self-consistent band-structure calculation one starts from a reasonable starting potential $v_s(\mathbf{r})$ for which the single-particle Schrödinger equation (5.22) is solved. Eq. (5.23) is then used to calculate the respective density of states $n(\mathbf{r})$ from which, using Eqs. (5.30) and (5.31), respectively, the Hartree potential v_H and the exchange-correlation potential v_{xc} can be computed. Together with Eq. (5.29) these give a new effective potential v_s for which the whole procedure is started anew etc.

The presented density-functional formalism may be extended to a spin-density formalism in which the spin-up and the spin-down densities $n_\uparrow(\mathbf{r})$ and $n_\downarrow(\mathbf{r})$ are the independent variables. As a result of the respective theory the exchange-correlation potential becomes spin-dependent,

$$v_{xc}^\sigma(n_\uparrow, n_\downarrow) = \frac{d[n\epsilon_{xc}(n_\uparrow, n_\downarrow)]}{dn_\sigma}, \tag{5.32}$$

with useful estimates given e. g. by von Barth and Hedin [116] and by Gunnarsson and Lundqvist [117].

Energy-band methods

The various band-structure methods are realizations of the discussed self-consistency cycle and differ from each other as to how the Schrödinger equation (5.22) is solved. They can be divided into those which express the wave functions as linear combinations of some fixed basis functions, and the classical methods, which employ matching of partial waves.

The classical approach is based on the approximate spherical symmetry of the effective potential (5.29), which applies especially to closed packed systems. As a result, the wave functions of the Schrödinger equation (5.22) at energy E and inside the

atomic polyhedron at the position **R** can be expressed in the form

$$\psi_j(\mathbf{k},\mathbf{r}) = \sum_{lm} b_{Rlm}^{j\mathbf{k}} \psi_{Rl}(E, |\mathbf{r}-\mathbf{R}|) \mathrm{i}^l Y_l^m(\widehat{\mathbf{r}-\mathbf{R}}) \tag{5.33}$$

with the spherical harmonics Y_l^m and the solutions of the radial Schrödinger equation ψ_{Rl}. In the *cellular method* [118, 119] the spherical symmetry of the potential is extended all the way to the boundaries of the atomic polyhedron. For a given Bloch vector **k**, the one-electron energies $E_j(\mathbf{k})$ of the system are now those values for which the coefficients of the Fourier series for the wave function $\psi_j(\mathbf{k},\mathbf{r})$ can be adjusted in such a way that the resulting wave function is continuous and differentiable across the boundary of the atomic polyhedron. The resulting complicated boundary conditions, however, have rendered the method little used in practice.

In the *augmented plane-wave* (APW) method [120] the troublesome boundary conditions of the cellular method are overcome by inscribing a so-called muffin-tin (MT) sphere in each atomic polyhedron. Inside the sphere the potential is assumed to be spherically symmetric and the wave functions are expanded as spherical harmonics. In the interstitial region, outside the spheres, the potential is assumed to be flat or slowly varying and a plane-wave expansion is used. As a result, the boundary conditions are transformed into a much more practical matching of the wave functions at the muffin-tin sphere. Other partial-waves approaches include the *Korringa-Kohn-Rostoker* (KKR) method [121, 122], where the difference with respect to the APW method is that in the interstitial region the wave functions are expanded in spherical waves.

In the linear band-structure methods the energy dependence of the basis functions (cf. Eq. (5.33)) from which the wave functions are constructed is neglected. Thus, the solution of the Schrödinger equation (5.22) is reduced to an algebraic eigenvalue problem. As a result, the linear methods vastly outperform the classical methods, at the price of slight inaccuracies.

Within the *linear combination of atomic orbitals* (LCAO) method [123, 124] one uses as basis functions the eigenfunctions of the bound states of the free atom. However, due to difficulties in the implementation of the LCAO method [110], it was not until the *linear muffin-tin orbital* (LMTO) and the *linear augmented plane-wave* (LAPW) method devised by Andersen [125] that the linear methods became widely used. In the LMTO method, the fixed basis set consists of muffin-tin orbitals. Inside the muffin-tin sphere the muffin-tin orbitals are constructed from partial waves and their first energy derivatives whereas outside the spheres they are spherical waves at fixed energy. Within the so-called *atomic sphere approximation* (ASA) the interstitial region is eliminated by allowing the muffin-tin spheres to overlap. The resulting band-structure technique is referred to as the LMTO-ASA. Further linear methods include the KKR-ASA, which is a variation of the LMTO-ASA method, and the *augmented spherical-wave* (ASW) method [126].

6 Calculations for EuO films

In this chapter we want to apply the theory for a real ferromagnetic semiconductor film presented in chapter 5 to EuO films. In Sec. 6.1 the calculation of the temperature dependence of the local-moment system presented in Sec. 4.1 for a model film will be tailored to the special situation in fcc EuO, where the next-nearest neighbor exchange interactions have to be taken into account. The following Sec. 6.2 is devoted to the band-structure calculations for bulk EuO and EuO films. Finally, in Sec. 6.3 we will combine the obtained $T = 0$ band structures with the *s-f* model calculation to obtain the temperature-dependent band structure of EuO films.

The europium chalcogenides crystallize in the NaCl crystal structure. Hence, the europium atoms are arranged on an fcc lattice. For all film calculations presented in this chapter, we assume the surfaces of the fcc film to be parallel to the fcc(100) crystal plane and refer to these films as fcc(100) or EuO(100) films.

6.1 Magnetic properties

The calculation of the magnetic properties of the EuO films follows the theory presented in Sec. 3.2.2. The main difference compared to the calculations for a model film presented in Sec. 4.1 is, however, that for EuO as well as for the other europium chalcogenides we have to take into account the next-nearest neighbor interactions J_2 in addition to the nearest neighbor interactions J_1 (cf. Eq. (2.3)) [61,62,63,60,91]. For the two ferromagnetic europium chalcogenides, we find [91]

$$\begin{aligned} &\text{EuO:} \quad J_1/k_\mathrm{B} = 0.625\,\mathrm{K}, \;\; J_2/k_\mathrm{B} = 0.125\,\mathrm{K}; \\ &\text{EuS:} \quad J_1/k_\mathrm{B} = 0.221\,\mathrm{K}, \;\; J_2/k_\mathrm{B} = -0.100\,\mathrm{K}. \end{aligned} \tag{6.1}$$

These values for J_1 and J_2 have been calculated by applying the renormalized spin-wave theory [91] to low-temperature neutron scattering experiments measuring the spin-wave dispersion, e. g. [61,62,63,60].

For a fcc(100) film, we have for the case of uniform J_1 and J_2 within the film, in analogy to Eqs. (4.1) and (4.2),

$$J_{ij}^{\alpha\beta} = \delta_{i,j+\Delta_{1\parallel}}^{\alpha\beta} J_1 + \delta_{i,j+\Delta_{1\perp}}^{\alpha,\beta\pm1} J_1 + \delta_{i,j+\Delta_{2\parallel}}^{\alpha\beta} J_2 + \delta_{ij}^{\alpha,\beta\pm2} J_2. \tag{6.2}$$

Here, $\Delta_{1\parallel}$, $\Delta_{1\perp}$ and $\Delta_{2\parallel}$ denote the relative parallel positions of nearest neighbors within the same layer, of nearest neighbors within the adjacent layers and of next

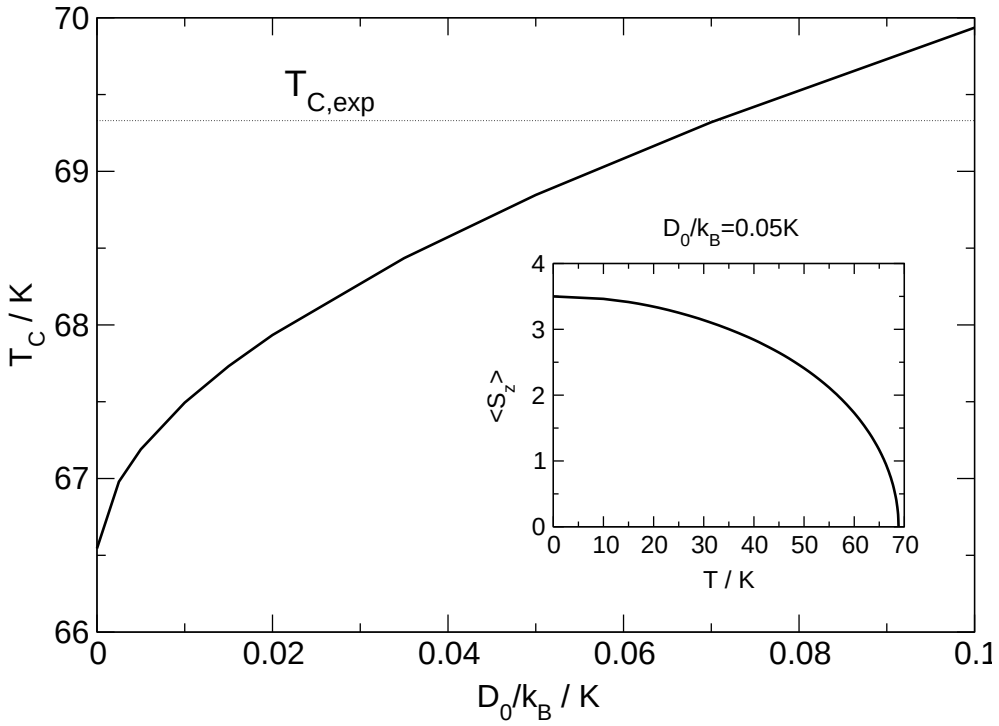

Figure 6.1: Dependence of the Curie temperature T_C on the single-ion anisotropy constant, D_0, calculated for bulk EuO including next-nearest neighbor interaction ($J_1/k_B = 0.625\,\mathrm{K}$, $J_2/k_B = 0.125\,\mathrm{K}$). The dotted line represents the experimental T_C [47]. **Inset:** Magnetization of bulk EuO as a function of temperature, calculated for $D_0/k_B = 0.05\,\mathrm{K}$.

nearest neighbors within the same layer, respectively,

$$\Delta_{1\parallel} = (\tfrac{1}{2}, \tfrac{1}{2}),\ (\tfrac{1}{2}, \bar{\tfrac{1}{2}}),\ (\bar{\tfrac{1}{2}}, \tfrac{1}{2}),\ (\bar{\tfrac{1}{2}}, \bar{\tfrac{1}{2}}), \qquad \Delta_{1\perp} = (0, \tfrac{1}{2}),\ (0, \bar{\tfrac{1}{2}}),\ (\tfrac{1}{2}, 0),\ (\bar{\tfrac{1}{2}}, 0),$$
$$\Delta_{2\parallel} = (0, 1),\ (0, \bar{1}),\ (1, 0),\ (\bar{1}, 0) \qquad (\Delta_{2\perp} = (0, 0)).$$

To determine a reasonable single-ion anisotropy constant D_0 for the case of EuO, in Fig. 6.1 the Curie temperature of bulk EuO calculated for the J_1 and J_2 values from Eq. (6.1) and for different values of D_0 is shown. As can be seen from Fig. 6.1, when increasing D_0/k_B from 0 to 0.1 K the Curie temperature rises from about 66.5 K to about 70 K. It should be stressed once again that the used values for J_1 and J_2 stem from low-temperature measurements of the spin-wave dispersion [91]. In this respect the agreement between the calculated Curie temperatures and the experimental value of $T_{C,\mathrm{exp}} = 69.33\,\mathrm{K}$ [47] which is documented in Fig. (6.1) is more than satisfying.

A side effect of this good agreement is that as long as $D_0 > 0$ we don't really have to be concerned with the choice of D_0/k_B within the range displayed in Fig. 6.1. Thus, for the further calculations for film geometries we have chosen $D_0/k_B = 0.05\,\mathrm{K}$, with the respective magnetization curve for bulk EuO plotted in the inset of Fig. 6.1. However, in the following, we still want to compare the chosen anisotropy constant to the spare experimental values.

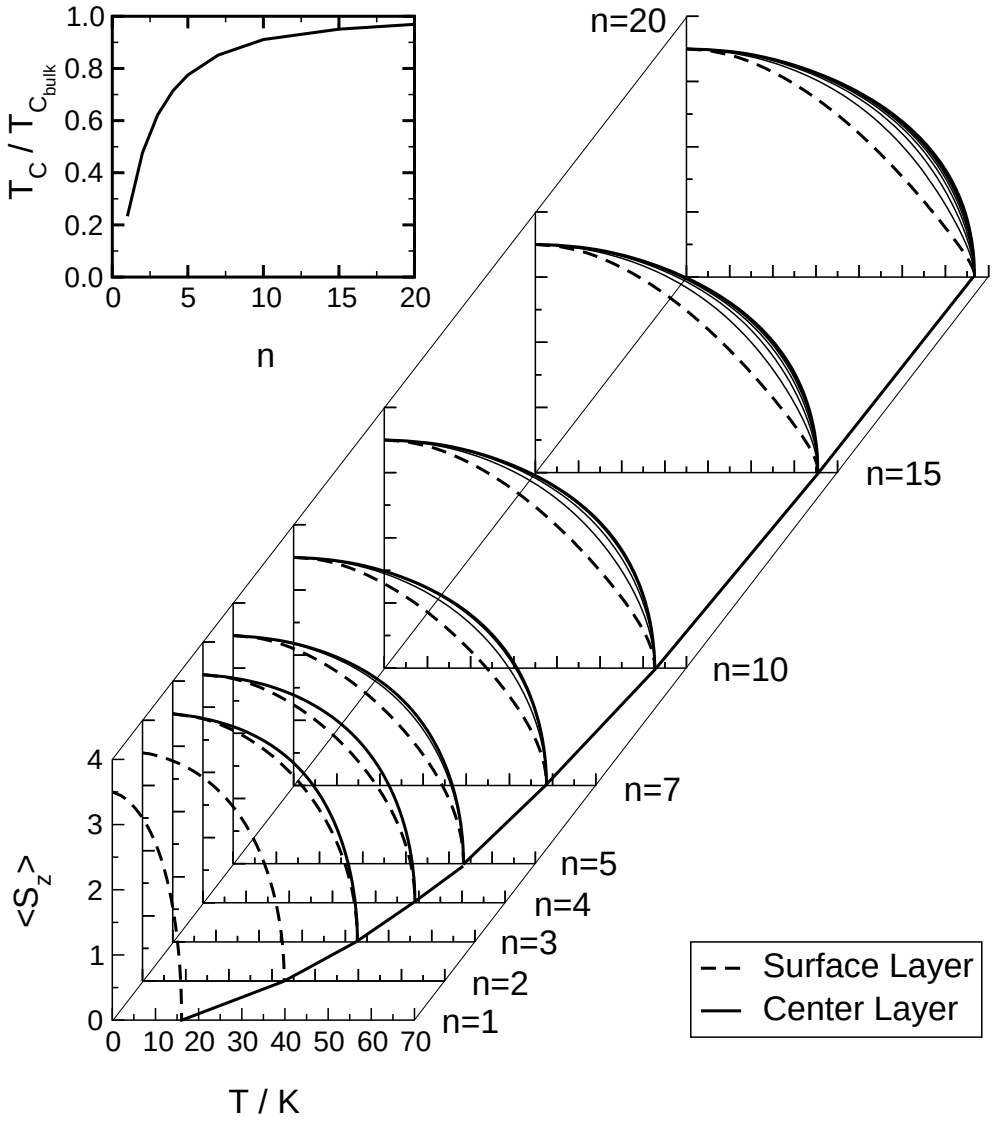

Figure 6.2: Layer-dependent magnetizations, $\langle S_\alpha^z \rangle$, of EuO(100) films as a function of temperature for $J_1/k_\mathrm{B} = 0.625\,\mathrm{K}$, $J_2/k_\mathrm{B} = 0.125\,\mathrm{K}$, $D_0/k_\mathrm{B} = 0.05\,\mathrm{K}$, for various thicknesses n of the films. For all temperatures and for all film thicknesses the $\langle S_\alpha^z \rangle$ increase monotonously from the surface layer towards the center of the films. **Inset:** Curie temperatures as a function of film thickness.

Known experimental results for the anisotropy exist for both EuO [127, 128] and EuS [129, 130]. Miyata and Argyle [128] measured the anisotropy constant for EuO at $T = 0$ to be $K_1 = -4.36 \times 10^5\,\mathrm{erg/cm^3} = -4.36 \times 10^4\,\mathrm{J/m^3}$. The magnetic anisotropy energy per europium atom can be calculated via $E_{\mathrm{A,exp}} = K_1 a^3/4$, where a denotes the lattice constant of EuO and $a^3/4$ is the volume occupied by a single europium atom. Inserting the lattice constant for EuO, $a = 5.142\,\text{Å}$ [47], we arrive at $E_{\mathrm{A,exp}}/k_\mathrm{B} = -0.11\,\mathrm{K}$. Bearing in mind that for the single-ion anisotropy, the

anisotropy energy at $T = 0$ has a value of $E_A = -6D_0$ (cf. Eq. (3.50) and Fig. 4.3), we have from the theory presented in Sec. 3.2.2 for $D_0/k_B = 0.05\,\mathrm{K}$ for the theoretical anisotropy energy per europium atom $E_{A,th}/k_B = -0.3\,\mathrm{K}$, which is of the same order of magnitude as the experimental value.

Fig. 6.2 displays the magnetization curves for EuO(100) films for thicknesses from $n = 1$ to $n = 20$. As in the case of the sc(100) film (cf. Fig. 4.1) the magnetization of the different layers of the films decreases monotonously from the center towards the surfaces of the films and the Curie temperature increases with film thickness. Here, the difference between the Curie temperature of a monolayer, $n = 1$, and that of the bulk crystal is significantly higher than that for the sc(100) model films in Fig. 4.1 due to the higher difference between the coordination number of the bulk crystal Z_b and the in-plane coordination number $Z_\parallel$ for the fcc(100) as compared to the sc(100) films ($Z_{b,sc} = 6$, $Z_{\parallel,sc(100)} = 4$, $Z_{b,fcc} = 12$, $Z_{\parallel,fcc(100)} = 4$).

Together with the higher correlation functions depicted in Fig. 4.2 as a function of magnetization, Fig. 6.2 provides the necessary temperature information needed to calculate the temperature-dependent band structures of europium films from the $T = 0$ LDA band structures of EuO films which will be calculated in the next section.

6.2 Band-structure calculations

For the band-structure calculations the TB-LMTO-ASA program from the Andersen group in Stuttgart has been used [125, 131, 132]. In this method, the original Hamiltonian of the band-structure problem is transformed to a tight binding Hamiltonian containing nearest neighbor interactions only. The transformation is obtained by linearly combining the original muffin-tin orbitals to obtain the short ranged tight-binding muffin-tin orbitals [131, 133].

In the following we will proceed with the band-structure calculations for bulk EuO. Here the three-dimensional EuO will serve us as a testing ground for choosing a reasonable approach for calculating the band structure of bulk EuO as well as of EuO films. Sec. 6.2.2 will then be devoted to the band-structure calculations for EuO(100) films.

6.2.1 Bulk calculations

The europium chalcogenides crystallize in the fcc rock-salt structure as depicted in Fig. 6.3 (a). For EuO, the lattice constant is $a = 5.142\,\text{Å} = 9.717\,\text{au}$ [46, 47]. The electronic configurations of europium and oxygen in the state of the free atom and in the ionic picture for EuO, respectively, are

$$\begin{aligned} &\text{free}: && [\text{Eu}] = [\text{Xe}](4f)^7(6s)^2, && [\text{O}] = [\text{He}](2s)^2(2p)^2; \\ &\text{EuO}: && [\text{Eu}] = [\text{Xe}](4f)^7, && [\text{O}] = [\text{Ne}]. \end{aligned}$$

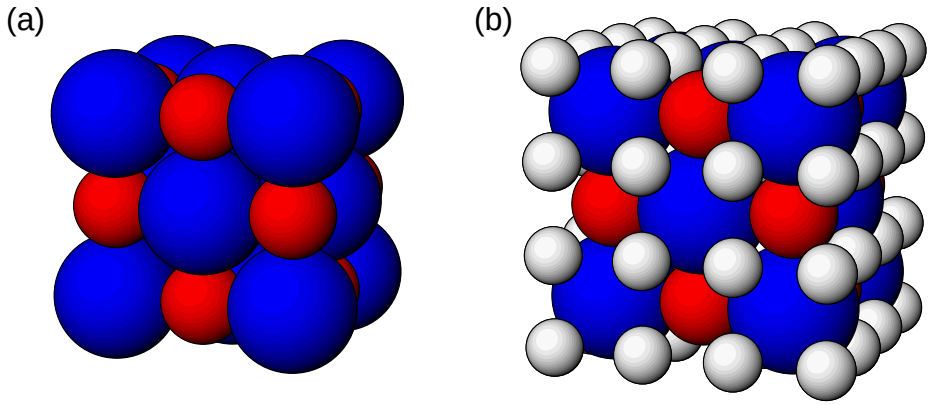

Figure 6.3: Crystal structure of EuO: (a) Unit cell of EuO with the large europium atoms at the corner positions, (b) Unit cell of EuO including the empty spheres (light colored). The sizes of the europium, oxygen and empty spheres correspond to the sizes of the respective muffin-tin spheres used in the band-structure calculations.

In accordance with Hund's coupling, the Eu-*4f* electrons couple to the maximum magnetic moment of $S = 7/2$. The difficulty in dealing with the *4f* levels within an LDA calculation lies in their strongly localized character, which is due to a strong Coulomb interaction between the *4f* electrons. As a result of the inability of the LDA to take into account the respective interactions correctly, a *normal* LDA calculation for EuO produces a metal with the *4f* levels lying well within the conduction band.

To overcome this situation, we have investigated two approaches for dealing with

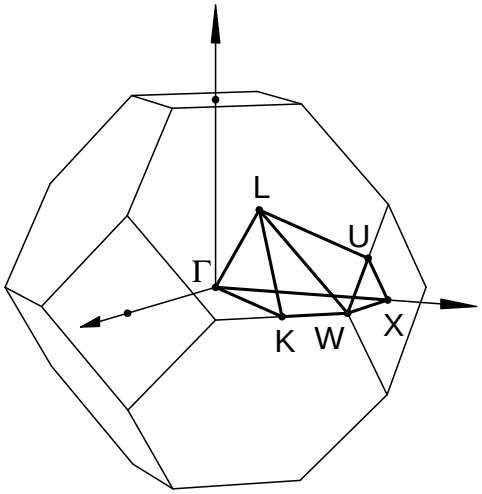

Figure 6.4: First Brillouin zone and irreducible Brillouin zone (**fat** lines) of the fcc crystal lattice. The high-symmetry points are indicated by their respective letters.

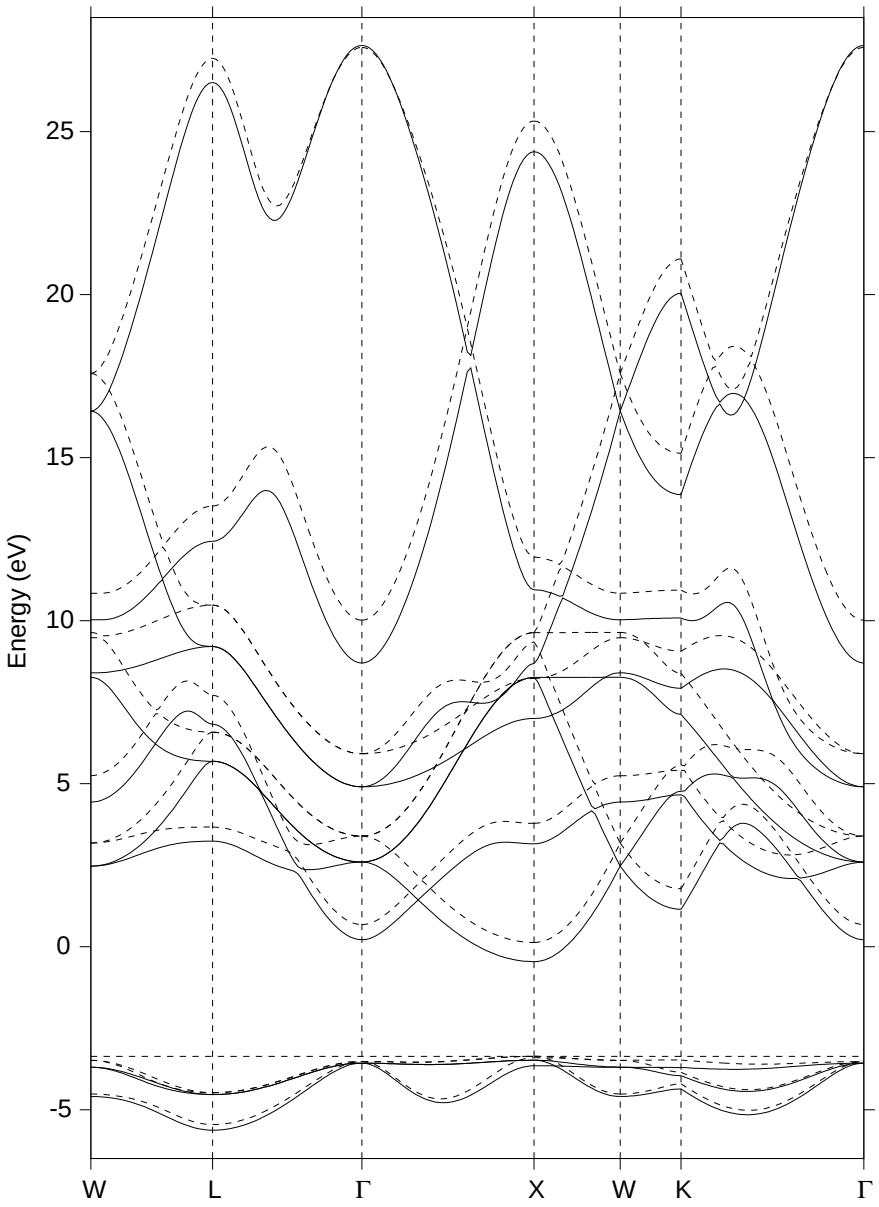

Figure 6.5: Spin-dependent (spin-↑: ——, spin-↓: - - -) band structure of bulk EuO calculated within an LSDA calculation with the *4f* levels treated as core electrons. The horizontal dashed line represents the Fermi energy.

the localized *4f* moments*. In the first, the *4f* moments are treated as localized core electrons. Fig. 6.5 shows the respective spin-dependent band structure of EuO. The positions of the high-symmetry points are given in Fig. 6.4. In Fig. 6.6, for the same calculation, the density of states is displayed. Here, the main contributions to the

*For the *4f* system Gd the different approaches have been reviewed by Eriksson *et al.* [98].

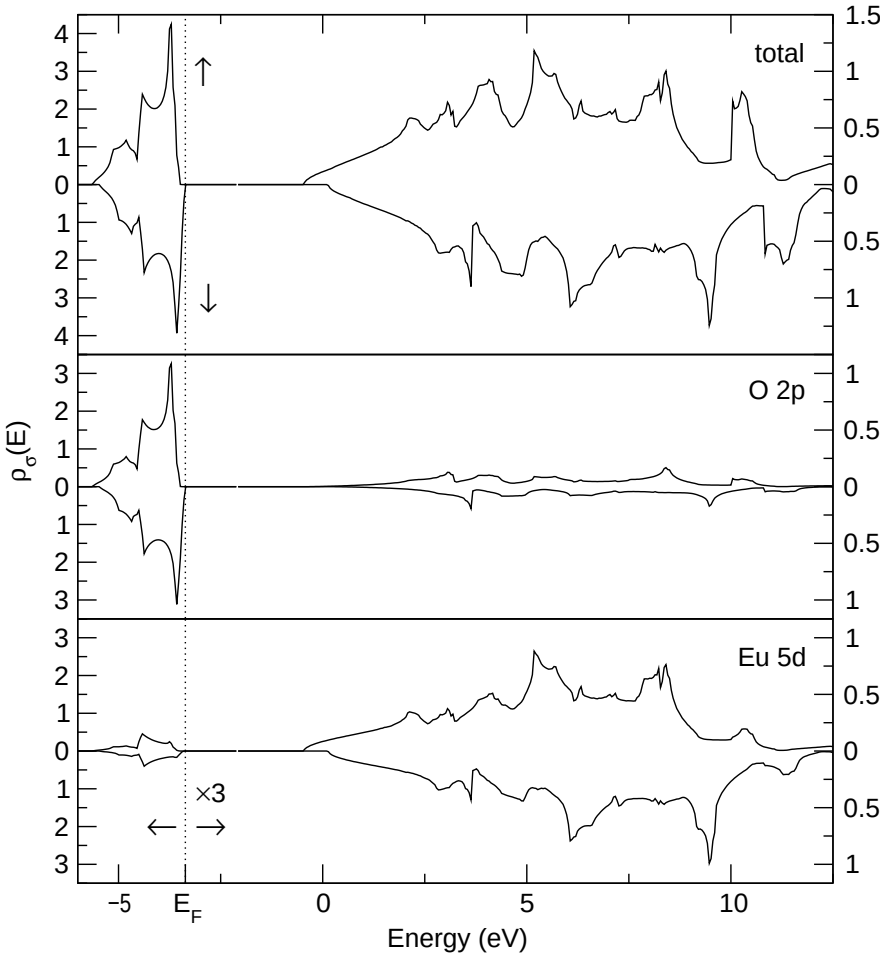

Figure 6.6: Density of states, $\rho_\sigma(E)$, of bulk EuO calculated within an LSDA calculation with the *4f* levels treated as core electrons. The upper graph shows the total density of states, whereas the lower two display the partial density of states of the O-*2p* and the Eu-*5d* bands. The dotted line represents the Fermi energy. The densities of states above the Fermi energy are multiplied by a factor of three and correspond to the left *y*-axis.

density of states originate from the O-*2p* levels, which constitute the valence band, and from the unoccupied Eu-*5d* levels. As a result of treating the *4f* levels as core electrons, we have the correct ground state of an insulator. Clearly, the conduction-band region is dominated by the Eu-*5d* electrons. Thus, for the model calculations which will be performed in Sec. 6.3 it is a reasonable approximation to restrict the single-particle input obtained within the band-structure calculations to the Eu-*5d* bands.

As a result of treating the *4f* electrons of europium as core electrons, in Figs. 6.5 and 6.6 the *4f* levels are missing. From photoemission experiments, however, it is known, that far from being out of the picture, the *4f* levels lie right between the O-*2p* bands and the Eu-*5d* bands [56, 58, 57]. To obtain the right position of the localized *4f* bands, an LDA+U calculation [134, 135] has to be performed. In this approach,

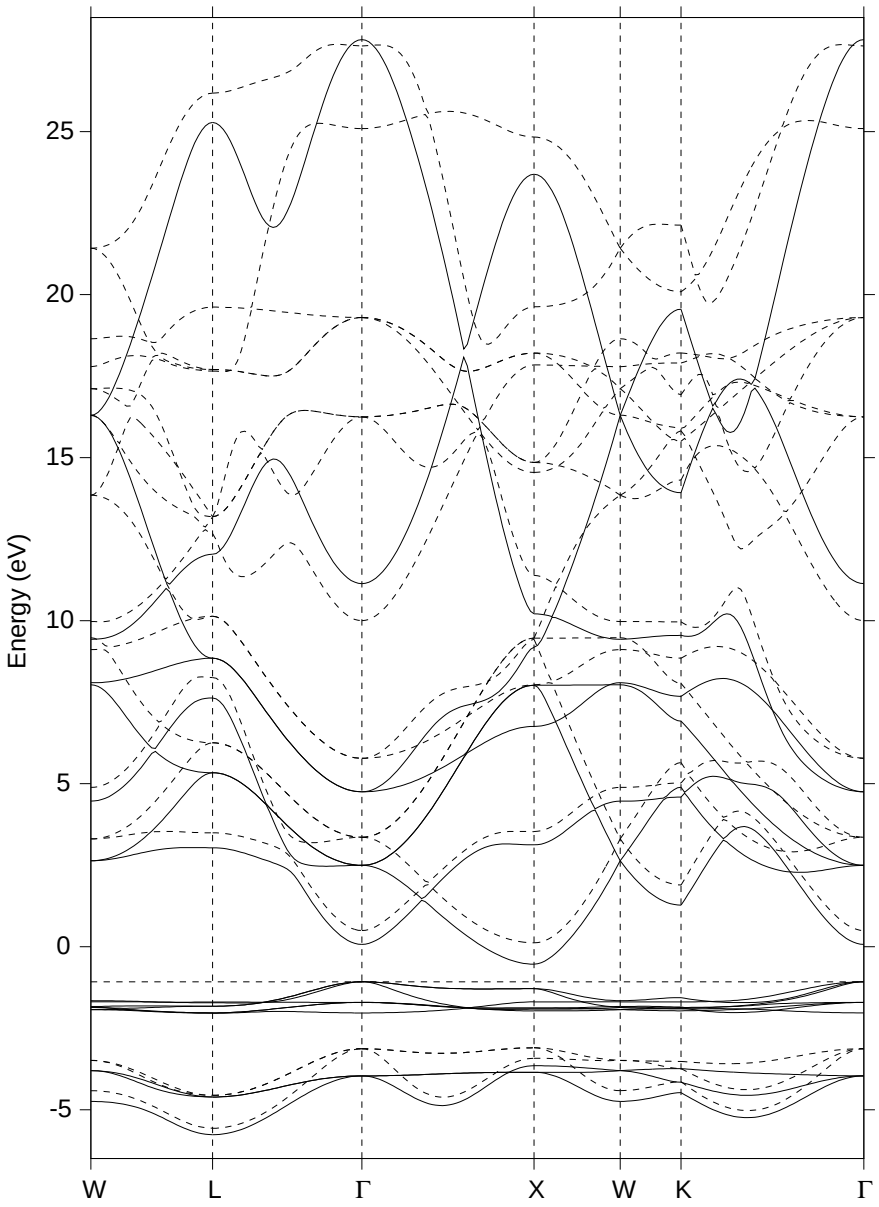

Figure 6.7: Spin-dependent (spin-↑: ——, spin-↓: - - -) band structure of bulk EuO calculated within an LSDA+U calculation with $U = 8\,\text{eV}$ and $J = 0.88\,\text{eV}$. The horizontal dashed line represents the Fermi energy.

a mean-field approximation for the Coulomb and the exchange interaction between the *4f* electrons is added to the LDA energy functional. The size of the respective interactions is given by two parameters, U and J.

Fig. 6.7 shows the LSDA+U band structure of bulk EuO calculated for the two parameters $U = 8\,\text{eV}$ and $J = 0.88\,\text{eV}$. Here, the parameter for the Coulomb interaction, U, has been adjusted in such a way, that the spin-↑ *4f* levels lie in the band gap

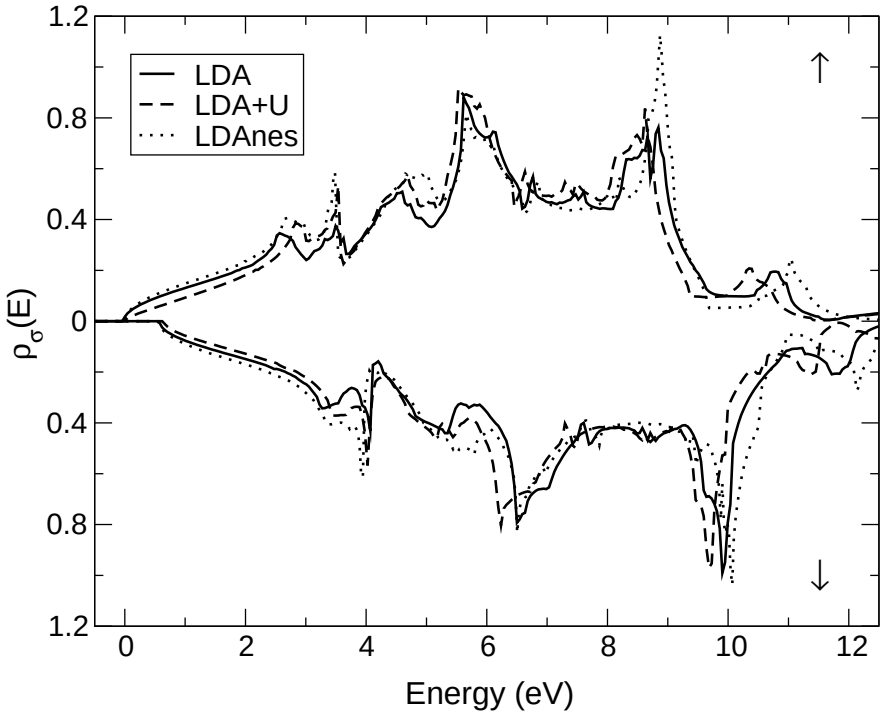

Figure 6.8: Partial Eu-*5d* density of states of bulk EuO calculated within different approaches, *LDA*: LSDA calculation of the *4f* electrons as core electrons, *LDA+U*: LSDA+U calculation with $U = 8\,\text{eV}$ and $J = 0.88\,\text{eV}$, *LDAnes*: same as LDA but without empty spheres (see text, Fig. 6.3). The spectra have been shifted for each method, such that lower band edges of the spin-↑ densities of states lie at $E = 0\,\text{eV}$.

between the O-*2p* and the Eu-*5d* levels. Again, apart from the strong contribution of the Eu-*4f* spin-↑ levels, the main contribution to the density of states stems from the O-*2p* and the Eu-*5d* bands with the latter dominating the conduction band.

Whereas the spin-resolved LDA+U calculation is able to reproduce the right position of the respective bands for EuO, the introduction of adjustable parameters U and J somehow corrupts the idea of a *first-principles* calculation. Furthermore, as can be seen in Fig. 6.8, the partial densities of states of the Eu-*5d* bands, which are the relevant bands for our model calculations, differ only slightly from those obtained with a "simple" LDA calculation, with the *4f* electrons treated as core electrons. All the main features of the partial density of states remain the same, so that the much simpler LDA calculation has to be preferred.

Also in Fig. 6.8, the partial density of states of the Eu-*5d* bands obtained within an LDA calculation without *empty spheres* is shown. The empty spheres have to be added to systems which are not closed packed to reduce the error which results from approximating the potential in the region between the muffin-tin spheres of the atoms by a constant. Both the LDA and the LDA+U calculations presented so far have been performed with empty spheres, the positions of which are depicted in Fig. 6.3 (b). As

	LDA	LDA+U	LDAnes
$4f^{\uparrow}$ bandwidth	—	0.96	—
$2p^{\uparrow(\downarrow)}$ bandwidth	2.14 (2.09)	2.12 (2.47)	2.04 (1.98)
$4f^{\uparrow}$–$2p^{\uparrow(\downarrow)}$ separation	—	1.61 (1.06)	—
$5d^{\uparrow(\downarrow)}$ bandwidth	9.67 (10.35)	9.39 (10.02)	9.69 (10.42)
$5d$–$2p^{\uparrow(\downarrow)}$ gap	3.02 (2.90)	3.11 (2.56)	3.21 (3.09)
$5d^{\uparrow}$–$4f^{\uparrow}$ gap	—	0.54	—

Table 6.1: Band-structure data (in eV) for EuO.

can be seen in Fig. 6.8, the partial densities of states of the Eu-*5d* bands calculated within the LDA without empty spheres correspond well to the respective partial densities calculated within the two other methods concerning the average distribution of spectral weight and the peak positions. Differences still occur as shows e. g. the strong peak around 9 eV in the spin-↑ DOS calculated within LSDA without empty spheres. However, since in this thesis we are mainly interested in the temperature-dependent modification in the spectra, these differences are acceptable.

The neglect of the empty spheres within the LDA calculation is not necessary for the case of bulk EuO. However, as will be seen in the next section, the band-structure calculations for film geometries require the definition of a supercell where the number of atoms in the supercell is proportional to the number of layers of the film. The resulting complexity of the band-structure calculations thus makes the LDA calculation without empty spheres the method of choice for film geometries.

Table 6.1 summarizes the relevant band-structure data of the different LSDA calculations. Here, the values from Table 6.1 agree reasonably well with the results of other LDA calculations [136, 137, 138] and with experimental data obtained with photoemission spectroscopy [55, 56].

6.2.2 Calculations for EuO films

For the band-structure calculations for EuO one has to employ a supercell geometry as depicted in Fig. 6.9. As a result of the supercell geometry, the system has a super-layered structure with the super-layers consisting of n consecutive EuO(100) layers followed by m layers of empty spheres. Here, the spacing between all layers is equidistant. As a result, we have a system of periodically stacked EuO n-layer films, which are isolated from each other by m layers of empty spheres.

The number m of empty layers has to be chosen large enough to have truly isolated EuO films. On the other hand, it is desirable to restrict the number of empty layers to cut down on the numerical effort. In Fig. 6.11, the partial density of states of the Eu-*5d* conduction bands of EuO(100) monolayers ($n = 1$) is displayed for different numbers

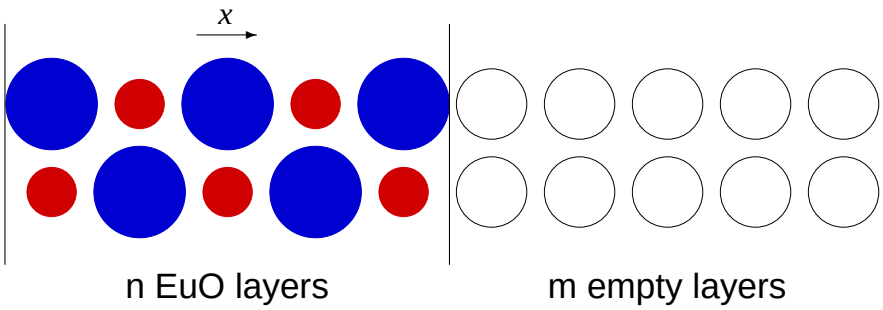

Figure 6.9: Supercell geometry for the EuO(100) film calculations, with the europium atoms (big), the oxygen atoms (small) and the empty spheres (circles). The vertical lines indicate the surfaces of the EuO film with the x-direction assumed to be perpendicular to them.

of spacer layers m and compared to the bulk case. As can be seen, the density of states of the EuO monolayer converges quite quickly as a function of the number of spacer layers m. For the following calculations we have chosen $m = 5$ which, according to Fig. 6.11, seems to be a reasonable approximation for the case of ideally isolated EuO films ($m \to \infty$).

Due to the effective decoupling of the EuO films in the x-direction, the band structures of the films show no dispersion in the k_x direction. As a result, the first Brillouin of the system is that of the fcc(100) surface sketched in Fig. 6.10.

In Fig. 6.12 the band structures of EuO films consisting of one, two, and five EuO(100) layers are displayed within the two-dimensional Brillouin zone of the fcc(100) surface. As can be seen, the number of bands increases with the number of

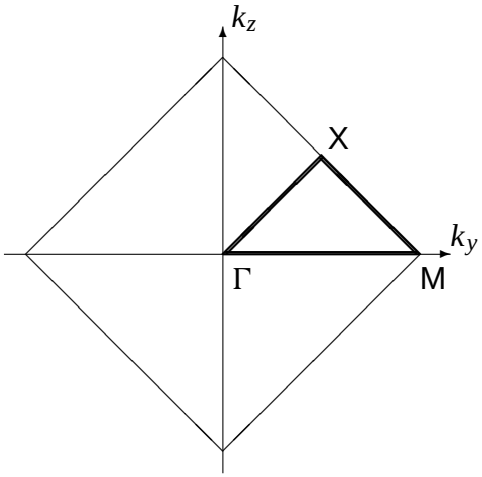

Figure 6.10: First Brillouin zone and irreducible Brillouin zone (**fat** lines) of the fcc(100) surface including the high-symmetry points. For simplicity, here and in the following, we have omitted the bars in the two-dimensional high-symmetry points, $\Gamma \equiv \overline{\Gamma}$, $\mathrm{X} \equiv \overline{\mathrm{X}}$, and $\mathrm{M} \equiv \overline{\mathrm{M}}$.

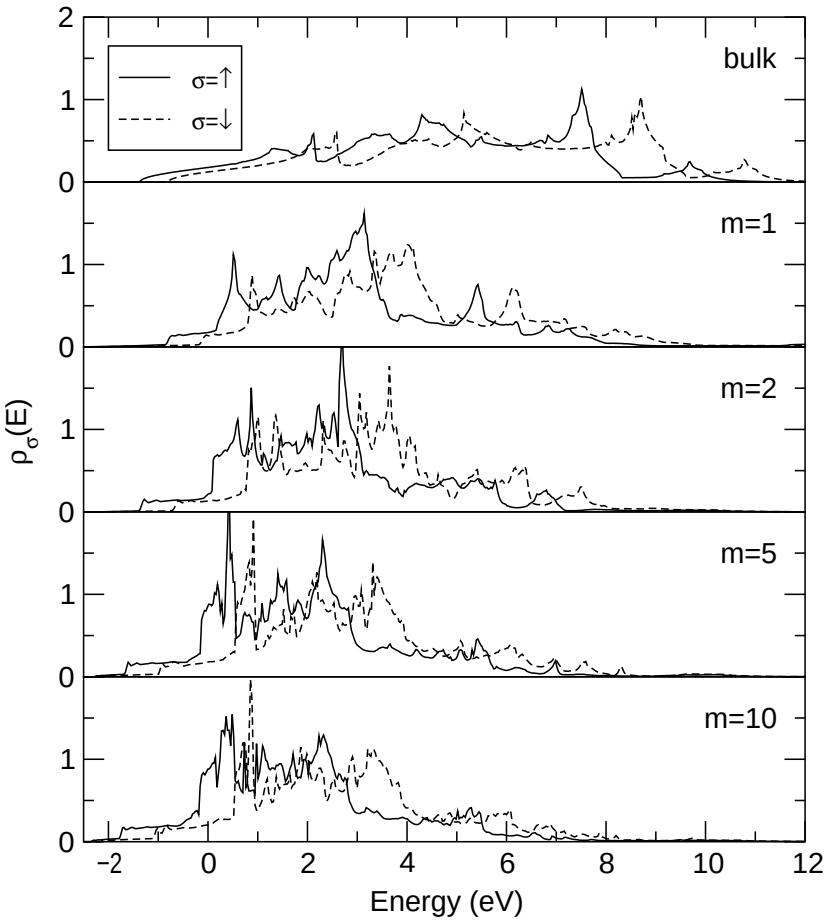

Figure 6.11: Partial densities of state for the Eu-*5d* bands of a EuO(100) monolayer calculated for different numbers *m* of spacer layers of empty spheres and for bulk EuO.

layers *n* of the film. This is due to the corresponding increase in nonequivalent lattice sites within the supercell. The plots on the left hand side of Fig. 6.12 show the complete band structures including the unphysical high-energetic bands originating from the orbitals of the empty spheres of the spacer layers. For the model calculations following in next section we are interested in the Eu-*5d* bands only. The band structures on the right hand side of Fig. 6.12 are reduced to the Eu-*5d* bands by cutting away the other parts (O-*2p*, Eu-*6s*, and bands of the empty spheres) of the tight-binding Hamiltonian. Thus, the respective band structures for the spin-↑ electron constitute the input for the model calculations.

Fig. 6.13 shows the partial densities of states of the *5d* bands of the center layer Eu atoms for films of various thicknesses *n* and for bulk EuO. The respective curves converge as a function of film thickness. Comparing the partial Eu-*5d* density of states of the center layer ($\alpha = 10$) of a 20-layer EuO(100) film with that of bulk EuO, we see that apart from an unimportant constant energy shift the main features of the densities of states match. Consequently, the center layer of the 20-layer film can be regarded as

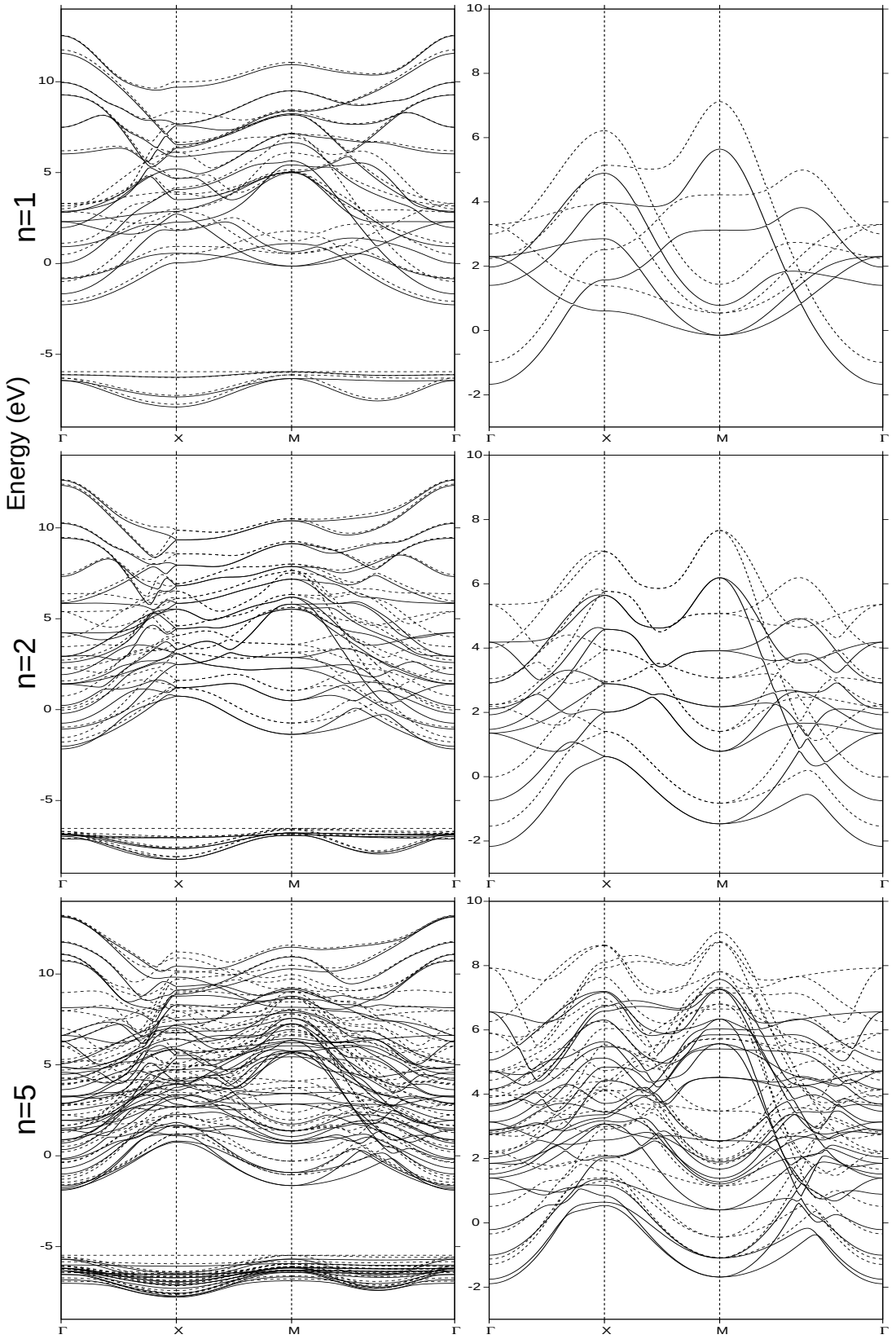

Figure 6.12: Band structures of n-layer EuO(100) films (spin-↑: ——, spin-↓: - - -). *Left*: total band structures, *Right*: band structures containing only the Eu-*5d* bands.

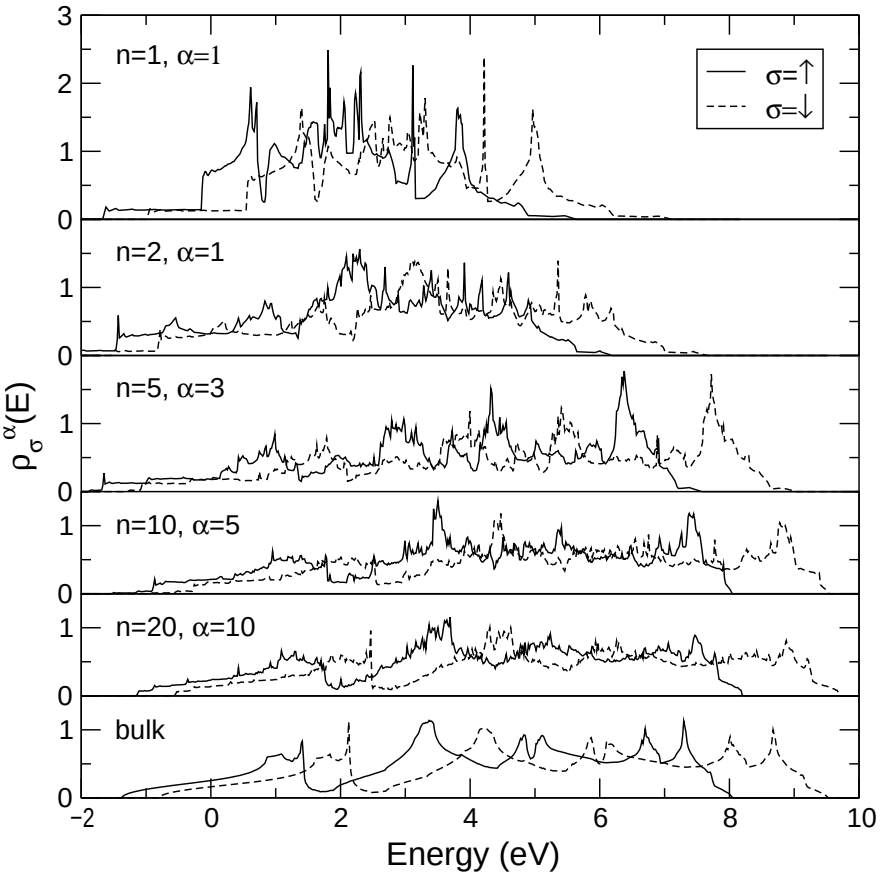

Figure 6.13: Partial densities of state for the Eu-*5d* bands of the center layers (layer index α) for EuO films of various thicknesses n and for bulk EuO.

a bulk-like environment.

The still existing slight discrepancy between the two spectra can be accounted for by two reasons. Firstly, due to the supercell geometry employed in the band-structure calculations for the EuO films, the cubic symmetry which is present in bulk EuO is broken. As a result, the splitting of the Eu-*5d* bands into t_{2g} and e_g orbitals is not valid anymore. Secondly, the center of a 20-layer EuO(100) film is only an approximation for the situation in bulk EuO. With respect to these two limiting factors, the slight discrepancy between the partial Eu-*5d* densities of states of the center layer of the 20-layer film and of bulk EuO is acceptable.

To round up the picture for the EuO(100) films, in Fig. 6.14 the partial Eu-*5d* densities of states of a 20-layer film are displayed for the two surface layers, $\alpha = 1,\ 2$, and for the two center layers, $\alpha = 9,\ 10$. The shown curves indicate that the local density of states in the center of the film is constant, but different from the local density of states in the vicinity of the surface of the film. Most notably, the centers of gravity of the local densities of state for the surface layer are at a lower energy and the densities of states are more narrowly distributed compared to the densities of state of the center

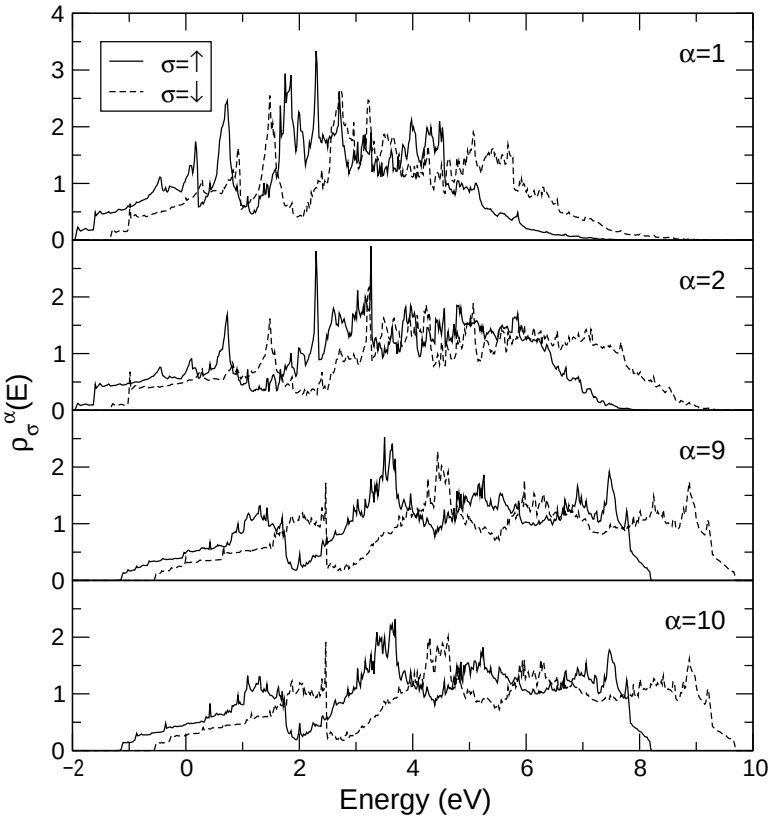

Figure 6.14: Partial densities of state of the Eu-*5d* bands for different layers α of a 20-layer EuO(100) film.

layers. The lower band edge of the Eu-*5d* bands of the surface layer compared to those of the center layer, which represent a bulk-like situation, indicates the existence of surface states. These surface states will we discussed in detail in Sec. 6.3.3.

6.3 Temperature-dependent band structures

In this section the LSDA band structures of bulk EuO and of the EuO(100) films shall be combined with an *s-f* model calculation to obtain the respective temperature-dependent band structures. To do this, we need the hopping integrals from Eq. (5.1). How the respective hopping integrals can be obtained from the **k**-dependent Hamilton operator and the overlap matrix of the TB-LMTO method is expounded in App. A. Due to the fact that within our model calculation for $T = 0$ the spin-↑ spectrum is rigidly shifted towards lower energies by the amount of $\frac{1}{2}JS$ (cf. e. g. Eq. (2.31)), the obtained **k**-dependent hopping matrices for the spin-↑ electron will serve us as the input for the kinetic Hamiltonian (5.1). Since the solution for $T = 0$ is exact, the problem of double counting of relevant interactions, which usually occurs when combining first-principles and model calculations, is elegantly avoided.

$\langle S_z\rangle/S$	bulk EuO	EuO(100) films (number of layers)				
		1	2	5	10	20
1	0	0	0	0	0	0
0.75	45.48	10.52	21.56	37.41	43.23	45.14
0.5	59.76	13.95	28.51	47.51	55.59	58.92
0.25	66.71	15.56	31.82	52.02	61.02	65.04
0 (T_C)	68.84	16.06	32.83	53.36	62.70	66.73

Table 6.2: Temperatures at which the magnetization of bulk EuO and of the center layers of EuO(100) films has assumed the values in the left column as obtained in Sec. 6.1 (cf. Figs. 6.1 and 6.2).

The temperature comes into play via the layer- and temperature-dependent *f*-spin correlation functions of Eqs. (3.32), which for the case of bulk EuO and EuO(100) films are given by Figs. 6.1 and 6.2 and by the dependence of the higher correlation functions on the magnetization displayed in Fig. 4.2. For the following calculations, the magnetization of bulk EuO and of the center layers of EuO(100) films, respectively, has been chosen as the temperature parameter. In Table 6.2 the different values of the magnetization $\langle S_z\rangle/S$ are related to the respective temperatures for bulk EuO and for EuO(100) films (cf. Figs. 6.1 and 6.2).

As for the LDA calculations, we will start our evaluation with the case of bulk EuO, firstly, because for bulk EuO there exists earlier work on the temperature-dependent band structure [138, 139]. Secondly, we need to get a reasonable estimate for the value of the *d-f* interaction in EuO, which then can be used to calculate the temperature-dependent band structures of EuO(100) films in Sec. 6.3.2.

6.3.1 Calculations for bulk EuO

Fig. 6.15 displays the partial Eu-*5d* densities of states of bulk EuO calculated within LSDA. It has been shown by several authors [140, 141, 142], that the standard LSDA band-structure calculations are quite compatible with the simple Stoner or mean-field picture, in which the exchange splitting is only slightly energy dependent. Therefore, in Fig. 6.15 we have marked prominent peaks in the LSDA spin-↑ and spin-↓ spectra. For the marked peaks the splitting varies in the quite big range from 0.57 eV to 1.37 eV. Obviously, these data somehow contradict the simple Stoner picture established in [140, 141, 142] but rather imply an energy-dependent exchange splitting of the LSDA spectra. However, the inclusion of a such an energy-dependent splitting of the spectra is not possible within the theory presented in chapter 3 and we have to take an averaged exchange interaction for the calculation of the temperature-dependent band structures.

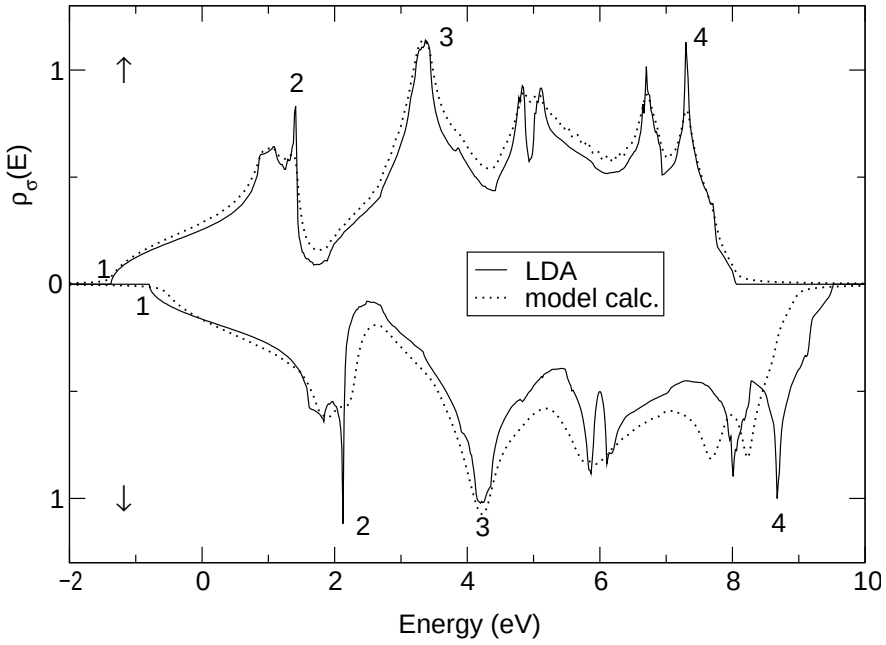

Figure 6.15: Partial Eu-*5d* densities of states of bulk EuO calculated within LSDA and with the *s-f* model calculation with $J = 0.25\,\text{eV}$, the latter corrected by an energy shift of $\frac{1}{2}JS$. The differences between the prominent peaks in the LSDA-spectra are (in eV): $1^{\downarrow} - 1^{\uparrow} = 0.57$, $2^{\downarrow} - 2^{\uparrow} = 0.7$, $3^{\downarrow} - 3^{\uparrow} = 0.86$, $4^{\downarrow} - 4^{\uparrow} = 1.37$.

Averaging the splitting of the spectra for the different marked peaks, one arrives at an average splitting of the spectra for the two spin directions of 0.875 eV. In the mean-field approximation of the *s-f* model[†] the spin-splitting is equivalent to JS. With $S = 7/2$ one gets for the *d-f* exchange splitting $J = 0.25\,\text{eV}$. This value will be used for all the further bulk and film *s-f* model calculations.

Also in Fig. 6.15, the spin-↑ and spin-↓ densities of states obtained within an *s-f* model calculations are displayed for $J = 0.25\,\text{eV}$ (dotted lines). The spin-↑ density of states agrees with that obtained within the LSDA calculation except for a slight smoothing of the features, which arises in the model calculation due to the numerical necessity of broadening the excitation energies by a small imaginary contribution. For the spin-↓ spectra it can be seen that the averaged value of $J = 0.25\,\text{eV}$ chosen for the model calculation results in a varying agreement between the model and the LSDA spectra depending on the energy position.

Fig. 6.16 shows the temperature-dependent spectral density of bulk EuO obtained within an *s-f* model calculation with $J = 0.25\,\text{eV}$. For $T = 0$ ($\langle S_z \rangle / S = 1$), the spin-↑ spectral density agrees, except for a constant energy shift, with that obtained by the LSDA calculation. However, still for $T = 0$ but for the spin-↓ spectrum a

[†]In the case of EuO the *s-f* model is actually a *d-f* model describing the intra-atomic interaction between the localized Eu-*4f* levels and the Eu-*5d* conduction bands. In the following, *s-f* and *d-f* will be used as synonyms.

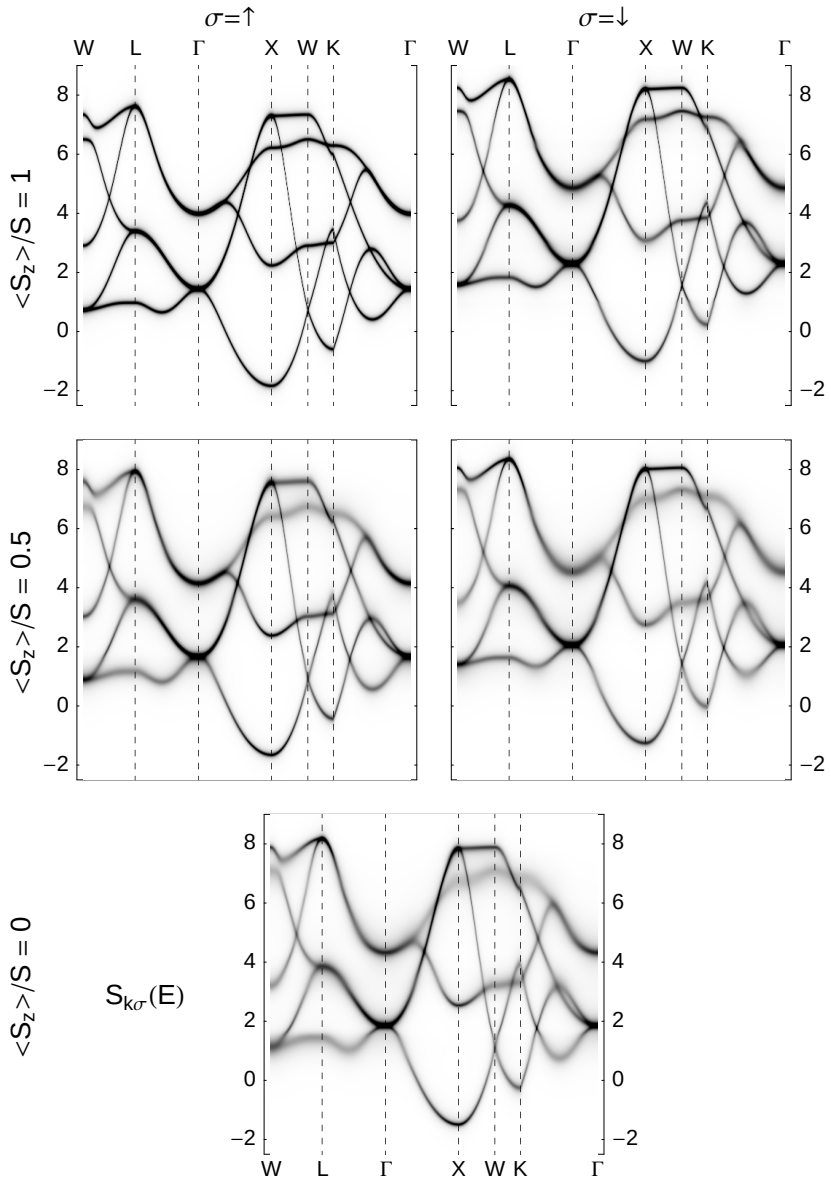

Figure 6.16: Spin-dependent spectral densities of the Eu-5*d* bands of bulk EuO for $J = 0.25\,\mathrm{eV}$ and for different magnetizations $\langle S_z\rangle/S$ (cf. Table 6.2).

broadening of the bands can be observed, most notably around the Γ-point, which indicates a finite lifetime of the respective quasiparticles due to correlation effects. In this respect already the $T = 0$ spin-↓ solution goes beyond LSDA by taking into account correlation more realistically.

For intermediate temperatures ($\langle S_z\rangle/S = 0.5$) a broadening of the bands sets in also for the spin-↑ spectra since the spin-↑ electron can now exchange its spin with the deviated local-moment system. For the spin-↓ spectral density, the correlation effects, already present at $T = 0$, increase, as can be seen by the further broadening

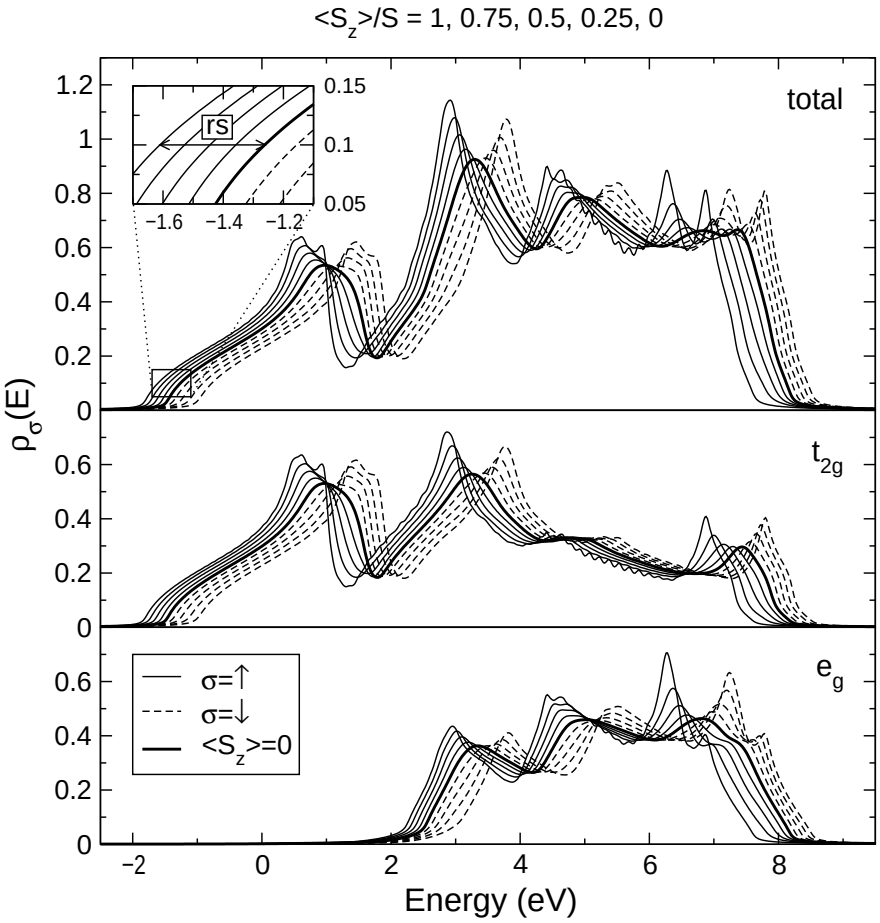

Figure 6.17: Temperature-dependent densities of states of the Eu-*5d* bands of bulk EuO. For $T = 0$ ($\langle S_z \rangle / S = 1$) the spectra for the two spin directions are furthest away from each other and approach each other when increasing the temperature. For $T = T_C$ ($\langle S_z \rangle / S = 0$) the densities of states for both spin directions are the same (**fat** lines).

of the bands. At the same time, the spin-↑ and the spin-↓ spectra are shifted towards higher and lower energies, respectively, reducing the effective splitting between the two spectra. This effect continues with increasing temperature, until finally, for $T = T_C$ ($\langle S_z \rangle / S = 0$), the spectra for both spin directions are equal. Clearly, the temperature-dependent effects displayed in Fig. 6.16 do not comply with the simple Stoner-picture which would imply a constant energy shift of the spectra. The reason for this more complicated behavior as a function of temperature is again that in the theory, the correlation is treated in a way which goes beyond mean-field.

The mentioned shift of the spin-↑ spectrum towards lower energies when going from $T = T_C$ down to $T = 0$ represents the red shift of the optical absorption edge in EuO [1, 2]. Fig. 6.17 displays the densities of states obtained for different magnetizations of the *4f* moments. It can be seen that the red shift of the optical absorption edge is due to the *4f*-$5d_{t_{2g}}$ transition. From Fig. 6.17 one obtains a red shift of

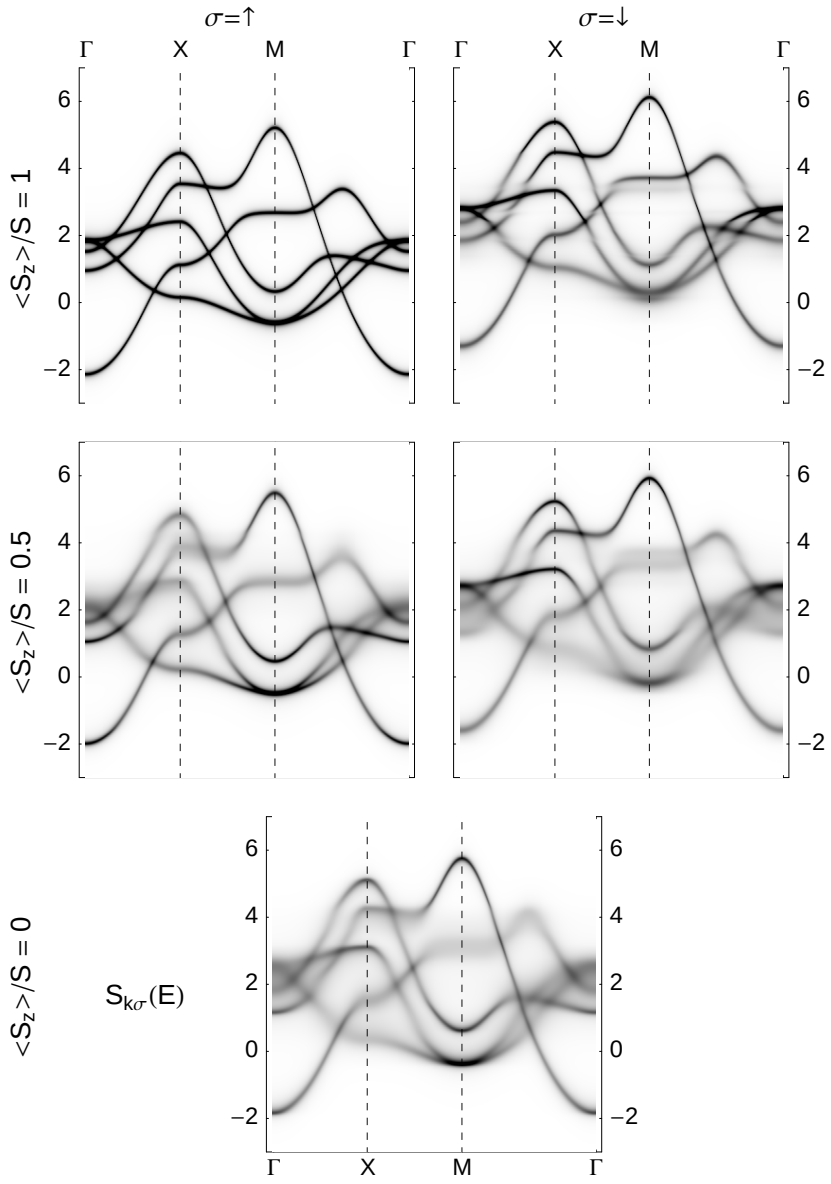

Figure 6.18: Spin-dependent spectral densities of the Eu-*5d* bands of an EuO(100) monolayer ($n = 1$) for $J = 0.25\,\mathrm{eV}$ and for different magnetizations $\langle S_z \rangle / S$ (cf. Table 6.2).

rs $= 0.35\,\mathrm{eV}$. This value agrees reasonably with the experimental value for the red shift of $0.27\,\mathrm{eV}$ [47]. Here, the agreement can be further improved when choosing the splitting of the lower edges of the LSDA Eu-*5d* bands in Fig. 6.15 to calculate the *d*-*f* exchange interaction for the model calculation.

There have been previous calculations by Nolting *et al.* concerning the temperature-dependent band structure of bulk EuO [138, 139]. In these works, the band structure of the Eu-*5d* bands has been split into five *s*-like bands with the lowest eigenstates belonging to the lowest band etc. The splitting into *s*-bands produces five consecutive

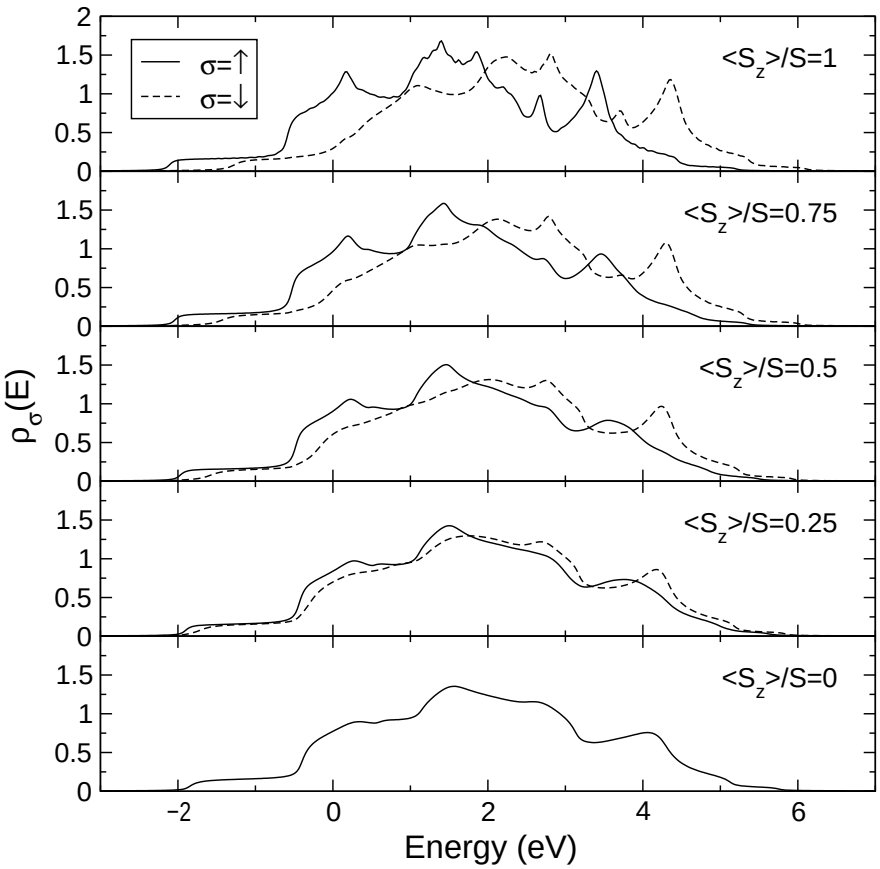

Figure 6.19: Temperature-dependent densities of states of the Eu-*5d* bands of an EuO(100) monolayer for different values of magnetization $\langle S_z \rangle / S$ of the local moment system (cf. Table 6.2).

bands of an average bandwidth of about $W = 3\,\mathrm{eV}$ [138, 139].

Contrary to these works, for the calculation of Figs. 6.16 and 6.17 the full band structure of the Eu-*5d* bands has been taken into account, thereby respecting the symmetry of the different Eu-*5d* orbitals. As a result, the Eu-*5d* bands of bulk EuO split into the t_{2g} and the e_g subbands with a bandwidth of about 10 eV and 6 eV, respectively. For the model calculations, the decisive entity for the magnitude of the correlation effects is the *s-f* interaction over bandwidth, J/W. In this respect, in the previous works [138, 139] the calculated correlation effects should be slightly overestimated, considering the more "natural" band decomposition employed in this thesis.

6.3.2 Calculations for EuO(100) films

Figs. 6.18–6.21 show the spectral densities and the partial densities of states of the Eu-*5d* bands for a EuO(100) monolayer ($n = 1$) and a double layer ($n = 2$) at varying magnetizations $\langle S_z \rangle / S$ of the local moment system. All calculations have been

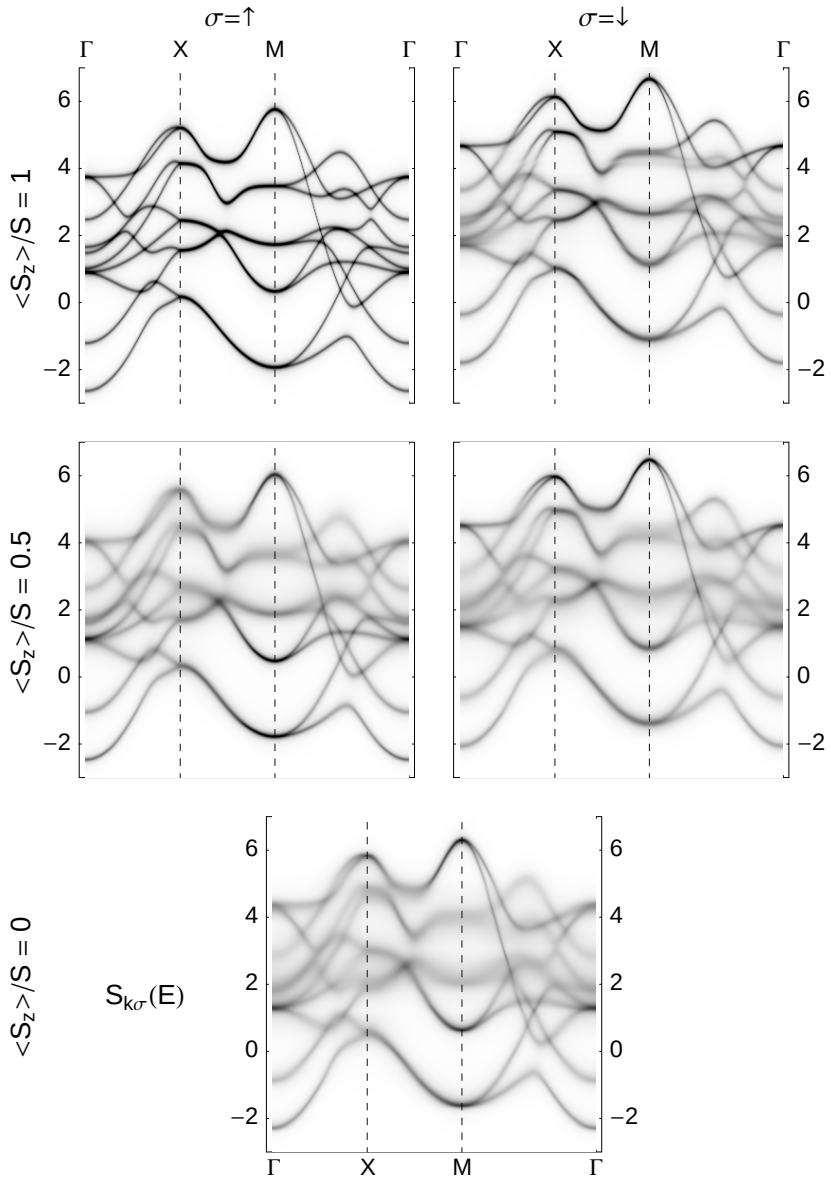

Figure 6.20: Spin-dependent spectral densities of the Eu-*5d* bands of an EuO(100) double layer ($n = 2$) for $J = 0.25\,\mathrm{eV}$ and for different magnetizations $\langle S_z \rangle / S$ (cf. Table 6.2).

performed with an *d-f* exchange interaction of $J = 0.25\,\mathrm{eV}$.

In Fig. 6.18 the influence of correlation effects on the spin-↓ spectral density can be seen. Thus, around the M-point, the band around 4 eV clearly splits into two parts. Here, in analogy to the discussion in Sec. 4.2, the low-energetic branch is due to scattering processes and the high-energetic band can be attributed to the existence of a polaron-like quasiparticle. This exchange-induced splitting, which can also be observed in other parts of the spin-↓ spectral density, clearly cannot be accounted for in an LSDA calculation.

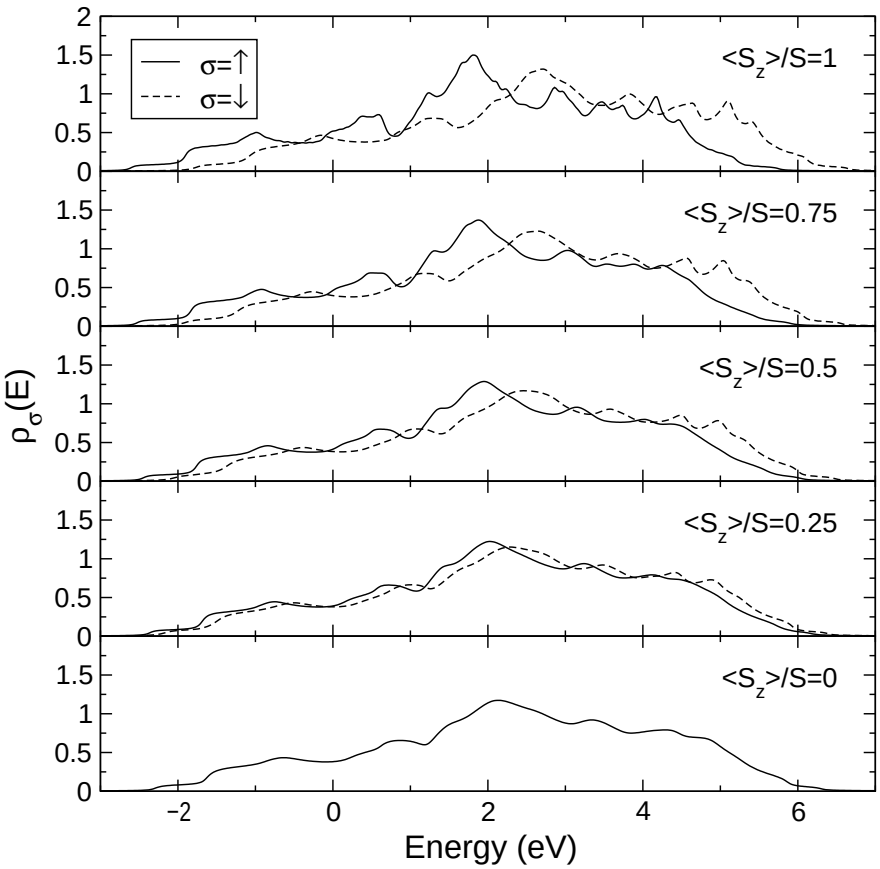

Figure 6.21: Temperature-dependent densities of states of the Eu-*5d* bands of an EuO(100) double layer for different values of magnetization $\langle S_z \rangle / S$ of the local moment system (cf. Table 6.2).

For intermediate magnetizations, $\langle S_z \rangle / S = 0.5$, as in the case of bulk EuO, the spin-↑ bands start to broaden, indicating spin-flip processes between the spin-↑ electron and the local-moment system. This broadening of the bands is also existent for the spin-↓ electron. Whereas the broadening of the bands starts on the lower energetic bands for the spin-↓ electron, for the spin-↑ electron first the higher energetic bands become broader when increasing the temperature form $T = 0$. The reason for this different behavior is that for a given spin-↑ polaron band the scattering, which is responsible for the broadening, occurs at higher energies, while for the spin-↓ electron, the scattering band is located at lower energies with respect to the polaron band (cf. Fig. 4.7 and Sec. 4.2). Finally, in the limiting case of $\langle S_z \rangle \to 0$ ($T \to T_C$) the lack of any magnetization results in the same spectral density for both spin directions of the electron.

As in the spectral densities, in the density of states displayed in Fig. 6.19 for a EuO(100) monolayer, the increase of temperature from $T = 0$ to $T = T_C$ leads to convergence of the densities of states for the two spin directions. It can clearly be seen,

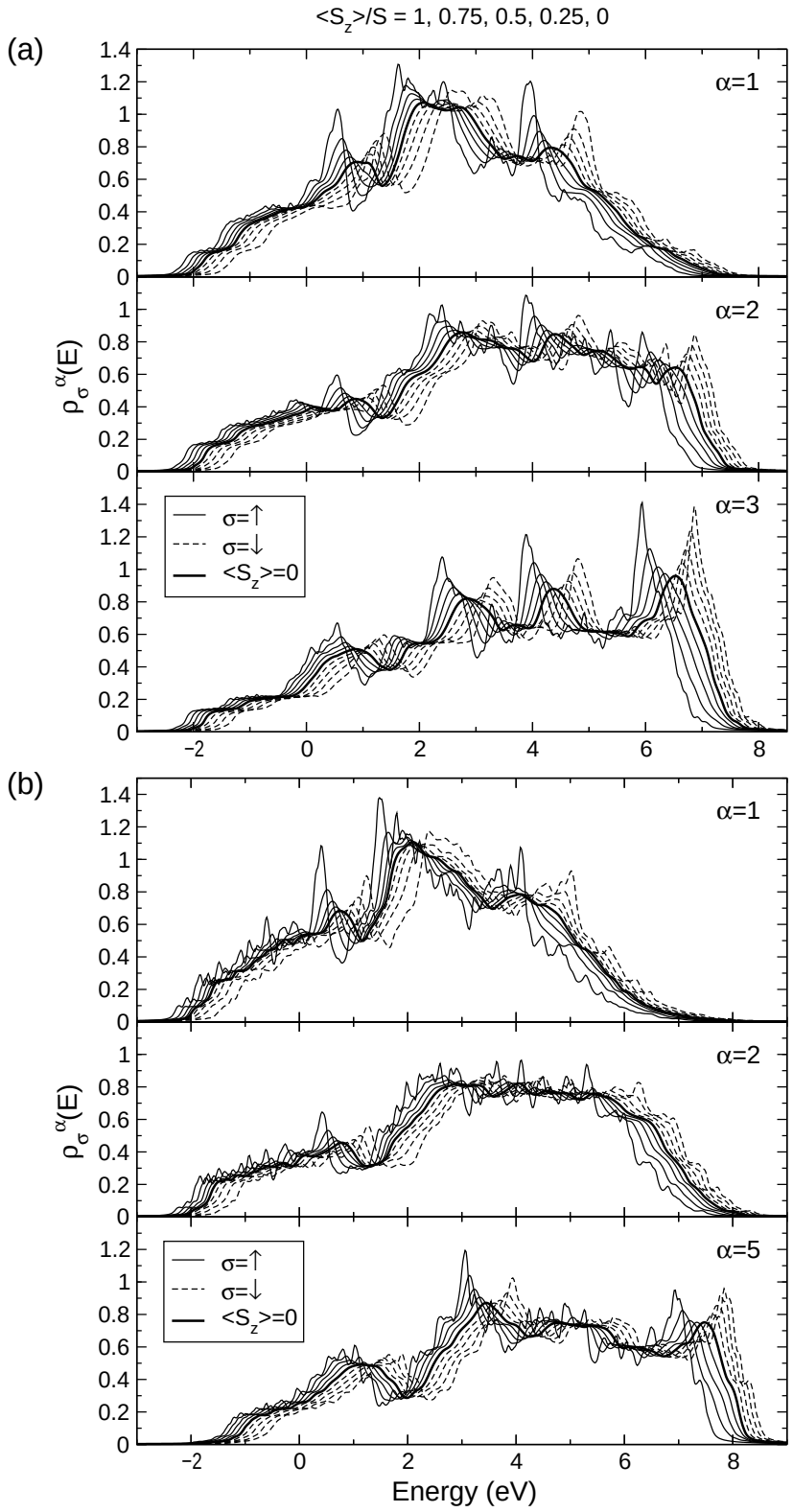

Figure 6.22: Local densities of states of the Eu-*5d* bands of the first, second and center layer of (a) a 5-layer and (b) a 10-layer EuO(100) film for different values of the center layer magnetization $\langle S_z \rangle / S$ (cf. Table 6.2).

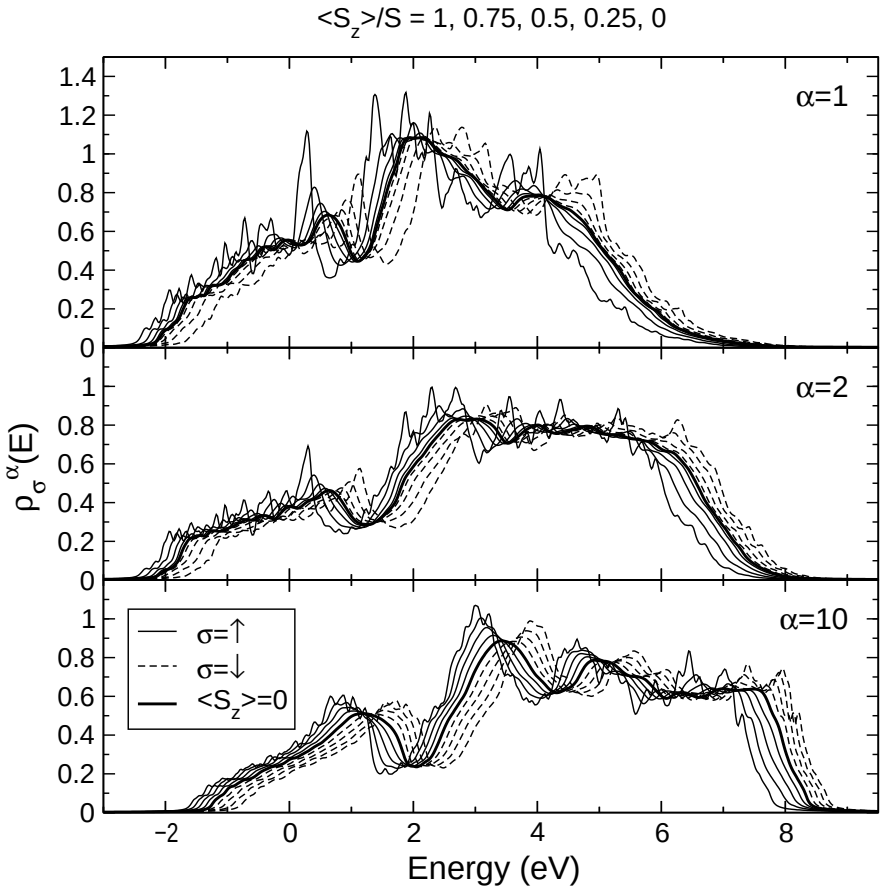

Figure 6.23: Same as Fig. 6.22 for a 20-layer EuO(100) film.

that the temperature dependence of the spectra goes beyond the Stoner picture, where the bands move rigidly towards each other when the temperature is increased. Thus, the temperature dependence shown in Fig. 6.19 is a result of taking the correlation effects into account.

Fig. 6.20 shows the spectral density of a EuO double layer with $J = 0.25\,\mathrm{eV}$ calculated for three different magnetizations, $\langle S_z \rangle / S = 1,\ 0.5,\ 0$, of the local-moment system. The same which has been said about the temperature-dependent tendencies of the spectra of the EuO(100) monolayer applies to the spectra of Fig. 6.20. However, due to the higher number of bands which originates from the interaction between the two EuO(100) layers, the temperature-dependent evolution of the bands becomes less clear for the EuO(100) double layer. Thus, the densities of states of the double layer displayed in Fig. 6.21 draw a clearer picture of the temperature-dependent behavior of the Eu-*5d* states.

Figs. 6.22 and 6.23 show the temperature-dependent local densities of states of a 5-layer, a 10-layer, and a 20-layer EuO(100) film. Different from the cases of the monolayer and the double layer, for these films the densities of states depend on the

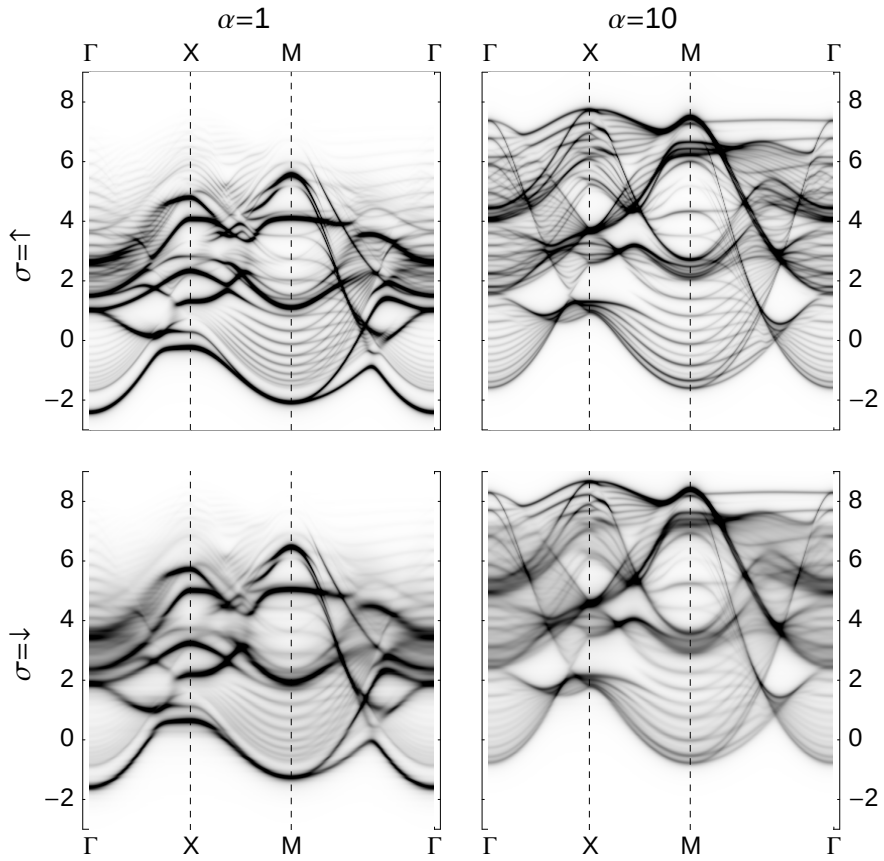

Figure 6.24: Local spectral densities $S^{\alpha\alpha}_{\mathbf{k}\sigma}$ of the surface ($\alpha = 1$) and the center layer ($\alpha = 10$) of a 20-layer EuO(100) film for $T = 0$ and $J = 0.25\,\mathrm{eV}$.

layer index α. Furthermore, the magnetization of the local-moment system is a layer-dependent entity. Here, the temperature parameter $\langle S_z \rangle / S$ refers to the magnetization of the center layer of the film, with the respective temperatures given in Table 6.2.

With increasing film thickness n, the densities of state of the center layer approach the densities of state of bulk EuO as in Fig. 6.17. As a result, the centers of gravity of the bands of the surface layers on the one hand and of the center layers on the other hand move away from each other, with the latter positioning at higher energies. This tendency leads to the existence of EuO(100) surface states, which will be discussed in the following section.

6.3.3 EuO(100) surface states

In Fig. 6.23 the lower band edges of the local densities of states of the surface layer ($\alpha = 1$) lies at lower energies than the respective local densities of state of the center layers, indicating the existence of a surface state at the lower edge of the Eu-*5d* bands.

In Fig. 6.24 the $T = 0$ local spectral density of the surface ($\alpha = 1$) and the center

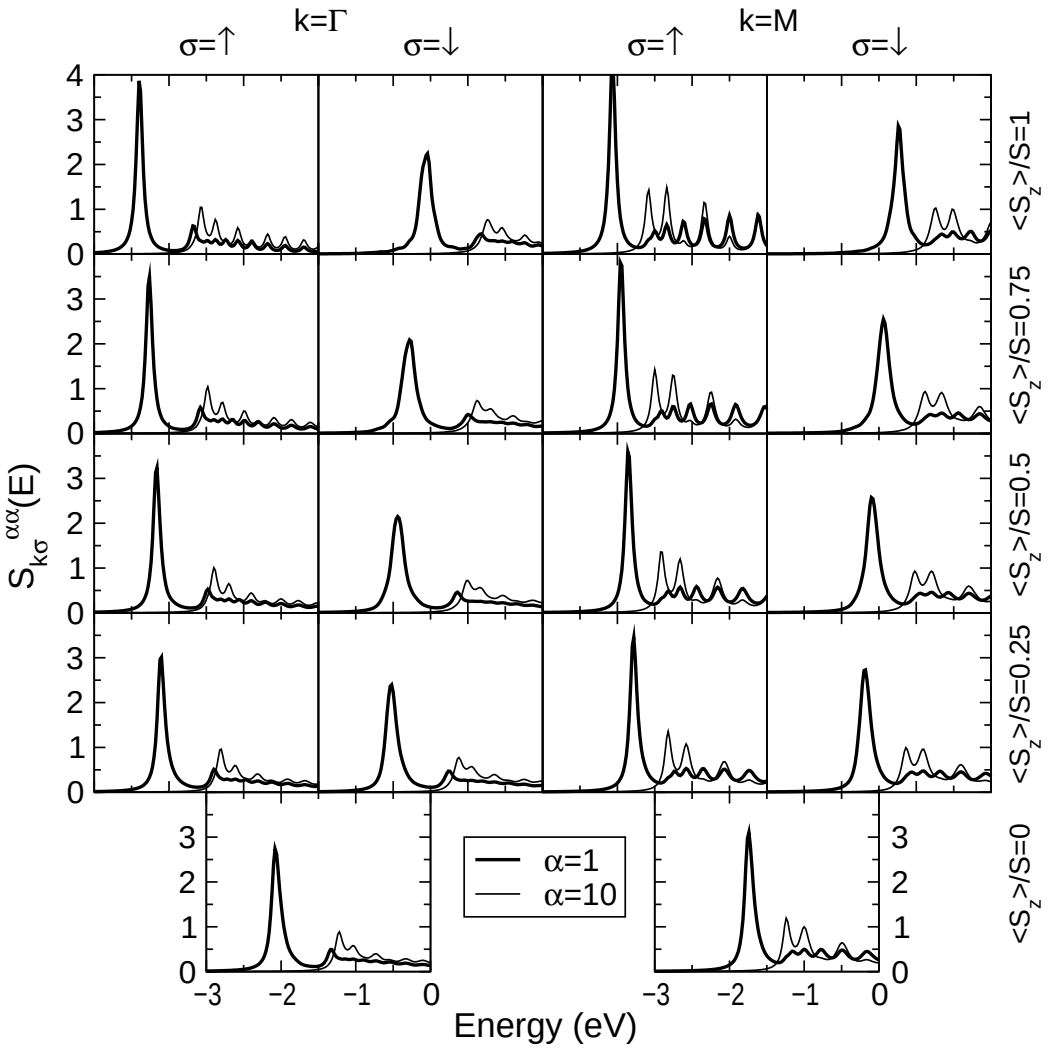

Figure 6.25: Local spectral densities $S_{\mathbf{k}\sigma}^{\alpha\alpha}$ of the surface ($\alpha = 1$) and the center layer ($\alpha = 10$) of a 20-layer EuO(100) film at the Γ-point and the M-point for $J = 0.25\,\mathrm{eV}$ and for different magnetizations $\langle S_z \rangle / S$ of the center layer (cf. Table 6.2).

($\alpha = 10$) layer of a 20-layer EuO(100) film can be seen for both spin directions. A surface state is a state which exists in the so-called forbidden region where no bulk states occur. For the bulk spectral density we take that of the center layer ($\alpha = 10$) of the 20-layer film (see Fig. 6.24). Apart from the still existing difference between the bulk spectral properties and those of the center of a 20-layer film, the respective local density of states corresponds to the bulk density of states projected onto the fcc(100) surface. The forbidden regions lie below and above the bulk bands but also includes "white regions" right in the middle of the bulk bands. In this respect, in Fig. 6.24, clearly the lowest bands of the spin-↑ and of the spin-↓ spectral densities of the surface layer ($\alpha = 1$) around the Γ-point and the M-point constitute surface

states. These surface states originate in the case of the spin-↑ electron from the LSDA calculation. With the *s-f* model calculation one can now investigate the temperature dependence of the surface state.

Fig. 6.25 shows the spectral density of the surface layer of a 20-layer film at $\mathbf{k} = \Gamma$ and $\mathbf{k} = \mathrm{M}$ for different values of the magnetization of the center layer. For comparison, the respective spectral densities of the center layer of the 20-layer films are plotted. The plotted spectral densities clearly indicate a surface state, which for $T = 0$ ($\langle S_z \rangle / S = 1$) lies at the Γ-point about 0.8 eV and at the M-point about 0.45 eV below the lower conduction-band edge of the "bulk" bands of the central layers. These splittings between the surface states and the lower edges of the bulk band are almost independent on the temperature. With increasing temperature both the surface states and the lower band edges of the bulk bands for the two spin directions converge Stoner-like.

As a result, the surface state does not change the red shift of system. However, the lower band edge of LDOS at the surface is lowered by about 0.8 eV compared to the bulk-like LDOS in the center of the film. Thus, for the 20-layer EuO(100) film, the band gap between the occupied $4f^{\uparrow}$ bands and the unoccupied $5d_{t_{2g}}$ bands will be reduced by the same 0.8 eV. When decreasing the temperature to $T = 0$ the red shift will reduce the band gap further: by 0.35 eV according to our calculations and by 0.27 eV according to the experimental results [47]. The overall reduction of the $4f$-$5d_{t_{2g}}$ gap will amount to 1.15 eV and 1.07 eV, respectively. These values are exactly in the range of the experimental band gap of the $4f$-$5d_{t_{2g}}$ transition of bulk EuO at 300 K of 1.12 eV [47]. These results indicate a possible surface insulator-metal transition in EuO(100) films as a function of decreasing temperature, $T \to 0$. Due to the exchange splitting of the conduction bands into the lower-energetic spin-↑ band and the higher-energetic spin-↓ band the respective phase for $T \to 0$ would be a half-metal. As a result, the resistivity of the EuO(100) films should be highly dependent on an applied magnetic field which would further increase the splitting of the states for the two spin directions and would result in the existence of a colossal magnetoresistance (CMR) effect.

There have been experimental works on the resistivity, the Hall effect and the insulator-metal transition in EuO by Shapira *et al.* [143, 144]. In these works it was found that Eu rich EuO samples both show a an insulator transition for temperatures of about 50 K, which lie significantly below the Curie temperature, and exhibit a colossal magnetoresistance effect. In these samples these effects are due to the impurity levels of the additional Eu^{2+} ions, which lie slightly below the lower conduction-band edge for $T \approx T_C$.

Different from the results by Shapira *et al.* [143, 144] the results presented in this section predict both the insulator-metal transition and the CMR effect for the surfaces of stoichiometric EuO(100) films. Conductivity and Hall effect measurements on EuO films therefore would be highly interesting.

7 Summary and Outlook

This dissertation has been concerned with the theoretical description of the temperature-dependent electronic structure and the magnetic properties of *4f* systems with film geometry. In the first part, a theory based on the *s-f* model has been presented and applied to a local-moment model film. Within this approach the temperature-dependent electronic structures of films of varying thicknesses have been obtained. In the second part of the thesis, the theory for the model films was extended to real systems. Finally, the temperature-dependent electronic structures of EuO(100) films have been presented.

The theory describes the local-moment films within the framework of the *s-f* model, which features a ferromagnetic intra-atomic exchange interaction between the localized magnetic moments of the *4f* shell and a single non-degenerated conduction band. A theoretical approach has been presented for the special situation of single electron in an otherwise empty conduction band which corresponds to the situation in a magnetic semiconductor. Due to the empty conduction band, the Hamiltonian of the system can be separated into a magnetic and an electronic part. The magnetic subsystem of localized magnetic moments can be described within the Heisenberg model. For the electronic subsystem the temperature dependence is mediated by certain *f*-spin correlation functions which are obtained within the calculations for the local-moment system. The approach for the electronic subsystem makes use of a moment-conserving decoupling approximation (MCDA) for suitably defined Green functions. The fact that the theory for finite temperatures presented in chapter 3 evolves continuously from the exactly solvable case of ferromagnetic saturation [94] gives it substance.

In chapter 4 the theory has been evaluated for sc(100) films. The exchange coupling of the conduction band to the local-moment system gives rise to a correlation induced splitting of the quasiparticle spectra. A polaron part may be interpreted as a repeated emission and reabsorption of magnons by the conduction electron resulting in a new quasiparticle, the magnetic polaron. A rather broad scattering peak is due to a simple magnon absorption or emission by the conduction electron. This pronounced splitting depends on the actual value of the exchange interaction over bandwidth, J/W. For small values, only a renormalization of the one-electron energy occurs, resulting in a deformation of the free dispersion. For higher values, $J/W \gtrapprox 0.2$, the mentioned splitting of the spectra into polaron part and scattering part sets in.

In systems with film geometry one gets a superposition of the correlation effects with the sheer geometrical dependence of the spectra on film thickness and layer index. A modified hopping in the vicinity of the surfaces of the film can lead to the

occurrence of surface states. The temperature dependence of these surface states has been investigated. Here, the results are in agreement with experimental works on a Gd(0001) surface state [38, 39].

The second part of the thesis is devoted to the temperature-dependent electronic structure and the magnetic properties of "real" EuO(100) films and bulk EuO. The step from the model calculations to the calculations for a real system is done by substituting the tight-binding band structure taken for the model films by a real band structure obtained within an LSDA calculation. For the in general multiple and degenerated conduction bands of a real system, the original *s*-*f* interaction describing the intra-atomic exchange between a localized moment and a single non-degenerated conduction band has to be replaced by a multi-band *s*-*f* interaction. In Sec. 5.1 the respective Hamiltonian has been derived from the general expression for the Coulomb interaction.

The numerical calculations for the EuO systems start with the calculation of the magnetic properties. Here, a Heisenberg model with an additional single-ion anisotropy contribution is employed. Taking the experimental value for the Heisenberg exchange interaction up to second nearest neighbors, the experimental values for the Curie temperature of bulk EuO is reproduced with a satisfying accuracy and the thickness-dependent Curie temperatures of EuO(100) films have been calculated. The band structure of bulk EuO and EuO(100) films have been calculated using the TB-LMTO-ASA method. Here, the film geometries are realized by introducing a supercell geometry, where consecutive EuO(100) films are isolated from each other by a stack of spacer layers. The obtained spin-dependent band structures of bulk EuO compare well to the results of other band-structure calculations for EuO. For the EuO(100) films one gets a convergence of the local densities of states of the center layer(s) of the film towards the bulk densities of states with increasing film thickness n.

For the calculation of the temperature dependent band structures of the EuO systems, the spin-↑ Eu-*5d* bands have been taken as input for the hopping matrices. The reason for taking the spin-↑ bands is that within the model calculation, the solution for the spin-↑ electron for the ferromagnetic saturation ($T = 0$) is only rigidly shifted compared to the free dispersion. As a result, due to the fact that the solution for the case of ferromagnetic saturation is exact, the problem of double counting of relevant interactions does not occur. The presented approach for including the band structure of the Eu-*5d* bands in the model calculation employs a decomposition into subbands, which takes into account the symmetry of the respective *5d* orbitals.

Already for the case of the ferromagnetic saturation of the local-moment system, the spin-↓ spectra of the EuO systems obtained within the model calculation exhibit strong deviations from the one-particle results obtained within the LSDA calculations, which can be attributed to correlation effects. These correlation effects for the spin-↓ electron spectra increase, when the temperature is switched on. The spin-↑ spectra, which for the case of $T = 0$ correspond to the spin-↑ LSDA spectra, develop these correlation effects with increasing temperature $T > 0$. The loss of magnetization of the local-moment system with increasing temperature for $T \to T_C$ leeds to a convergence of the spectra for both spin directions.

For the *d-f* interaction a value of $J = 0.25\,\mathrm{eV}$ has been deduced from the spin-dependent splitting of the LSDA spectra. Within the model calculation this *s-f* interaction leeds to a red shift of the optical absorption edge of the *4f*-$5d_{t_{3g}}$ transition in bulk EuO of about 0.35 eV when decreasing the temperature from $T = T_\mathrm{C}$ to $T = 0$. This value compares well to the experimental value for the red shift in EuO of about 0.27 eV [47].

For the EuO(100) films the correlation effects, already existing for the case of bulk EuO, are superimposed with the geometrical dependence of the spectral properties on the film thickness and with the local variation of the spectral properties within the films. Most interestingly, for a 20-layer film, the LSDA calculations result in the existence of a surface state, which lies about 0.8 eV below the bulk conduction band. The respective shift of the lower conduction-band edge towards lower energies due to the EuO(100) surface state is comparable to the experimental *4f*-$5d_{t_{2g}}$ gap at $T = 0$ of 0.85 eV. This implies, that a surface insulator-half-metal transition appears possible for thick EuO(100) films. Here, the limitations of the LSDA calculations presented in this thesis are, that no relaxation of the interlayer distance in the vicinity of the surfaces of the films has been taken into account.

The most interesting and immanent extension of the present thesis is the extension of the theory presented in chapters 3 and 5 to a non-zero occupation of the conduction bands. For the three-dimensional case and for a single non-degenerated model band this theory has been given by Nolting *et al.* [81]. In this theory the exchange interactions between the local magnetic moments are given by an indirect exchange via the conduction band. As a result, the magnetization and the higher correlation functions of the local-moment system have to be calculated self-consistently as opposed to the case of $n = 0$ discussed in this thesis. The theory for $n \neq 0$ has been applied to bulk Gd [145], however, with a band decomposition of the Eu-*5d* bands into simple non-interacting *s* bands by assigning the lowest-energetic eigenstates to the lowest band etc. (cf. Sec. 6.3.1). The flaw of these calculations is that the self-consistent calculations yield no ferromagnetism for the local-moment system. Therefore, for the calculations the magnetization of the local-moment system had to be kept at a fixed value [145]. A reason for this result is that the employed band decomposition yields a set of consecutive bands whose band occupancy is not related to the real band occupancy of the Gd-*5d* bands. Here, the band decomposition proposed in this thesis promises to result in a realistic band occupancy of the subbands which would give the chance of getting the ferromagnetic Gd within a completely self-consistent calculation.

Concerning the aspect of reduced dimensionality discussed in this thesis, the dependence of the magnetic and electronic properties of Gd films are of high experimental and theoretical interest. Respective investigations would shed light on some extraordinary physical properties of the lanthanides [19], in particular the enhanced Curie temperature of the Gd(0001) surface [26, 27, 28, 30] and its relation to the temperature-dependent behavior of the Gd(0001) surface state [34, 35, 36, 33, 37, 95, 96, 38, 39, 40, 41, 42].

The theory for the *s-f* model with finite band occupation holds a couple of fur-

ther interesting applications. These include the calculation of the electronic, magnetic and conductive properties of Eu rich EuO systems. These systems exhibit interesting physical properties like the temperature-dependent insulator-metal transition which is accompanied by a colossal magnetoresistance (CMR) phenomenon. In the same direction aims the calculation of magnetic and conductive properties of the perovskite manganites, $La_{1-x}Sr_xMnO_3$ and $La_{1-x}Ca_xMnO_3$. These materials have become popular due to the observation of colossal magnetoresistance phenomena [8, 9]. Furthermore, they exhibit a complicated phase diagram as a function of doping x and temperature including regions with ferromagnetic phases, but also regions with charge ordering and antiferromagnetic correlation [11].

The model of reference for the manganites is the double-exchange (DEX) or the ferromagnetic Kondo-lattice model (FKLM) [10, 12, 11] which both are other names for the *s-f* model discussed in this thesis. The perovskite manganites $La_{1-x}A_xMnO_3$ (A = Sr, Ca) have $(4-x)$ *3d* electrons per atom in the $(t_{2g})^3(e_g)^{(1-x)}$ configuration [12]. The three t_{2g} electrons couple to a maximum spin of $S = 3/2$ and represent a localized magnetic moment which is exchange coupled to the e_g electrons. The accepted approach for the FKLM is the dynamical mean-field theory (DMFT), first introduced by Metzner and Vollhardt [146], which assumes the self-energy of the system to be a local entity. This is an exact statement in the limit of infinite dimensions $d \to \infty$ or, equivalently, infinite coordination number Z. The application of the DMFT to the FKLM [147, 148, 12, 149] assumes the spin of the t_{2g} electrons to be classical, $S \to \infty$. Here, the theoretical approach for the *s-f* model for finite band occupation [81] to the perovskite manganites holds the prospect of investigating the influence of a quantized t_{2g} spin on the physics of these materials.

A Combination of LDA and model calculation

Within the TB-LMTO method it is possible, to directly extract the **k**-resolved Hamilton operator $\hat{\mathrm{H}}^{ll'}_{\mathbf{k}}$ and overlap matrix $\mathrm{S}^{ll'}_{\mathbf{k}}$. In the three-dimensional case the indices l and l' correspond to the band indices m and m', respectively, whereas in the of film structures, they are multi-indices including the layer indices, $l = (\alpha, m)$, $l' = (\beta, m')$. The Schrödinger equation for the band structure problem reads,

$$\sum_{l'} \left(\hat{\mathrm{H}}^{ll'}_{\mathbf{k}} - E^{a}_{\mathbf{k}} \mathrm{S}^{ll'}_{\mathbf{k}}\right) \hat{u}^{a}_{l'}(\mathbf{k}) = 0 \tag{A.1}$$

where the $\hat{u}^{a}_{l}(\mathbf{k})$ are the eigenfunctions to the eigenvalue $E^{a}_{\mathbf{k}}$. Via coefficiencts $c^{a}_{ll'}(\mathbf{k})$ they are related to the Bloch sums $\hat{\psi}_{l}(\mathbf{k})$,

$$\hat{u}^{a}_{l}(\mathbf{k}) = \sum_{l'} c^{a}_{ll'}(\mathbf{k}) \hat{\psi}_{l'}(\mathbf{k}), \qquad \hat{\psi}_{l}(\mathbf{k}) = N^{-\frac{1}{2}} \sum_{\mathbf{R}} \mathrm{e}^{i\mathbf{k}\mathbf{R}} \hat{\psi}_{l}(\mathbf{r} - \mathbf{R}). \tag{A.2}$$

Here, the $\hat{\psi}_{l}(\mathbf{r} - \mathbf{R})$ are the muffin-tin orbitals of the atom at the position $\mathbf{R}$. The $\hat{\mathrm{H}}^{ll'}_{\mathbf{k}}$ represents the matrix elements of the Hamilton operator $\mathcal{H}$ with respect to the basis functions $\hat{\psi}_{l}(\mathbf{k})$ and $\mathrm{S}^{ll'}_{\mathbf{k}}$ is the overlap matrix,

$$\hat{\mathrm{H}}^{ll'}_{\mathbf{k}} = \langle \hat{\psi}_{l}(\mathbf{k}) | \mathcal{H} | \hat{\psi}_{l'}(\mathbf{k}) \rangle \tag{A.3}$$

$$\mathrm{S}^{ll'}_{\mathbf{k}} = \langle \hat{\psi}_{l}(\mathbf{k}) | \hat{\psi}_{l'}(\mathbf{k}) \rangle. \tag{A.4}$$

The transformation to an orthogonal set of basis functions, $\langle \psi_{l}(\mathbf{k}) | \psi_{l'}(\mathbf{k}) \rangle = \delta_{ll'}$, is given by

$$\mathbf{H}_{\mathbf{k}} = \mathbf{S}^{-\frac{1}{2}}_{\mathbf{k}} \cdot \hat{\mathbf{H}}_{\mathbf{k}} \cdot \mathbf{S}^{-\frac{1}{2}}_{\mathbf{k}}, \qquad \mathbf{u}^{a}(\mathbf{k}) = \mathbf{S}^{+\frac{1}{2}}_{\mathbf{k}} \hat{\mathbf{u}}^{a}(\mathbf{k}). \tag{A.5}$$

As a result, the **k**-dependent eigenvalues of the system can be obtained from the such transformed Hamilton matrix,

$$\sum_{l'} \left(\mathrm{H}^{ll'}_{\mathbf{k}} - E^{a}_{\mathbf{k}}\right) u^{a}_{l'}(\mathbf{k}) = 0, \tag{A.6}$$

which directly corresponds to the hopping intergrals from Eq. (5.1).

Bibliography

[1] P. WACHTER. *Helv. phys. Acta* **37**, 637 (1964). 7, 12, 81

[2] G. BUSCH, J. JUNOD, AND P. WACHTER. *Phys. Lett.* **12**, 11 (1964). 7, 12, 81

[3] B. BATLOGG, E. KALDIS, A. SCHLEGEL, AND P. WACHTER. *Phys. Rev. B* **12**, 3940 (1975). 7, 12

[4] W. NOLTING. *J. Phys. C* **12**, 3033 (1979). 7, 17

[5] C. ZENER. *Phys. Rev.* **81**, 440 (1951). 7, 14, 20

[6] T. KASUYA. *Prog. Theor. Phys. (Kyoto)* **16**, 45 (1956). 7, 14, 20, 21

[7] K. YOSIDA. *Phys. Rev.* **106**, 893 (1957). 7, 14, 20

[8] K. CHAHARA, T. OHNO, M. KASAI, AND Y. KOZONO. *Appl. Phys. Letters* **63**, 1990 (1993). 7, 94

[9] S. JIN, T. H. TIEFEL, M. MCCORMACK, R. A. FASTNACHT, R. RAMESH, AND L. H. CHEN. *Science* **264**, 413 (1994). 7, 94

[10] N. FURUKAWA. *J. Phys. Soc. Japan* **63**, 3214 (1994). 7, 94

[11] E. DAGOTTO, S. YUNOKI, A. L. MALVEZZI, A. MOREO, J. HU, S. CAPPONI, D. POILBLANC, AND N. FURUKAWA. *Phys. Rev. B* **58**, 6414 (1998). 7, 94

[12] N. FURUKAWA. http://arXiv.org/abs/cond-mat/9812066 (1998). 7, 94

[13] T. WOLFRAM AND R. E. DEWAMES. *Prog. Surf. Sci.* **2**, 233 (1972). 7

[14] D. L. MILLS. Surface spin waves on magnetic crystals. In V. M. AGRANOVICH AND R. LOUDON, editors, "Surface Excitations". North Holland, Amsterdam (1984). 7

[15] A. J. FREEMAN AND C. L. FU. "Magnetic Properties of Low Dimensional Systems", vol. 14 of "Springer Proceedings in Physics", p. 16. Springer, Berlin (1986). 7

[16] K. BINDER. "Phase Transitions and Critical Phenomena", vol. 8. Academic Press, London (1989). 7

[17] P. J. JENSEN. "Magnetische Eigenschaften dünner ferromagnetischer Filme". Habilitationsschrift, Freie Universität Berlin (1994). 7

[18] R. ALLENSPACH. *J. Magn. Magn. Mater.* **129**, 160 (1994). 7

[19] P. A. DOWBEN, D. N. MCILROY, AND D. LI. In K. A. GSCHNEIDNER, JR. AND L. EYRING, editors, "Handbook of the Physics and Chemistry of Rare Earth", vol. 24, ch. 159. Elsevier, Amsterdam (1997). 7, 48, 93

[20] C. SCHÜSSLER-LANGEHEINE. "Magnetic Properties of Thin Films of Heavy Lanthanide Metals Studied by Magnetic X-Ray Diffraction and High-Resolution Photoemission". Doktorarbeit, Freie Universität Berlin (1999). 7, 8

[21] T. HERRMANN. "Ferromagnetismus und temperaturabhängige elektronische Struktur in metallischen dünnen Filmen". Doktorarbeit, Humboldt-Universität zu Berlin (1999). 7

[22] M. POTTHOFF. "Correlated Electrons at Metal Surfaces". Habilitationsschrift, Humboldt-Universität zu Berlin (1999). 7

[23] T. HERRMANN AND W. NOLTING. *J. Phys.: Condens. Matter* **11**, 89 (1999). 7

[24] P. POULOPOULOS AND K. BABERSCHKE. *J. Phys.: Condens. Matter* **11**, 9495 (1999). 7

[25] H. ZABEL. *J. Phys.: Condens. Matter* **11**, 9303 (1999). 7

[26] D. WELLER, S. F. ALVARADO, W. GUDAT, K. SCHRÖDER, AND M. CAMPAGNA. *Phys. Rev. Lett.* **54**, 1555 (1985). 8, 93

[27] C. RAU AND S. EICHNER. *Phys. Rev. B* **34**, 6347 (1986). 8, 93

[28] C. RAU AND M. ROBERT. *Phys. Rev. Lett.* **58**, 2714 (1987). 8, 93

[29] C. RAU, C. JIN, AND M. ROBERT. *J. Appl. Phys.* **63**, 3667 (1988). 8

[30] H. TANG, D. WELLER, T. G. WALKER, J. C. SCOTT, C. CHAPPERT, H. HOPSTER, A. W. PANG, D. S. DESSAU, AND D. P. PAPPAS. *Phys. Rev. Lett.* **71**, 444 (1993). 8, 93

[31] C. RAU, C. JIN, AND M. ROBERT. *Phys. Lett. A* **138**, 334 (1989). 8

[32] C. RAU, C. LIU, A. SCHMALZBAUER, AND G. XING. *Phys. Rev. Lett.* **57**, 2311 (1986). 8

[33] M. DONATH, B. GUBANKA, AND F. PASSEK. *Phys. Rev. Lett.* **77**, 5138 (1996). 8, 47, 93

[34] R. WU AND A. J. FREEMAN. *J. Magn. Magn. Mater.* **99**, 81 (1991). 8, 47, 93

[35] D. LI, C. W. HUTCHINGS, P. A. DOWBEN, C. HWANG, R.-T. WU, M. ONELLION, A. B. ANDREWS, AND J. L. ERSKINE. *J. Magn. Magn. Mater.* **99**, 85 (1991). 8, 47, 93

[36] A. V. FEDOROV, K. STARKE, AND G. KAINDL. *Phys. Rev. B* **50**, 2739 (1994). 8, 47, 93

[37] E. WESCHKE, C. SCHÜSSLER-LANGEHEINE, R. MEIER, A. V. FEDEROV, K. STARKE, F. HÜBINGER, AND G. KAINDL. *Phys. Rev. Lett.* **77**, 3415 (1996). 8, 47, 93

[38] M. DONATH AND B. GUBANKA. In M. DONATH, P. A. DOWBEN, AND W. NOLTING, editors, "Magnetism and Electronic Correlations in Local-Moment Systems: Rare-Earth Elements and Compounds", p. 217. World Scientific, Singapore (1998). 8, 47, 54, 92, 93

[39] M. BODE, M. GETZLAFF, R. PASCAL, S. HEINZE, AND R. WIESENDANGER. In M. DONATH, P. A. DOWBEN, AND W. NOLTING, editors, "Magnetism and Electronic Correlations in Local-Moment Systems: Rare-Earth Elements and Compounds", p. 235. World Scientific, Singapore (1998). 8, 47, 54, 92, 93

[40] C. WALDFRIED, D. N. MCILROY, T. MCAVOY, D. WELIPITIYA, P. A. DOWBEN, AND E. VESCOVO. *J. Appl. Phys.* **83**, 6284 (1998). 8, 47, 93

[41] C. WALDFRIED, T. MCAVOY, D. WELIPITIYA, T. KOMESU, P. A. DOWBEN, AND E. VESCOVO. *Phys. Rev. B* **58**, 7434 (1998). 8, 47, 93

[42] T. KOMESU, C. WALDFRIED, AND P. A. DOWBEN. *Phys. Lett. A* **256**, 81 (1999). 8, 47, 93

[43] E. L. NAGAEV. *phys. stat. sol. (b)* **65**, 11 (1974). 11

[44] W. NOLTING. *phys. stat. sol. (b)* **96**, 11 (1979). 11, 12, 14, 15, 17

[45] S. G. OVCHINNIKOV. *Phase Transitions* **36**, 15 (1991). 11

[46] F. HOLTZBERG, T. R. MCGUIRE, AND S. METHFESSEL. In K.-H. HELLWEGE AND A. M. HELLWEGE, editors, "Magnetic and Other Properties of

Oxides and Related Compounds", vol. 4a of "Landoldt-Börnstein – Numerical Data and Functional Relationships in Science and Technology", ch. 2.2. Springer-Verlag, Berlin (1970). 11, 66

[47] P. WACHTER. In K. A. GSCHNEIDNER, JR. AND L. EYRING, editors, "Alloys and Intermetallics", vol. 2 of "Handbook of the Physics and Chemistry of Rare Earths", ch. 19. Elsevier, Amsterdam (1991). 11, 12, 13, 16, 64, 65, 66, 82, 90, 93

[48] W. NOLTING. "Vielteilchentheorie", vol. 7 of "Grundkurs Theoretische Physik". Viehweg, Braunschweig/Wiesbaden, 4th ed. (1997). 11, 14, 17, 19

[49] P. FAZEKAS. "Lecture Notes on Electron Correlation and Magnetism", vol. 5 of "Series in Modern Condensed Matter Physics", ch. 11. World Scientific, Singapore (1999). 11, 20

[50] I. TSUBOKAWA. *J. Phys. Soc. Japan* **15**, 1664 (1960). 12

[51] B. T. MATTHIAS, R. M. BOZORTH, AND J. H. VAN VLECK. *Phys. Rev. Lett.* **7**, 160 (1961). 12

[52] G. BUSCH, P. JUNOD, M. RISI, AND O. VOGT. "Proceedings of the International Conference on Semiconductors, Exeter 1962", p. 727. Institute of Physics and Physical Society, London (1962). 12

[53] T. R. MCGUIRE, B. E. ARGYLE, M. W. SHAFER, AND J. S. SMART. *Appl. Phys. Letters* **1**, 17 (1962). 12

[54] S. VAN HOUTEN. *Phys. Rev. Lett.* **2**, 215 (1962). 12

[55] G. BUSCH, P. COTTI, AND P. MUNZ. *Solid State Commun.* **7**, 795 (1969). 12, 72

[56] D. E. EASTMAN, F. HOLTZBERG, AND S. METHFESSEL. *Phys. Rev. Lett.* **23**, 226 (1969). 12, 69, 72

[57] G. GÜNTHERODT, P. WACHTER, AND D. M. IMBODEN. *Phys. kondens. Materie* **12**, 292 (1971). 12, 69

[58] D. E. EASTMAN AND M. KUZNIETZ. *J. Appl. Phys.* **42**, 1396 (1971). 12, 69

[59] R. GRIESSEN, M. LANDOLDT, AND H. R. OTT. *Solid State Commun.* **9**, 2219 (1971). 13

[60] H. G. BOHN, W. ZINN, B. DORNER, AND A. KOLLMAR. *Phys. Rev. B* **22**, 5447 (1980). 13, 63

[61] L. PASSELL, O. W. DIETRICH, AND J. ALS-NIELSEN. *Phys. Rev. B* **14**, 4897 (1976). 13, 63

[62] J. ALS-NIELSEN, O. W. DIETRICH, AND L. PASSELL. *Phys. Rev. B* **14**, 4908 (1976). 13, 63

[63] O. W. DIETRICH, J. ALS-NIELSEN, AND L. PASSELL. *Phys. Rev. B* **14**, 4923 (1976). 13, 63

[64] U. KÖBLER, I. APFELSTEDT, K. FISCHER, W. ZINN, E. SCHEER, J. WOSNITZA, H. V. LÖHNEYSEN, AND T. BRÜCKEL. *Z. Phys. B* **92**, 475 (1993). 13

[65] U. KÖBLER, R. MUELLER, L. SMARDZ, D. MAIER, K. FICHER, B. OLEFS, AND W. ZINN. *Z. Phys. B* **100**, 497 (1996). 13

[66] S. V. VONSOVSKII. *Zh. eksper. teor. Fiz.* **16**, 981 (1946). 14

[67] T. WOLFRAM AND J. CALLAWAY. *Phys. Rev.* **127**, 1605 (1962). 14

[68] T. WOLFRAM AND J. CALLAWAY. *Phys. Rev.* **130**, 45 (1963). 14

[69] A. FETTER AND J. D. WALECKA. "Quantum Theory of Many-Particle Systems". McGraw-Hill Publ. Co., San Francisco (1969). 17

[70] A. C. HEWSON. "The Kondo Problem to Heavy Fermions", vol. 2 of "Cambridge Studies in Magnetism", ch. 1. Cambridge University Press, Cambridge (1997). 20, 21, 22

[71] A. H. WILSON. "The Theory of Metals", p. 282. Cambridge University Press, Cambridge (1953). 21

[72] W. J. DE HAAS, J. H. DE BOER, AND G. J. VAN DEN BERG. *Physica* **1**, 1115 (1934). 21

[73] P. W. ANDERSON. *Phys. Rev.* **124**, 41 (1961). 21

[74] J. KONDO. *Prog. Theor. Phys. (Kyoto)* **32**, 37 (1964). 22

[75] P. W. ANDERSEN. *J. Phys. C* **3**, 2346 (1970). 22

[76] K. G. WILSON. *Nobel Symposia* **24**, 68 (1974). 22

[77] K. G. WILSON. *Rev. Mod. Phys.* **47**, 773 (1975). 22

[78] J. KONDO. vol. 23 of "Solid State Physics", p. 184. Academic Press, New York and London (1969). 22

[79] R. B. COLES. *Phys. Lett.* **8**, 243 (1964). 22

[80] J. R. SCHRIEFFER AND P. A. WOLFF. *Phys. Rev.* **149**, 491 (1966). 23, 24

[81] W. NOLTING, S. REX, AND S. M. JAYA. *J. Phys. C* **9**, 1301 (1997). 26, 93, 94

[82] R. SCHILLER. "Das magnetische Polaron in dimensionsreduzierten Systemen". Diplomarbeit, Humboldt-Universität zu Berlin (1996). 26, 31, 50, 51, 58

[83] R. SCHILLER AND W. NOLTING. *Phys. Rev. B* **60**, 462 (1999). 26

[84] W. NOLTING, S. M. JAYA, AND S. REX. *Phys. Rev. B* **54**, 14455 (1996). 31, 40, 45

[85] N. M. MERMIN AND H. WAGNER. *Phys. Rev. Lett.* **17**, 1133 (1966). 33

[86] A. GELFERT AND W. NOLTING. *phys. stat. sol. (b)* **217**, 805 (2000). 33

[87] R. SCHILLER AND W. NOLTING. *Solid State Commun.* **110**, 121 (1999). 33

[88] H. B. CALLEN. *Phys. Rev.* **130**, 890 (1963). 33, 35

[89] M. E. LINES. *Phys. Rev.* **156**, 534 (1967). 34

[90] E. PRAVECZKI. *Phys. Lett.* **6**, 147 (1963). 35

[91] W. NOLTING. "Quantentheorie des Magnetismus, Teil 2: Modelle". Teubner, Stuttgart (1986). 35, 63, 64

[92] S. R. ALLAN AND D. M. EDWARDS. *J. Phys. C* **15**, 2151 (1982). 40

[93] W. NOLTING AND U. DUBIL. *phys. stat. sol. (b)* **130**, 561 (1985). 40

[94] R. SCHILLER, W. MÜLLER, AND W. NOLTING. *J. Magn. Magn. Mater.* **169**, 39 (1997). 40, 42, 46, 91

[95] M. DONATH, P. A. DOWBEN, AND W. NOLTING, editors. "Magnetism and Electronic Correlations in Local-Moment Systems: Rare-Earth Elements and Compounds". World Scientific, Singapore (1998). 47, 93

[96] C. WALDFRIED AND P. A. DOWBEN. In M. DONATH, P. A. DOWBEN, AND W. NOLTING, editors, "Magnetism and Electronic Correlations in Local-Moment Systems: Rare-Earth Elements and Compounds", p. 171. World Scientific, Singapore (1998). 47, 93

[97] D. A. PAPACONSTANTOPOULOS. "Handbook of the Band Structure of Elemental Solids", p. 20. Plenum Press, New York (1986). 49

[98] O. ERIKSSON, R. AHUJA, A. ORMECI, J. TRYGG, O. HJORTSTAM, P. SÖDERLIND, B. JOHANSSON, AND J. M. WILLS. *Phys. Rev. B* **52**, 4420 (1995). 49, 68

[99] R. SCHILLER, W. MÜLLER, AND W. NOLTING. *Eur. Phys. J. B* **2**, 249 (1998). 50, 52

[100] R. SCHILLER, W. MÜLLER, AND W. NOLTING. *J. Phys.: Condens. Matter* **11**, 9589 (1999). 50

[101] W. MÜLLER, R. SCHILLER, AND W. NOLTING. *Eur. Phys. J. B* **16**, 705 (2000). 50, 51

[102] S. LUDQVIST AND N. H. MARCH, editors. "Theory of the Inhomogeneous Electron Gas". Plenum Press, New York (1983). 59

[103] P. PHARISEAU AND W. M. TEMMERMANN, editors. "The Electronic Structure of Complex Systems". Plenum Press, New York (1984). 59

[104] R. M. DREIZLER AND J. DE PROVIDÊNCIA, editors. "Density Functional Methods in Physics". Plenum Press, New York (1985). 59

[105] R. M. DREIZLER AND E. K. U. GROSS. "Density Functional Theory". Springer, Berlin (1990). 59

[106] H. ESCHRIG. "The Fundamentals of Density Functional Theory", vol. 32 of "Teubner-Texte zur Physik". Teubner, Stuttgart (1996). 59

[107] J. KÜBLER AND V. EYERT. In K. H. J. BUSCHOW, editor, "Electronic and Magnetic Properties of Metals and Ceramics – Part I", vol. 3A of "Materials Science and Technology – A Comprehensive Treatment", ch. 1. VCH, Weinheim (1992). 59

[108] V. EYERT. In M. SPRINGBORG, editor, "Density Functional Methods: Applications in Chemistry and Materials Science", p. 233. J. Wiley, Chichester (1997). 59

[109] V. EYERT. *Int. J. Quant. Chem.* **77**, 1007 (2000). 59

[110] H. L. SKRIVER. "The LMTO Method", vol. 41 of "Springer Series in Solid-State Sciences". Springer, Berlin (1984). 59, 62

[111] D. J. SINGH. "Planewaves, Pseudopotentials and the LAPW Method". Kluwer Academic Publishers, Boston (1994). 59

[112] E. WIMMER. "Prediction of Materials Properties". In P. VON RAGUÉ-SCHLEYER, editor, "Encyclopedia of Computational Chemistry". J. Wiley, New York (1998). 59

[113] P. HOHENBERG AND W. KOHN. *Phys. Rev.* **136**, B 864 (1964). 59

[114] W. KOHN AND L. J. SHAM. *Phys. Rev.* **140**, A 1133 (1965). 59, 60

[115] L. HEDIN AND B. I. LUNDQVIST. *J. Phys. C* **4**, 2064 (1971). 61

[116] U. VON BARTH AND L. HEDIN. *J. Phys. C* **5**, 1629 (1972). 61

[117] O. GUNNARSSON AND B. I. LUNDQVIST. *Phys. Rev. B* **13**, 4274 (1976). 61

[118] E. P. WIGNER AND F. SEITZ. *Phys. Rev.* **43**, 804 (1933). 62

[119] E. P. WIGNER AND F. SEITZ. *Phys. Rev.* **46**, 509 (1934). 62

[120] J. C. SLATER. *Phys. Rev.* **51**, 846 (1937). 62

[121] J. KORRINGA. *Physica* **13**, 392 (1947). 62

[122] W. KOHN AND N. ROSTOKER. *Phys. Rev.* **94**, 1111 (1954). 62

[123] F. BLOCH. *Z. Phys.* **52**, 555 (1928). 62

[124] N. F. MOTT AND J. H. "The Theory of Metals and Alloys". Oxford University Press, London (1936). 62

[125] O. K. ANDERSEN. *Phys. Rev. B* **12**, 3060 (1975). 62, 66

[126] A. R. WILLIAMS, J. KÜBLER, AND C. D. GELATT, JR. *Phys. Rev. B* **19**, 1990 (1979). 62

[127] J. F. DILLON AND C. E. OLSEN. *Phys. Rev.* **135**, A 434 (1964). 65

[128] N. MIYATA AND B. E. ARGYLE. *Phys. Rev.* **157**, 448 (1967). 65

[129] S. VON MOLNAR AND A. W. LAWSON. *Phys. Rev.* **139**, A 1598 (1965). 65

[130] M. C. FRANZBLAU, G. L. EVERETT, AND A. W. LAWSON. *Phys. Rev.* **164**, 716 (1967). 65

[131] O. K. ANDERSEN AND O. JEPSEN. *Phys. Rev. Lett.* **53**, 2571 (1984). 66

[132] G. KRIER, O. JEPSEN, A. BURKHARDT, AND O. K. ANDERSEN. "The TB-LMTO-ASA program". Max-Planck-Institut für Festkörperforschung, Heisenbergstr. 1, D-70569 Stuttgart, Germany (April 1995). 66

[133] O. K. ANDERSEN, Z. PAWLOWSKA, AND O. JEPSEN. *Phys. Rev. B* **34**, 5253 (1986). 66

[134] V. I. ANISIMOV, J. ZAANEN, AND O. K. ANDERSEN. *Phys. Rev. B* **44**, 943 (1991). 69

[135] V. I. ANISIMOV, F. ARYASETIAWAN, AND A. I. LICHTENSTEIN. *J. Phys.: Condens. Matter* **9**, 767 (1997). 69

[136] S. J. CHO. *Phys. Rev. B* **1**, 4589 (1970). 72

[137] O. V. FABEROVICH AND S. V. VLASOV. *phys. stat. sol. (b)* **105**, 755 (1981). 72

[138] W. NOLTING, G. BORSTEL, AND W. BORGIEL. *Phys. Rev. B* **35**, 7015 (1987). 72, 78, 82, 83

[139] W. NOLTING, G. BORSTEL, AND W. BORGIEL. *Phys. Rev. B* **35**, 7025 (1987). 78, 82, 83

[140] J. T. JANAK AND A. R. WILLIAMS. *Phys. Rev. B* **14**, 4199 (1976). 78

[141] U. K. POULSEN, J. KOLLER, AND O. K. ANDERSEN. **F6**, L241 (1976). 78

[142] O. GUNNARSON. *Physica B* **91**, 329 (1977). 78

[143] Y. SHAPIRA, S. FONER, AND T. B. REED. *Phys. Rev. B* **8**, 2299 (1973). 90

[144] Y. SHAPIRA, S. FONER, R. L. AGGARWAL, AND T. B. REED. *Phys. Rev. B* **8**, 2316 (1973). 90

[145] S. REX, V. EYERT, AND W. NOLTING. *J. Magn. Magn. Mater.* **192**, 529 (1999). 93

[146] W. METZNER AND D. VOLLHARDT. *Phys. Rev. Lett.* **62**, 324 (1989). 94

[147] T. PRUSCHKE, M. JARRELL, AND J. FREERICKS. *Adv. Phys.* **44**, 187 (1995). 94

[148] A. GEORGES, G. KOTLIAR, W. KRAUTH, AND M. J. ROZENBERG. *Rev. Mod. Phys.* **68**, 13 (1996). 94

[149] K. HELD AND D. VOLLHARDT. *Phys. Rev. Lett.* **84**, 5168 (2000). 94

Lebenslauf

Persönliche Daten

Name:	Roland Schiller
Geburtstag:	13. Mai 1972
Geburtsort:	Berlin
Nationalität:	deutsch

Ausbildung

06/1990	Abitur am Heinrich-Hertz-Gymnasium in Berlin (Note: 1.2)
10/1991–09/1994	Physikstudium an der Friedrich-Schiller-Universität Jena und an der Humboldt-Universität zu Berlin
02/1994–01/1997	Stipendiat der Studienstiftung des deutschen Volkes
10/1994–09/1995	Studium and der Loughborough University in England, Abschluss: Master of Science (MSc)
10/1995–03/1997	Übungsleiter am Institut für Physik der Humboldt-Universität zu Berlin
12/1995–12/1996	Diplomarbeit an der Humboldt-Universität zu Berlin mit dem Thema “Das magnetische Polaron in dimensionsreduzierten Systemen”, betreut von Prof. Dr. W. Nolting (Lehrstuhl “Festkörpertheorie”)
01/1997	Physik-Diplom an der Humboldt-Universität zu Berlin (Note: 1.2)
seit 09/1997	Doktorand an der Humboldt-Universität zu Berlin, betreut von Prof. Dr. W. Nolting (Lehrstuhl “Festkörpertheorie”), Promotionsstipendiat der Studienstiftung des deutschen Volkes
02/1999–09/1999	Forschungsaufenthalt in der Forschungsgruppe von Prof. Arthur J. Freeman an der Northwestern University in Evanston, Illinois; Bandstrukturrechnungen für die Dissertation

Berlin, den 15. Juli 2000

Veröffentlichungen

- R. Schiller, W. Müller und W. Nolting, “Electronic Quasiparticle Structure of a Thin Ferromagnetic Local-Moment Film”, *J. Magn. Magn. Mater.* **169**, 39 (1997).
- R. Schiller, W. Müller und W. Nolting, “On the Origin of Surface States in a Correlated Local-Moment Film”, *Eur. Phys. J. B* **2**, 249 (1998).
- R. Schiller und W. Nolting, “Thickness Dependent Curie Temperatures of Ferromagnetic Heisenberg Films”, *Solid State Commun.* **110**, 121 (1999).
- R. Schiller und W. Nolting, “Temperature-Dependent Band Structure of a Ferromagnetic Semiconductor Film”, *Phys. Rev. B* **60**, 462 (1999).
- R. Schiller, W. Müller und W. Nolting, “The Temperature-Dependent Behaviour of Surface States in Ferromagnetic Semiconductors”, *J. Phys.: Condens. Matter* **11**, 9589 (1999).
- W. Müller, R. Schiller und W. Nolting, “Understanding Surface States in a Correlated Electron System”, *Eur. Phys. J. B* **16**, 705 (2000).

Berlin, den 15. Juli 2000

Danksagung

Ich möchte mich bei allen bedanken, die mich bei der Anfertigung dieser Arbeit unterstützt haben.

Insbesondere danke ich Prof. Dr. W. Nolting für die intensive fachliche Betreuung sowie für die nachhaltige Unterstützung meines Forschungsaufenthaltes an der Northwestern University;

I wish to thank Prof. Arthur J. Freeman from Northwestern University in Evanston for his support during my stay in his research group and all the lunches at the "Mandarin House". Furthermore I would like to thank all the members of the Freeman group, in particular my tutor Dr. Oleg Myrasov and Carolyn Ashley, the secretary of the group.

Also from my time in Evanston I want to thank the following people for the nice time I had during my 8-months stay: Dr. Oliver Warschkow, Dr. Cathy Stampfl, Prof. Don Ellis, and Gianni Profeta.

Ich bedanke mich bei

M. Götsch für Ihre Unterstützung bei allen organisatorischen Fragen für das Korrekturlesen der deutschsprachigen Passagen und für das angenehme Klima an unserem Lehrstuhl;

PD Dr. Volker Eyert und Dr. Michael Potthoff für viele fruchtbare Diskussionen;

meinen "Kollegen" Robert Metzke, Dietrich Meyer und Torsten Wegner für die entspannte Atmosphäre in unserem Zimmer;

Friedbert Lewin und noch einmal Torsten Wegner für unzählige Zigaretten;

Dietrich Meyer, Wolf Müller, Sören Rex und Carlos Santos für die Administration der Rechner und Ihre Hilfe bei auftretenden Fragen;

und allen anderen, teilweise ehemaligen, Angehörigen des Lehrstuhls "Festkörpertheorie".

Bei der Studienstiftung des deutschen Volkes bedanke ich mich für das Promotionsstipendium sowie für die Unterstützung meines Forschungsaufenthaltes an der Northwestern University. Des weiteren möchte ich mich bei meinem Vertrauensdozenten Prof. Dr. J. Sauer sowie bei Dr. N. Weidtmann von der Studienstiftung bedanken.

Thomas Anders danke ich für das Korrekturlesen. Meiner Mutter Marianne Schiller, meiner Frau Patricia Schiller sowie den Eltern meiner Frau, Melitta und Till Geml, danke ich für Ihre bedingungslose Unterstützung, ohne die insbesondere der Aufenthalt an der Northwestern University unmöglich gewesen wäre. Meinem Sohn Adrian danke ich für seine Hilfe bei der Literaturrecherche :)

Selbständigkeitserklärung

Hiermit erkläre ich, die vorliegende Arbeit selbständig ohne fremde Hilfe verfasst und nur die angegebene Literatur und Hilfsmittel verwendet zu haben.

Berlin, den 15. Juli 2000